

Section 6.2: Clean Mo Surfaces

Table 6.1 shows the rates of product formation over clean Mo(100) single crystals and clean Mo polycrystalline foils. Table 6.1 expresses the rate of product formation as a turnover frequency (product molecules/metal site \cdot sec) versus the hydrocarbon used in each experiment. No differences in selectivity or rate were observed between Mo(100) single crystals and polycrystalline foils. We found the rate of HDO reactions to be 10-100 times faster than HDN reactions for similar model compounds under identical reaction conditions.

Hydrodeoxygenation reactions over clean Mo mainly produced propene and CO and some methane. The HDO activity for furan was found to be \sim 10 times greater than for tetrahydrofuran (THF). The product distributions of furan and THF were found to be significantly different over the range of conditions used in this study. Furan produced propene and CO almost exclusively, while THF gave a product distribution similar to the HDN reactions studied. During THF HDO reactions, we found that furan was produced at approximately the same rate as the sum of the formation rates of the four carbon (Σ C₄'s of Table 6.1) products combined.

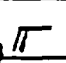

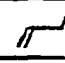

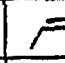

Table 6.2 shows the product distribution in mole percent of C₃ and C₄ hydrocarbons produced from each model compound. The mole percent of propene was found to be approximately equal for THF and all the nitrogen-containing model compounds. The distribution of C₄ hydrocarbons produced from the THF and pyrrolidine HDO reactions was similar. Product distributions and overall rates for both the paraffinic and olefinic nitrogen-containing ring compounds were found to be the same. The rate of formation of C₅ hydrocarbons from pyridine and piperidine was found to be approximately twice the rate of C₄ hydrocarbon formation.

Table 6.1. Rates of product formation are shown. Conditions were 10 Torr hydrocarbon and 750 Torr H₂ at 610 K.

Reactants	Products											
	C ₃ H ₆	C ₃ H ₄	C ₃ H ₂	C ₃ H	C ₃ H ₂	C ₃ H	C ₃ H ₂	C ₃ H	C ₄	C ₅	CO	CH ₄
furan	1.05	0.005	0.017	0.009	0.014	0.007	0.045	0.045	1.0	0.04		
THF	0.07	0.006	0.019	0.013	0.017	0.004	0.049	0.049	0.05	0.02		
pyridine	0.007	ND ^a	0.003	0.002	0.002	ND	0.005	0.10				0.10
piperidine	0.009	ND	0.002	0.004	0.004	ND	0.006	0.10				0.10
pyrrole	0.004	0.001	0.001	0.001	0.001	~ 0.001	0.002					0.04
pyrrolidine	0.009	0.001	0.003	<0.002	<0.002	~ 0.001	0.005					0.09

ND = not detectable by methods used in this study. Turnover frequency = molecules produced/metal site • sec.

Table 6.2. Product distribution of C₃ and C₄ hydrocarbons from each model compound over clean Mo are shown. Conditions were 10 Torr hydrocarbon and 750 Torr hydrogen at 610 K.

Reactants	Products (mole %)						overall rate ^a
	C ₃ 						
furan	95	0.5	1.5	0.8	1.2	1.0	1.1
THF	54	5	15	10	13	3	0.13
pyridine	58	NDb	25	17		-	0.012
piperidine	60	ND	13	27		-	0.015
pyrrole	50	12	12	12		12	0.014
pyrrolidine	56	6	19	12		-	0.016

^aunits of molecules produced/site · sec. bND ≡ not detectable by methods used in this study.






Experiments were performed to determine the effect of hydrogen pressure on the overall rate and selectivity of the HDO reaction. For the HDO reaction with furan, higher hydrogen pressures increased the overall rate and shifted the product distribution toward more C₄ hydrocarbons (see Fig. 6.1). All of the HDN reactions and also the HDO reaction with THF showed an increase in the overall rate of reaction but no change in selectivity.

We also studied the effect of temperature and partial pressure of hydrogen on the poisoning rate. Higher temperatures or a lower partial pressure of hydrogen increased the rate of poisoning of the reaction as shown in Fig. 6.2. The rate of poisoning, for the overall rate of product formation, can be fit to an Arrhenius curve which shows that the rate of poisoning (expressed as the half-life of the reaction rate) decreased exponentially with increased temperature.

Section 6.3: Sulfided Mo Surfaces

Addition of 0.5 ML of S to the Mo surface results in a decrease in the overall rate of reaction and an increase in the relative rate of production of C₄ hydrocarbons. Table 6.3 shows the product distribution (in mole percent) and overall rate (molecules produced/metal site • sec \equiv turnover frequency) of reaction for HDO and HDN reactions over a sulfided Mo surface. An increase in the olefin-to-paraffin ratio in the product distribution was noted. The HDO reaction was found to be more sensitive to addition of S to the Mo surface than was the HDN reaction. The overall rate of HDO reactions decreased 35-75% upon S addition, while the HDN reaction rates decreased by ~ 20%.

Table 6.3. Product distribution of C₃ and C₄ hydrocarbons from each model compound over sulfur-covered Mo (0.5 ML S) are shown. Conditions were 10 Torr hydrocarbon and 750 Torr hydrogen at 610 K.

Reactant	Products (mole %)					overall rate ^a
						
furan	88	1.3	4.6	2.1	3.5	0.37
THF	64	ND ^b	14	11	11	0.08
pyridine	50	ND	25	25		0.010
piperidine	50	ND	17	33		0.012
pyrrole	56	ND	22	22		0.010
pyrrolidine	82	ND	9	9		0.011

^aunits of molecules produced/metal site · sec. ^bND ≡ not detectable by methods used in this study.

Section 6.4: Discussion

There has been a tremendous amount of work done on determining the mechanism and best catalysts for the hydrodesulfurization reactions because of their great economic value. Much less work has been done on the HDN and HDO reactions because under the conditions necessary for HDS these two reactions also occur. We have found that HDO and HDN of model compounds, in fact, do occur over clean and sulfided Mo catalysts.

The product distributions from HDN and HDO reactions appear similar to that found for the HDS reactions, using the sulfur analogues of the model compounds used in this work.¹⁻¹⁰ Sulfur on the Mo surface increased the C₄ to C₃ and the alkene to alkane mole ratios of the products. Increasing the hydrogen over-pressure also increased the C₄ to C₃ ratio of the products; but, decreased the alkene to alkane ratio.

The reaction mechanism for the HDO reaction using furan and THF, where the major products were propene and CO, was studied in more detail than the nitrogen HDN reactions. The rate of formation of propene from furan was found to be 10 times faster than from THF. A rate of production of furan was also observed from THF. The mechanism appears to involve dehydrogenation followed by ring opening and CO extraction to form propene and CO. The details of this simplistic scheme need more careful experiments designed to probe each step individually.

Section 6.5: References

1. Furinsky, E., Catal. Rev. Sci. Eng. 22 (3), 371 (1980).
2. Chianelli, R.R., Catal. Rev. Sci. Eng. 26 (3,4), 361 (1984).
3. Owens, P.J., and Amberg, C.H., Can. J. Chem. 40, 941 (1962).
4. Owens, P.J., and Amberg, C.H., Can. J. Chem. 40, 947 (1962).
5. Owens, P.J., and Amberg, C.H., Can. J. Chem. 41, 1966 (1963).
6. Owens, P.J., and Amberg, C.H., Can. J. Chem. 42, 843 (1964).
7. Owens, P.J., and Amberg, C.H., Can. J. Chem. 44, 2623 (1966).
8. Flening, J.E., and Lynton, H., Can. J. Chem. 45, 353 (1967).
9. Nag, N.K., Appl. Catal. 10, 53 (1984).
10. Rollmann, L.D., J. Catal. 46, 243 (1977).
11. Sonnemans, J., Van Den Berg, G.H., and Mars, P., J. Catal. 31, 220 (1973).
12. Ledoux, M.J., Puges, P.E., and Marie, G., J. Catal. 76, 285 (1982).
13. Ledoux, M.J., Appl. Catal. 9, 31 (1984).
14. Satherfield, C.N., and Gulfekin, S., Ind. Eng. Chem. Proc. Des. Dev. 20, 62 (1981).
15. McIlvried, H.G., Ind. Eng. Chem. Proc. Des. Dev. 10, 125 (1971).
16. Stern, E.N., J. Catal. 57, 390 (1979).
17. Furimsky, E., Ind. Eng. Chem. Prod. Res. Dev. 22, 34 (1983).
18. Furimsky, E., Ind. Eng. Chem. Prod. Res. Dev. 22, 31 (1983).
19. Krishnamurthy, S., Panvelker, S., and Shah, Y.T., Al. Ch. E. 27 (6) 994 (1981).
20. Furimsky, E., Appl. Catal. 6, 159 (1983).

CHAPTER SEVEN: THE CONVERSION OF ACETYLENE TO
FORM BENZENE OVER PALLADIUM SINGLE CRYSTAL SURFACES

Section 7.1: Introduction

Palladium surfaces have been noted¹⁻¹² to possess the distinctive property that catalytic reactions of various classes can be observed both at high pressures and under ultrahigh vacuum conditions. An example is the trimerization of acetylene, which has been shown to occur both in ultrahigh vacuum and at higher pressures over a number of Pd surfaces (single crystals¹⁻⁹, foils⁶ and supported⁶ catalysts) as well as over many homogeneous catalysts¹⁰⁻¹². The low temperature formation of benzene has been observed using temperature programmed desorption (TPD)¹⁻⁶, high resolution electron energy loss spectroscopy (HREELS)⁷⁻⁹, angle resolved ultraviolet photoemission spectroscopy (ARUPS)^{1,2}, metastable noble gas deexcitation spectroscopy (MDS)⁴, X-ray photoelectron spectroscopy (XPS)^{1,2}, low energy electron diffraction (LEED)^{1,2} and molecular beam measurements². This paper deals with the effect of pressure and additives on Pd single crystal surfaces on the trimerization of acetylene to form benzene.

The cyclization of acetylene to benzene was first reported to occur in small yields by Berthelot in 1866 at elevated temperatures (300-400°C)⁵³. In the 1940's, Reppe discovered that certain homogeneous nickel complexes produced benzene from acetylene in good yield under mild experimental conditions⁵⁴. Since that discovery, other research groups have found numerous homogeneous transition metal systems that catalyze substituted and functionalized acetylenes to form benzene derivatives¹². For example, cobalt complexes such as $\text{CpCo}(\text{CO})_2$ are used in cyclization steps in the

synthesis of natural products such as steroids and Vitamin B6. Also, it has been shown that palladium chloride will easily oligomerize acetylene¹¹.

Additives, such as potassium, silicon, phosphorus, sulfur and chlorine, have been shown to modify the behavior of catalysts for many different reactions¹³⁻¹⁷, and their interaction with surfaces has been studied extensively by many surface-sensitive techniques¹⁸⁻²⁴. Two effects are possible - (1) a geometric effects due to site blocking; and (2) an electronic effect due to electron donation (as in the case of K¹⁸) or electron depletion (as in the case of Cl²⁵) of the near surface region.

In this chapter, a systematic study of both surface composition effects and pressure effects on the chemisorptive and catalytic properties of palladium (111), (100) and (110) single crystal surfaces on the cyclotrimerization of acetylene is described.

Section 7.2: Results: Introduction

This study investigated similarities and differences in the trimerization of acetylene to benzene using palladium single crystal catalysts under varying pressure conditions (10^{-12} atm - 1 atm) and with different additives on the single crystal surface. Under UHV condition, the cyclo-trimerization of acetylene on all three surfaces ((111), (110) and (100)) was detected by observing the thermal desorption of molecular benzene after dosing with acetylene. All doses were at 130 K. Table 7.1 shows the dose molecules, desorption products, desorption temperature, E_A of desorption and relative areas for the products of acetylene adsorption for the clean (111), (100) and (110) surfaces in UHV.

Section 7.3: Ultra-High Vacuum Studies: Pd(111)

On the Pd(111) face, dosing 6 Langmuirs (L) of acetylene produced benzene with two distinct desorption peaks at 250 K and 490 K. The low temperature peak was 2.5 times larger than the high temperature (see Fig. 7.1). Acetylene, ethylene and hydrogen were also detected as desorption products. The acetylene and ethylene desorbed at 190 K and 305 K, respectively. Hydrogen, the only other product detected, had a broad desorption peak from 430-830 K, with a maximum at 450 K (Table 7.1). At low acetylene coverages (0.5 L), the benzene desorption maxima remained unchanged. The amount of benzene formed decreased, with the area under the high temperature peak decreasing more rapidly than the area under the low temperature peak. No C_4 products were detected. In order to determine whether the product formation was desorption rate-limited or reaction rate-limited, C_6H_6 , C_2H_4 and H_2 were adsorbed on clean Pd(111) and a TPD spectrum was taken. Benzene undergoes both reversible and irreversible chemisorption, with the fraction of reversibly bound benzene increasing with exposure. At low coverages (1.0 L), there was primarily decomposition as characterized by a broad hydrogen trace extending from 520 K to 720 K with a maximum at 545 K. Benzene had two weak desorption peaks at 260 K and 520 K. With exposures greater than 2 L, the hydrogen spectrum remained unchanged and the benzene maxima occurred at 235 K and 510 K with a 1:10 intensity ratio (Fig. 7.2). No C_2H_2 or C_2H_4 fragments were detected. Hydrogen dosing yielded a desorption peak at 310 K with only the peak area changing at higher coverages. With ethylene (1.0 L), reversible desorption occurred at 300 K with hydrogen desorbing at 370 K and 430 K in a 1:1 ratio. Higher coverages of ethylene (>2L) increased molecular desorption of ethylene only.

Table 7.1. Desorption products from acetylene, ethylene and benzene over Pd(111), Pd(100) and Pd(110) single crystal surfaces.

Crystal Face	Dose Molecule	Desorption Product	Desorption Temperature (K)	E _A (kcal/mol)	Relative Areas (for acetylene adsorption)	
(111)	C ₂ H ₂	H ₂	450 (430-830)	26.3 (25.1-49.5)	4.3	
		C ₂ H ₂	190	10.8	1.0	
		C ₂ H ₄ C ₆ H ₆	350 250, 490	20.3 14.3, 28.7	0.22 0.9	
(100)	C ₂ H ₄ C ₆ H ₆	C ₂ H ₄	300	17.3		
		H ₂ C ₆ H ₆	545 (520-720) 260, 520	32.0 (30.5-42.7) 14.9, 30.5		
		C ₂ H ₂	420 (495-625 sh) 180 (250 sh) 305 260, 380, 470	24.5 (29.0-36.9 sh) 10.2 (14.3) 17.6 14.9, 22.1, 27.5	2.8 1.0 0.1 0.04	
(110)	C ₂ H ₄ C ₆ H ₆	C ₂ H ₄	260, 310	14.9, 17.9		
		H ₂ C ₆ H ₆	575 (665 sh) 220, 375, 525	33.8 (39.3) 12.5, 21.8, 30.8		
		C ₂ H ₂	490 180 (to 500 sh) 260 250, 420	28.7 10.2 (to 29.3 sh) 14.9 14.3, 24.5	1.43 1.0 0.09 0.06	
(110)	C ₂ H ₄ C ₂ H ₆	C ₂ H ₄	475, 535 250 (to 425 sh)	27.8, 31.4 14.3 (to 24.8 sh)		
		H ₂ C ₆ H ₆				
		C ₂ H ₂				

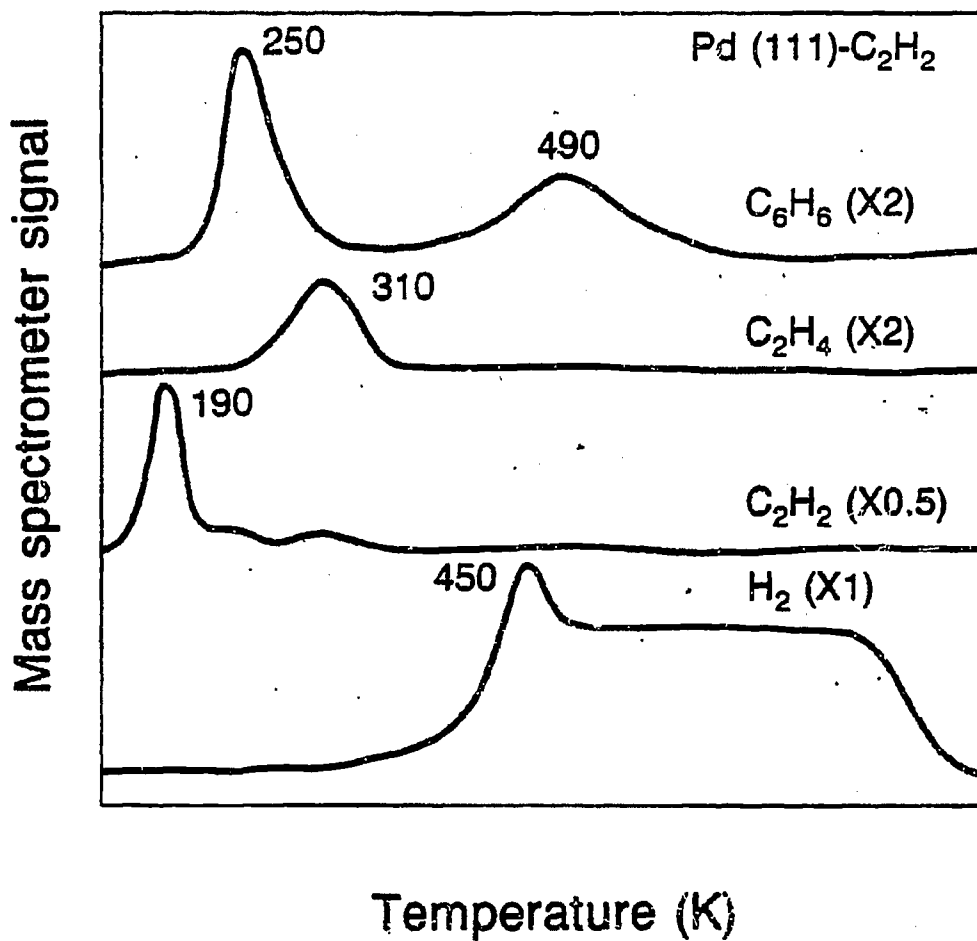


Fig. 7.1. The TPD spectra of acetylene on clean Pd(111) (6 L of acetylene dosed at 130 K) are displayed. The four products from the desorption are shown - benzene, from the trimerization of acetylene; ethylene, due to self-hydrogenation of acetylene; hydrogen, from acetylene decomposition; and molecular desorption of acetylene itself.

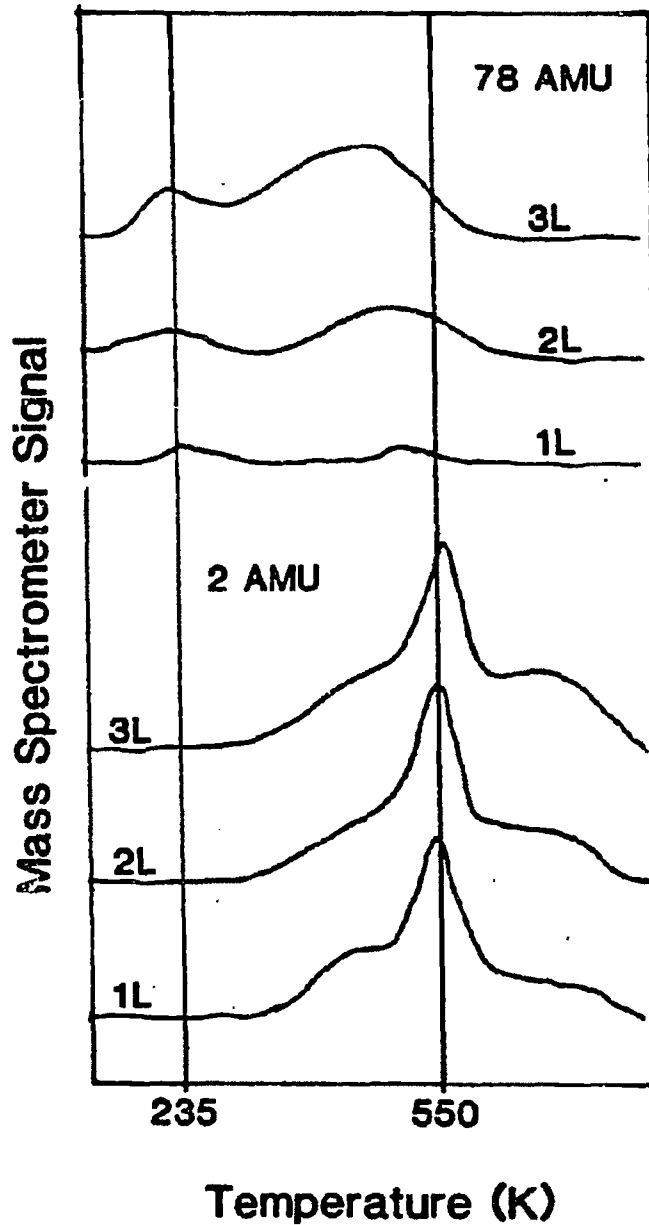


Fig. 7.2. Benzene was found to undergo both reversible and irreversible adsorption on clean Pd(111). The desorption signal of benzene and hydrogen from 1,2 and 3 Langmuir doses of benzene on Pd(111) at 130 K are shown. At higher exposures, a large increase in reversible desorption of benzene is observed.

Section 7.4: Effect of Adatoms on Cyclotrimerization at Low Pressures: Pd(111)

Adsorption of 0.25 monolayer (ML) of silicon on Pd(111) did not significantly perturb the chemisorption of acetylene, as shown by the thermal desorption results (see Fig. 7.3). As shown in Fig. 7.3, the only effect of Si was a slight decrease in the extent of acetylene decomposition (to form H_2 and C) and some enhancement of the high temperature desorption peak of benzene. Phosphorus, however, greatly suppressed the acetylene decomposition, increased the yield of ethylene, and yielded a complex thermal desorption spectrum of benzene (from the cyclotrimerization processes) with maxima at 200, 300, 400 and 470 K, while doubling the benzene yield.

Like P, S adatoms affected the thermal behavior of chemisorbed acetylene (see Fig. 7.3). At low coverages of S (< 0.2 ML), the ethylene yield and decomposition to hydrogen decreased, but the benzene yield significantly increased. The low temperature benzene peak intensity increased and a new peak appeared at ~ 430 K. At high S coverages (> 0.25 ML), the formation of ethylene was fully suppressed and the decomposition to H_2 was also very low. At these high S coverages, the benzene desorption spectrum was comprised mostly of a broad peak with a single maximum at 260 K.

Like P and S, Cl adatoms also shifted the acetylene surface chemistry toward benzene formation (see Fig. 7.3); but, in contrast to S, the benzene desorbed largely in the high temperature regions with maxima at 415 and 490 K, although there was a smaller peak at 270 K. Chlorine also suppressed ethylene formation and acetylene decomposition to H_2 and carbon.

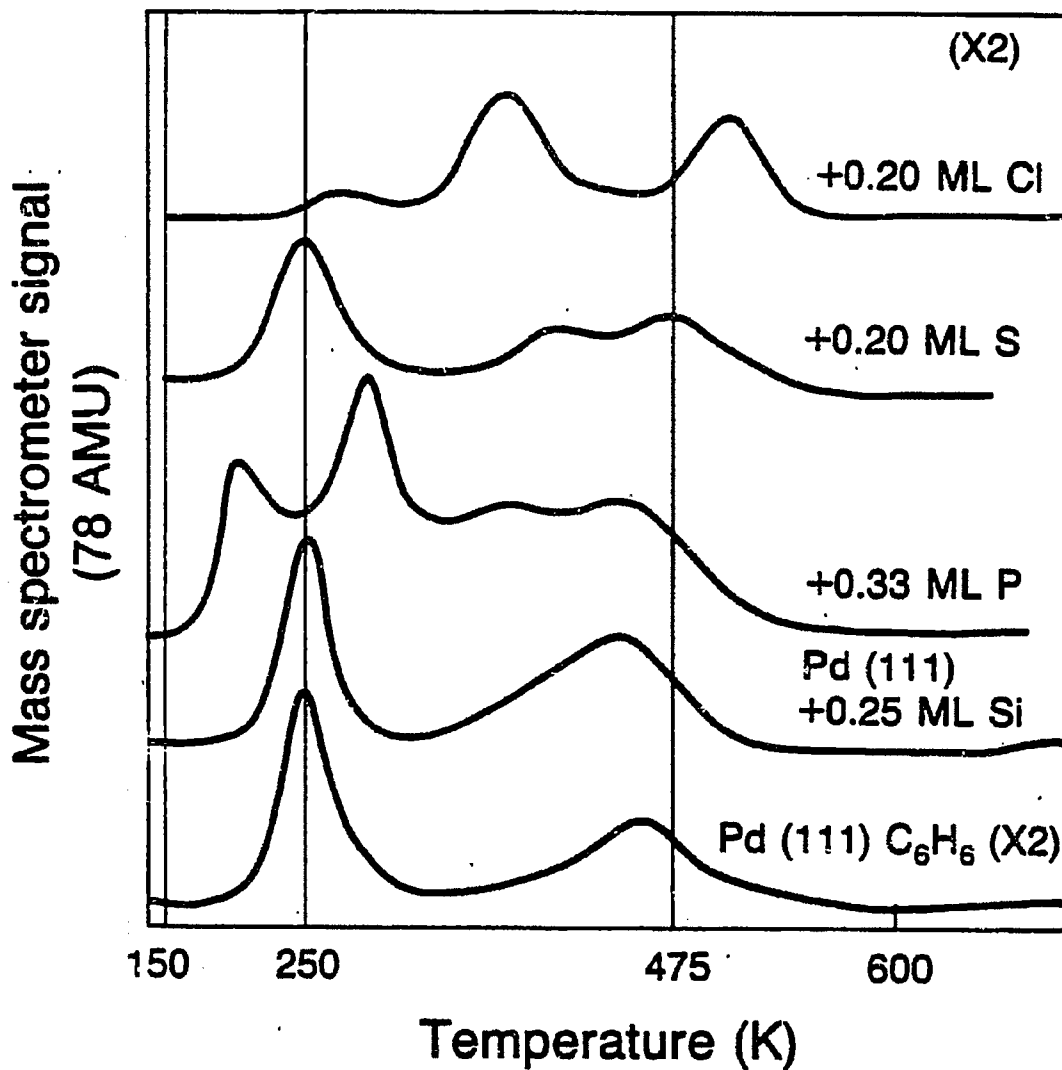


Fig. 7.3. Six L of acetylene were dosed on additive-covered Pd(111) at 130 K. The benzene TPD spectrum was then recorded and is displayed for each surface. The high temperature peak is observed to shift upwards from 470 K on the Si-dosed surface to 490 K on the Cl-covered Pd(111) surface. Phosphorus is observed to have a complex thermal desorption spectrum with four maxima.

The adatom effect upon the acetylene cyclotrimerization yield increased in the presence of adatoms in order from Si to P to S. Chlorine was not quite as effective as S, which basically fully suppressed all acetylene reactions except cyclotrimerization. Thus, Pd(111)-S is an impressively selective catalyst for benzene formation from acetylene under ultra-high vacuum conditions. The main difference in the TPD spectra between the Pd(111)-S and Pd(111)-Cl surfaces was that the Pd(111)-S surface mostly promoted the low temperature cyclotrimerization reaction and the Pd(111)-Cl surface promoted the high temperature process.

Using TPD studies to observe the effect of adsorbed benzene on adatom-covered palladium surfaces led to the same trends as found with acetylene adsorbed on adatom-covered Pd surfaces. For example, Fig. 7.4 shows the effect of 0.25 ML of Si on Pd(111). As in the case of acetylene adsorption, Si enhanced the high temperature TPD peak of benzene. Higher exposures of both acetylene and benzene led to an enhancement of the high temperature (470 K) benzene desorption peak.

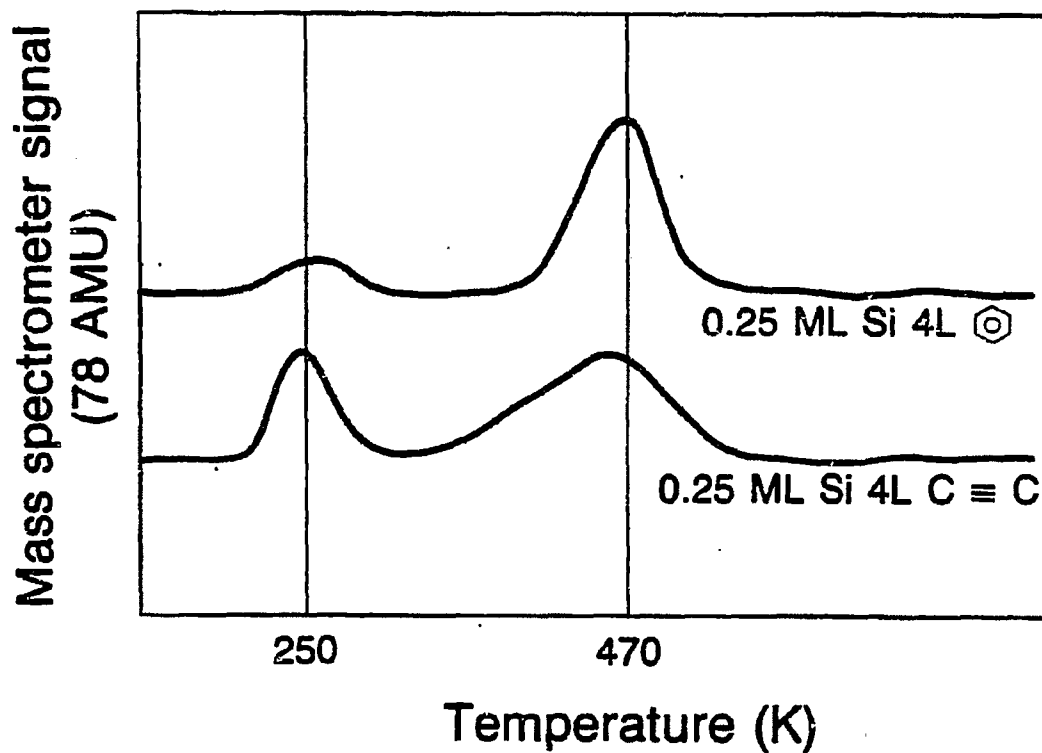


Fig. 7.4. Benzene TPD spectra are compared on a Si-doped Pd(111) surface after benzene or acetylene desorption (4 L adsorption at 130 K). Acetylene gives a broader high temperature peak. More acetylene exposure enhances the high temperature benzene peak, whereas more benzene exposure enhances the low temperature desorption maxima.

Section 7.5: Ultra-High Vacuum Studies: Pd(110)

The Pd(110) surface produced four times less benzene than the (111) face. On the (110) face, benzene desorbed at 250 K and 420 K in a 1:3 ratio after a 6L dose of acetylene (see Fig. 7.5). At coverages below 3L of acetylene, no benzene was detected. Molecular desorption of acetylene occurred at 180 K with a broad shoulder plateau extending to 500 K. Ethylene desorbed at 260 K, and hydrogen desorbed in a broad peak centered at 490 K. When the surface was dosed with 6 L of benzene, molecular desorption occurred at 250 K, with a shoulder extending to 425 K. At low coverages (1.0 L), a single peak at 260 K was observed. The hydrogen from decomposed benzene had maxima at 475 K and 535 K which increased in area with increasing amounts of benzene up to 3 L, after which they remained constant. Hydrogen desorbed at 310 K at all coverages, when adsorbed on the surface alone.

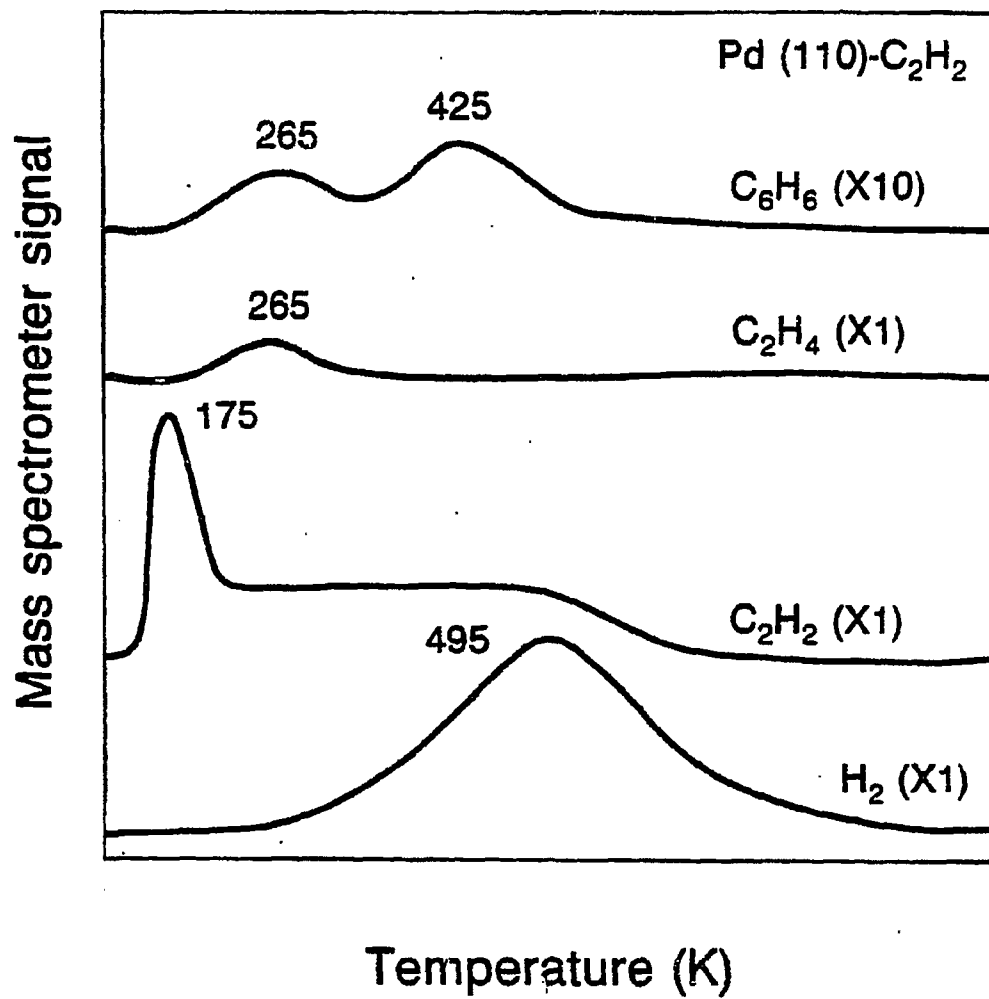


Fig. 7.5. The TPD spectra of acetylene on clean Pd(110) (6 L acetylene dosed at 130 K) are shown. The four products from the desorption are shown - benzene, ethylene, hydrogen and acetylene.

Section 7.6: Effect of Adatoms on Cyclotrimerization at Low Pressures: Pd(110)

Silicon at low surface coverages (<0.25 ML) enhanced the benzene yield through the high temperature desorption peak (see Fig. 7.6), and decreased the decomposition of hydrogen. At $\Theta_{Si}=0.37$ ML, the yield of benzene increased further to a factor of 3.5 (relative to the clean surface), while the ethylene and hydrogen yields were less than that observed for the clean Pd(110) surface.

Phosphorus on the (110) surface of Pd also increased the cyclotrimerization and self-hydrogenation reactions of acetylene. Benzene desorption was found to increase at P coverages greater than 0.2 ML. As on Pd(111), the gain in benzene yield was in the high temperature desorption peak (see Fig. 7.6). At higher coverages of P, two benzene TPD maxima were observed at 270 K and 440 K. The high temperature maximum was increased by as much as a factor of 4 ($\Theta_P=0.42$ ML) relative to the clean surface, while the ethylene yield remained at the level of the low coverage surface. A decrease in the amount of hydrogen desorbing from the surface was observed.

On sulfur-covered Pd(110), the yield of benzene showed a slight increase while the yield of ethylene decreased with increasing S coverage. The molecular desorption of acetylene increased with increasing sulfur coverage. At higher coverages of S, $\Theta_S=0.4$ ML, no ethylene was detected, very little hydrogen desorbed, and the amount of benzene formed was approximately the same as on clean Pd(110).

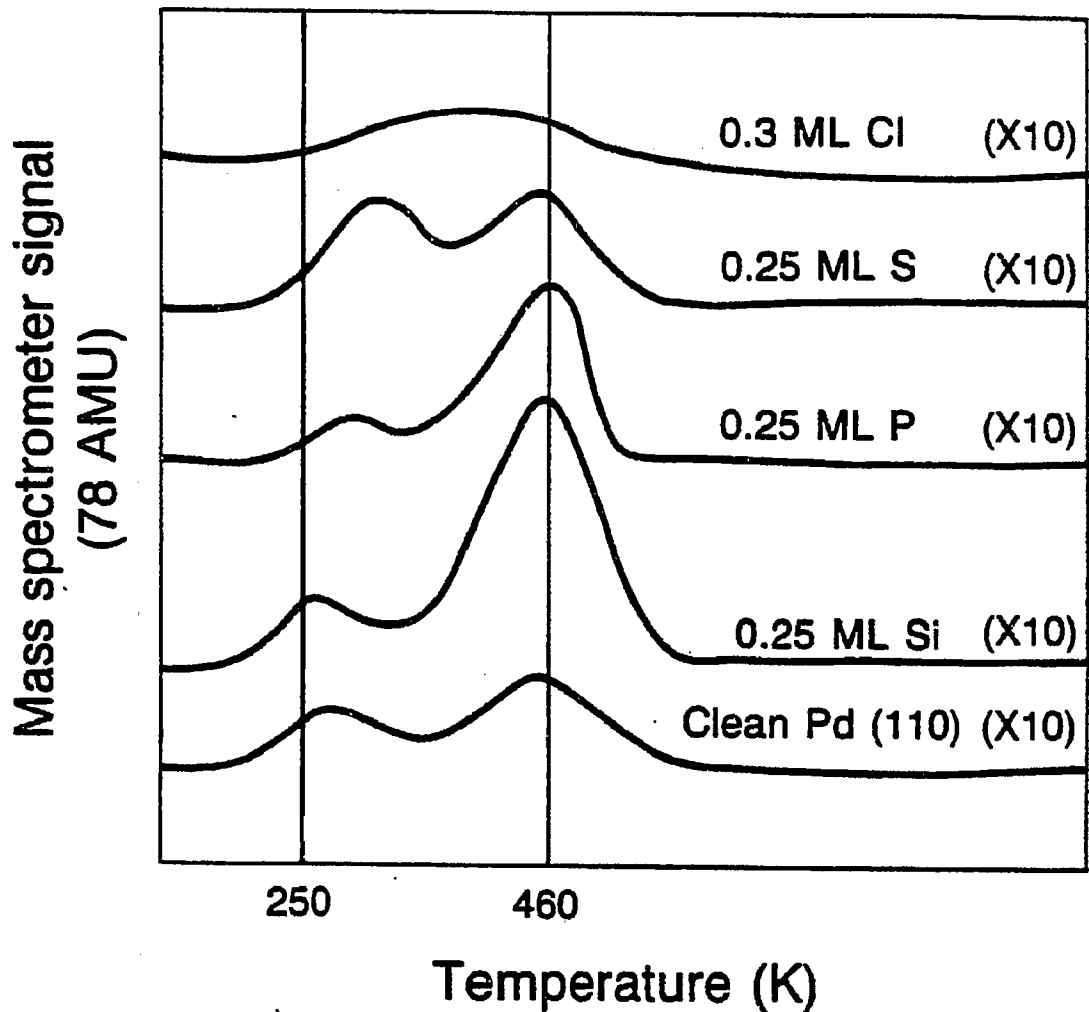


Fig. 7.6. The benzene TPD spectra from additive-covered Pd(110) after a 6 L exposure of acetylene at 130 K. Silicon and P add to the benzene yield in the high temperature peak, similar to their effect on Pd(111) and Pd(100). Sulfur, on the other hand, enhances the low temperature benzene desorption maximum slightly and Cl reduces the overall yield and broadens the two maxima into one peak.

Addition of Cl to Pd(110) resulted in decomposition, hydrogenation and cyclotrimerization of acetylene. At a Cl coverage of 0.30 ML, a very weak ethylene desorption was observed at 290 K and a broad benzene desorption maximum was observed at 370 K (see Fig. 7.6).

Section 7.7: Ultra-High Vacuum Studies: Pd(100)

On the Pd(100) surface, dosing 6 L of acetylene produced benzene continuously from 250 K to 490 K with three maxima at 260, 380 and 470 K. At exposures below 3 L, no benzene was detected. This surface formed 20 times less benzene than the (111) crystal face. With a 6 L dose of acetylene, in addition to trimerization, reversible desorption, hydrogenation and decomposition were also observed (see Fig. 7.7). Acetylene desorbed at 180 K with a shoulder at 250 K, and ethylene desorbed in a single peak at 305 K. The hydrogen desorption from the decomposition reached a maximum at 420 K, followed by a broad plateau from 495 to 625 K. At low coverages of acetylene (1.0 L), there was primarily decomposition. Benzene dosed on the crystal at low coverages (1.0 L) yielded a weak maximum at 310 K with a tail extending to 535 K. At an exposure of 6.0 L, three poorly resolved benzene maxima at 220, 375 and 525 K were observed, along with a hydrogen peak at 575 K, which had a high temperature shoulder at 665 K. When hydrogen alone was dosed on the surface, at all coverages, it desorbed in one peak at 310 K. Ethylene (0.5 L) gave molecular desorption at 260 K and 310 K in a 1:5 ratio with hydrogen desorbing at 365 K. Larger ethylene doses increased the low temperature reversible desorption peak without affecting the hydrogen desorption.

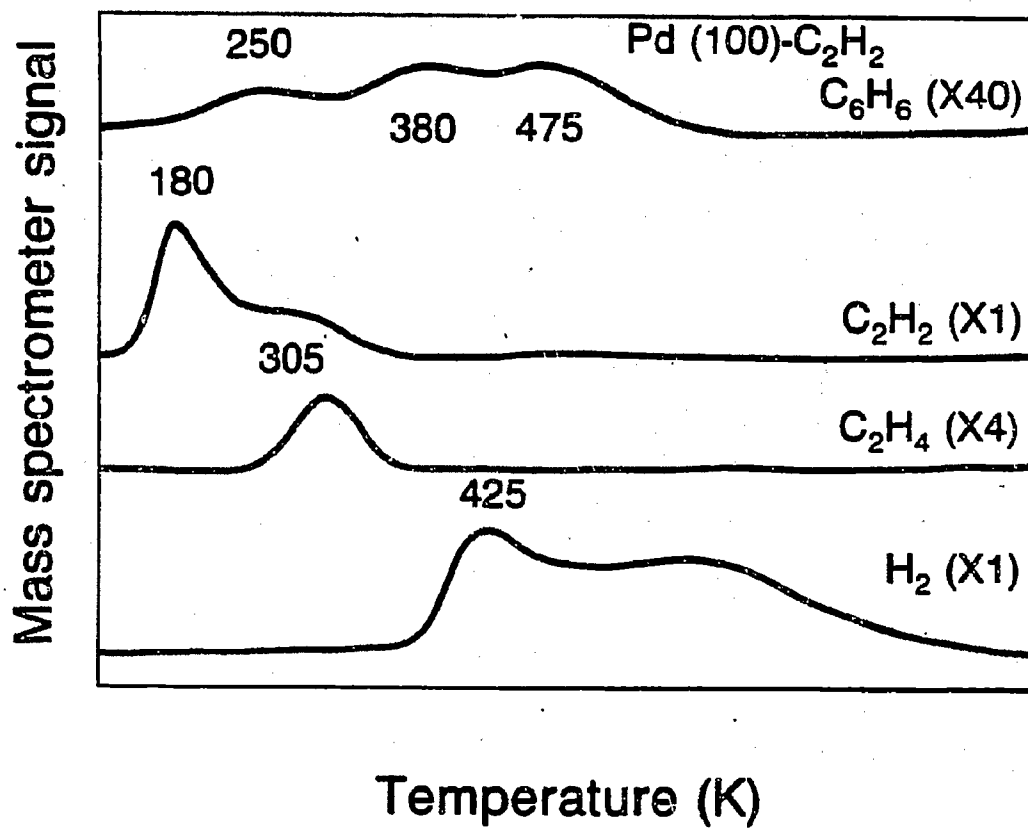


Fig. 7.7. The TPD spectra of acetylene from clean Pd(100) (6 L acetylene dosed at 130 K), showing the four products of the desorption reaction - benzene, ethylene, hydrogen and acetylene.

Section 7.8: Effect of Adatoms on Cyclotrimerization at Low Pressures: Pd(100)

Potassium on the (100) face of palladium had a large negative effect on the formation of benzene from acetylene (see Fig. 7.8). The yield of ethylene and hydrogen was decreased by ~ 95% (see Fig. 7.9,11). The molecular desorption of acetylene was slightly reduced, ~ 20-25% (see Fig. 7.10). At 0.25 ML (or higher) coverage of K, no benzene formation was observed.

Silicon has a substantial effect on acetylene chemisorbed on Pd(100). The yield of both ethylene and benzene was found to increase markedly (see Fig. 7.8,9). The two benzene TPD peaks were similarly affected by Si promotion on Pd(100) and Pd(111); that is, the high temperature peak increased and accounted for a six-fold increase in the yield of benzene at a Si coverage of 0.10 ML. Higher coverages of Si on Pd(100) further increased the yield of benzene, up to ~ 20 times that of the clean surface at Si coverages of 0.38 ML. Concomitantly, the ethylene yield was also enhanced by a factor of ~ 10. The decomposition reaction increased also, although the hydrogen desorption remained constant (see Fig. 7.11).

Phosphorus adsorbed on Pd(100) also influenced the chemistry of chemisorbed acetylene. The yield of benzene was enhanced, but not to the extent observed on silicon-covered Pd(100). At a coverage of 0.17 ML of P, two benzene maxima were observed, at 350 and 520 K. Low coverages of P, <0.2 ML, resulted in no change in the benzene or ethylene yields; however, at coverages of $0.3 < \theta_p < 0.5$ ML, the yield of both benzene and ethylene was found to increase by a factor of 3-5 (see Fig. 7.8,9). With increasing P coverages, benzene desorption maxima were also observed

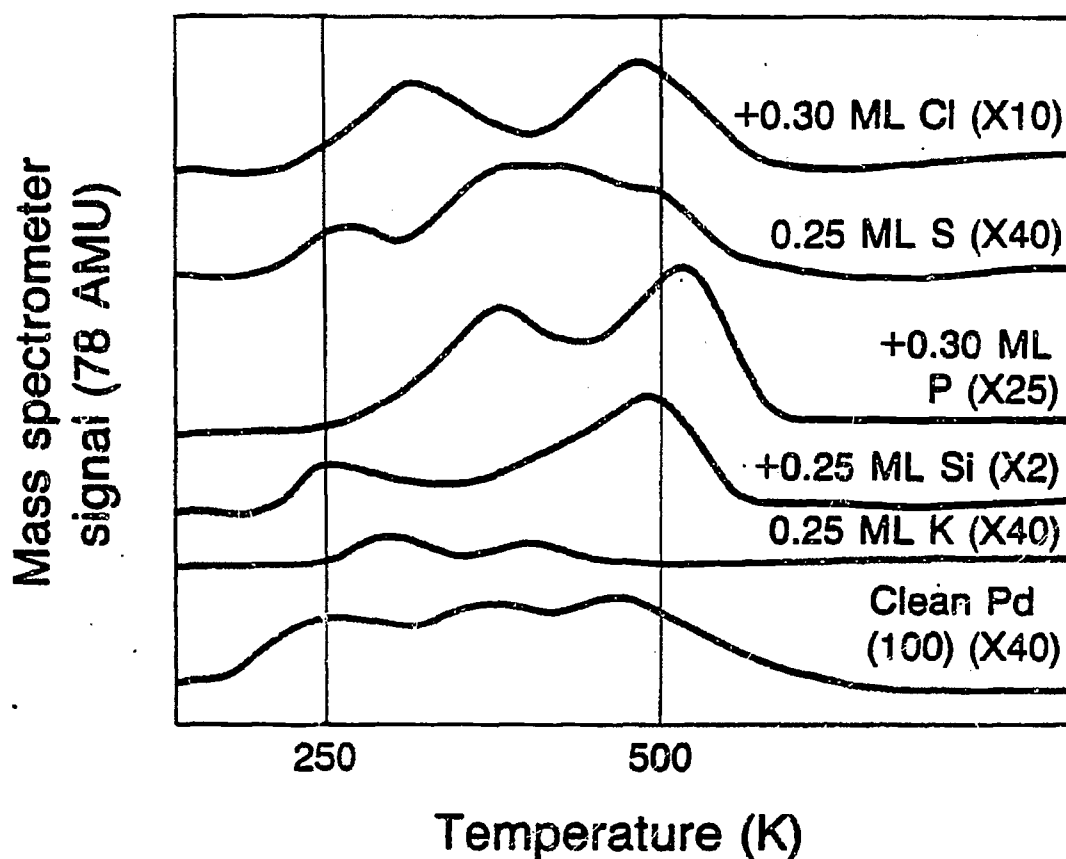


Fig. 7.8. Benzene TPD spectra from adatom-covered Pd(100), after a 6 L exposure of acetylene at 130 K, are displayed. Silicon, 0.25 ML, is found to enhance the formation of benzene ~ 15 times relative to the clean surface. For Si- and P-covered surfaces, the high temperature desorption maximum was enhanced further at higher additive coverages.

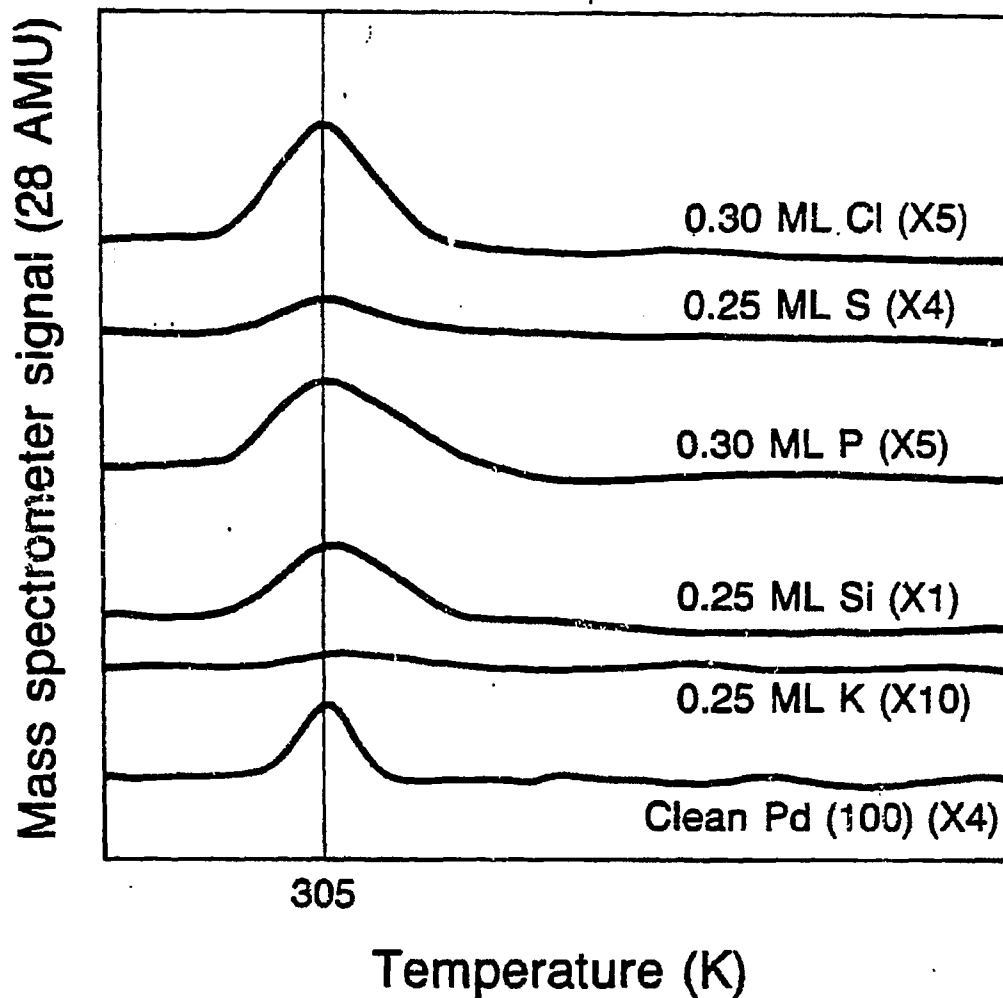


Fig. 7.9. Ethylene TPD spectra, after a 6 L dose of acetylene on Pd(100), are displayed. The more electron-withdrawing additives, S and Cl, completely block ethylene desorption at higher additive coverages. Potassium-covered surfaces produces very little ethylene. At coverages of more than ~ 0.1 ML, Si-covered Pd(100) enhances the formation of ethylene, as well as benzene, much more than the other additives.

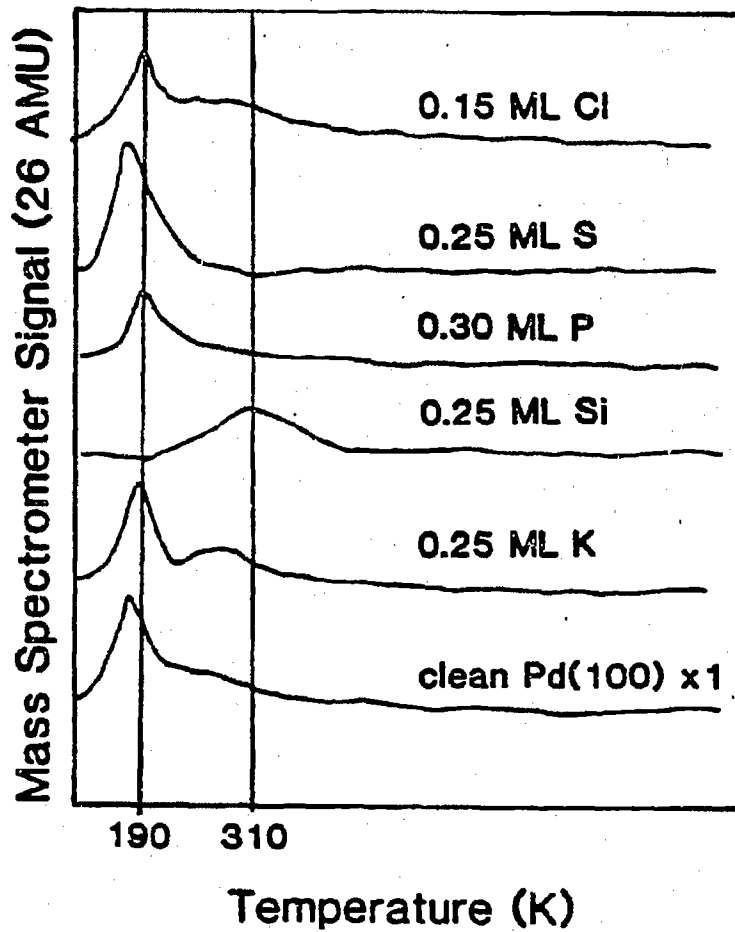


fig. 7.10. Acetylene TPD spectra, after a 6 L dose of acetylene on Pd(100) at 130 K, are displayed. Clean Pd(100), K-, P-, S- and Cl-covered surfaces have similar TPD traces for acetylene desorption. Silicon appears to have the strongest binding site for acetylene.

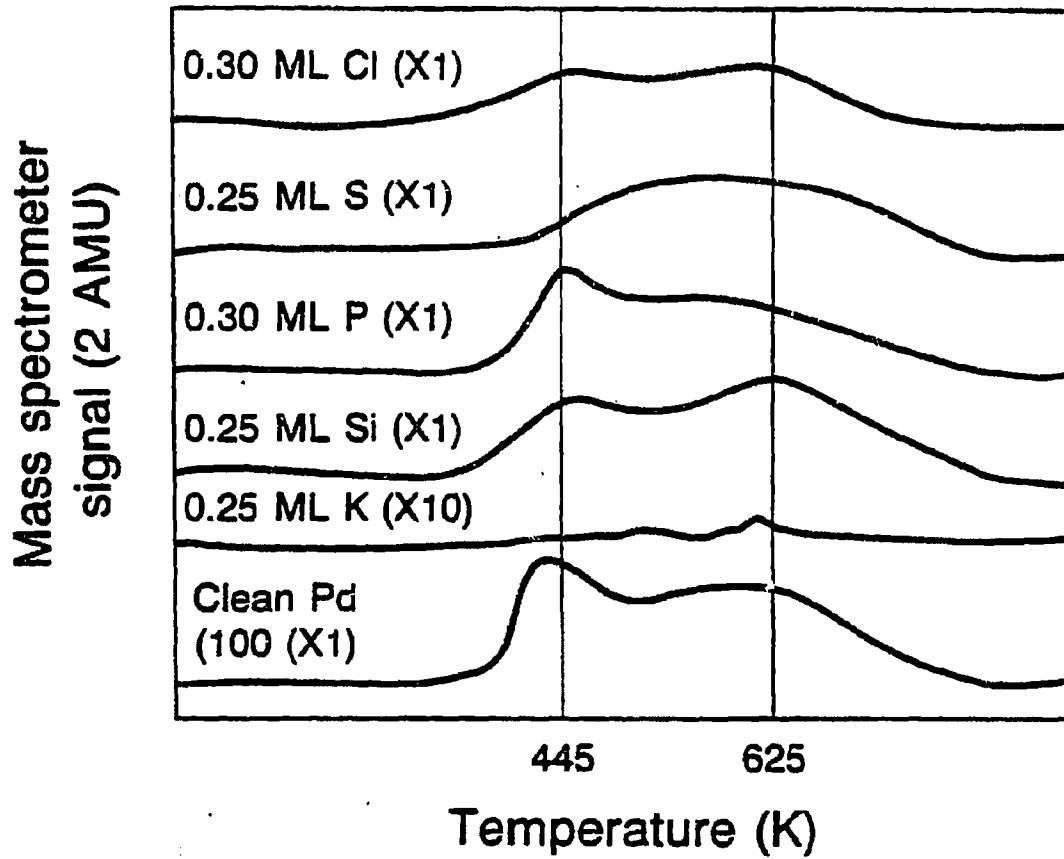


Fig. 7.11. The hydrogen TPD spectra, after a 6 L dose of acetylene at 130 K on Pd(100), are displayed. All the additives reduced the amount of H₂ desorption, K > Cl > S > P > Si > clean. Higher coverages of P, S and Cl further reduce the H₂ yield.

to shift to higher temperatures, with the increased yield coming mainly from the high temperature desorption peak, 470-490 K.

Low coverage sulfur on Pd(100) ($\theta_S < 0.25$ ML) decreased the yield of ethylene and only slightly increased the benzene yield. The desorption of hydrogen was decreased markedly for all S coverages, and the desorption spectra was very broad, from 435-610 K (see Fig. 7.11). The major change observed at higher S coverages was the decrease in ethylene yield. For example, at $\theta_S = 0.25$ ML, the ethylene yield was one-half that for the clean surface (see Fig. 7.9).

Chlorine was found to enhance the yield of both ethylene and benzene (see Fig. 7.8,9). The effect, however, was much smaller than that observed for either Si or P. For coverages of 0.3 ML of Cl, the yield of benzene was found to be 5 times higher than for the clean surface.

Section 7.9: Coverage Dependence of Additives

Coverage dependence of additives for the conversion of acetylene to benzene was studied on all three Pd surfaces. Fig. 7.12 shows the additive coverage for the formation of benzene on Pd(100). For coverages of S and Cl (>0.25 ML), the amount of benzene produced is decreased. Higher coverages of Si and P, up to 0.38 ML, increased the rate of benzene formation in this study.

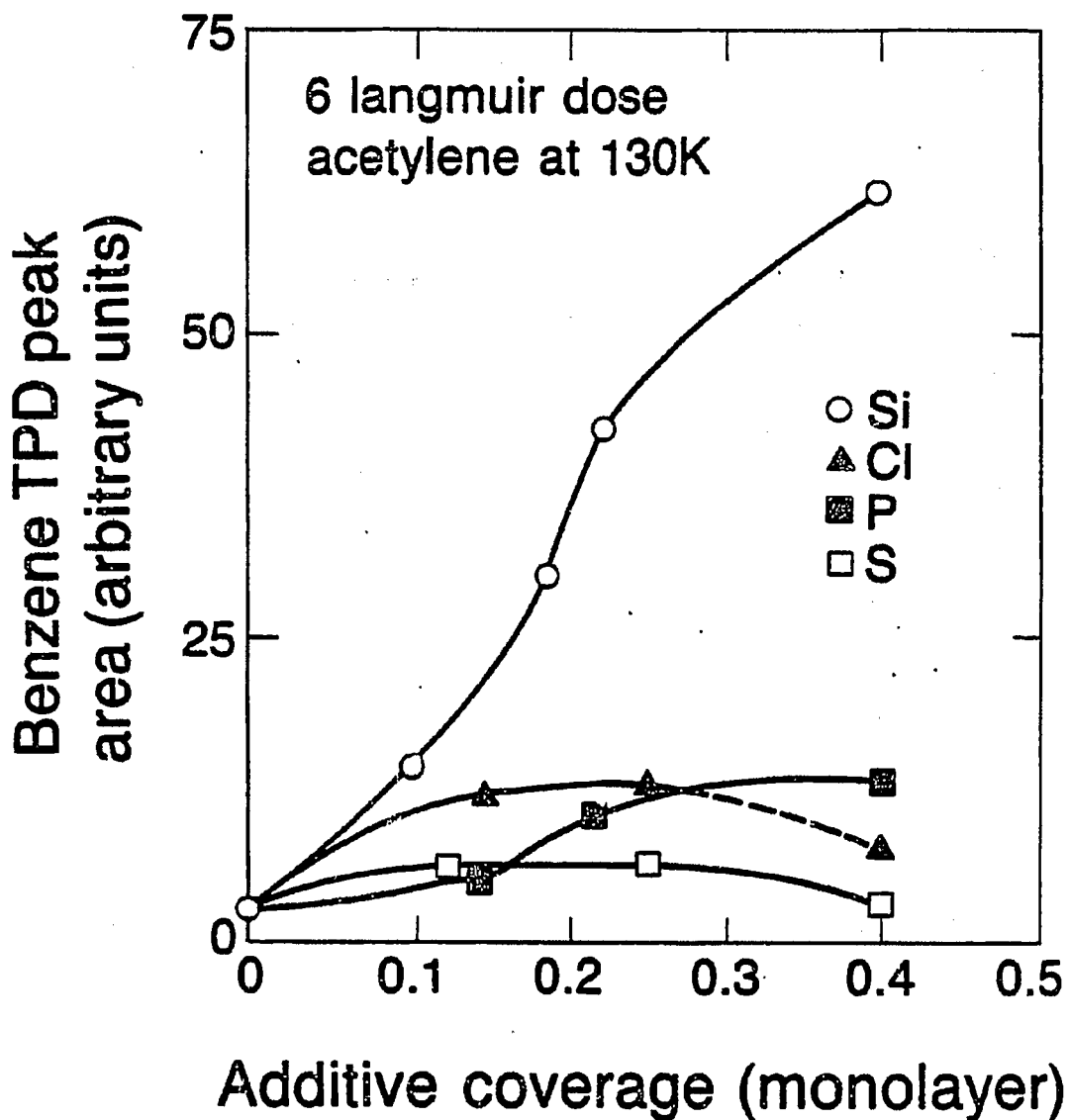


Fig. 7.12. The effect of varying the additive coverage at a constant exposure of acetylene, at 130 K, is shown. Electron-withdrawing additives, S and Cl, and electron-neutral P have similar overall effects on formation of benzene. Silicon, for coverages up to 0.38 ML, enhances the benzene yield in the high temperature peak. At 0.38 ML, the Si-doped surface increased the yield 20-fold over the clean surface.

Section 7.10: Conversion of Acetylene to Benzene at High Pressures

The cyclotrimerization of acetylene on three low Miller index planes of palladium ((111), (110) and (100)) was extensively studied at atmospheric pressures (200-1200 Torr). For all the temperature and pressure conditions used in this study, benzene was the only product detected. Due to the large acetylene peak in the gas chromatograms, trace ethylene could not be detected.

As also seen under UHV conditions, the reaction showed structure sensitivity for the formation of benzene (see Fig. 7.13) at atmospheric pressure. It was found that the (111) and the (100) surfaces were approximately equal in catalytic activity and the (100) surface was $\sim 1/4$ as active. The (111) and (100) surfaces had a turnover frequency (T.F. \equiv number of molecules produced/ metal atom \cdot sec, assuming 1×10^{15} metal atoms on the single crystal surface) of 0.014 molecules/site \cdot sec (200 Torr acetylene, 850 Torr N_2 or Ar at 570 K). No correction was made for the slight differences in metal surface atoms on the various faces. On the more active surfaces, the reaction had up to 50% conversion of acetylene to benzene or roughly a 20 mole percent yield of benzene. At these conversions, the reaction was limited by either surface poisoning or product concentration. The slope of the turnover frequency versus $1/T$ plot, assuming Arrhenius kinetics, yields the apparent activation energy of the reaction, calculated as 2 kcal/mol on all three surfaces (Fig. 7.14). Plotting the reaction rate as a function of acetylene pressure showed that the reaction was first order in acetylene, with the rate law (Fig. 7.15):

$$\text{Rate} = kP^{+1} C \equiv C \cdot$$

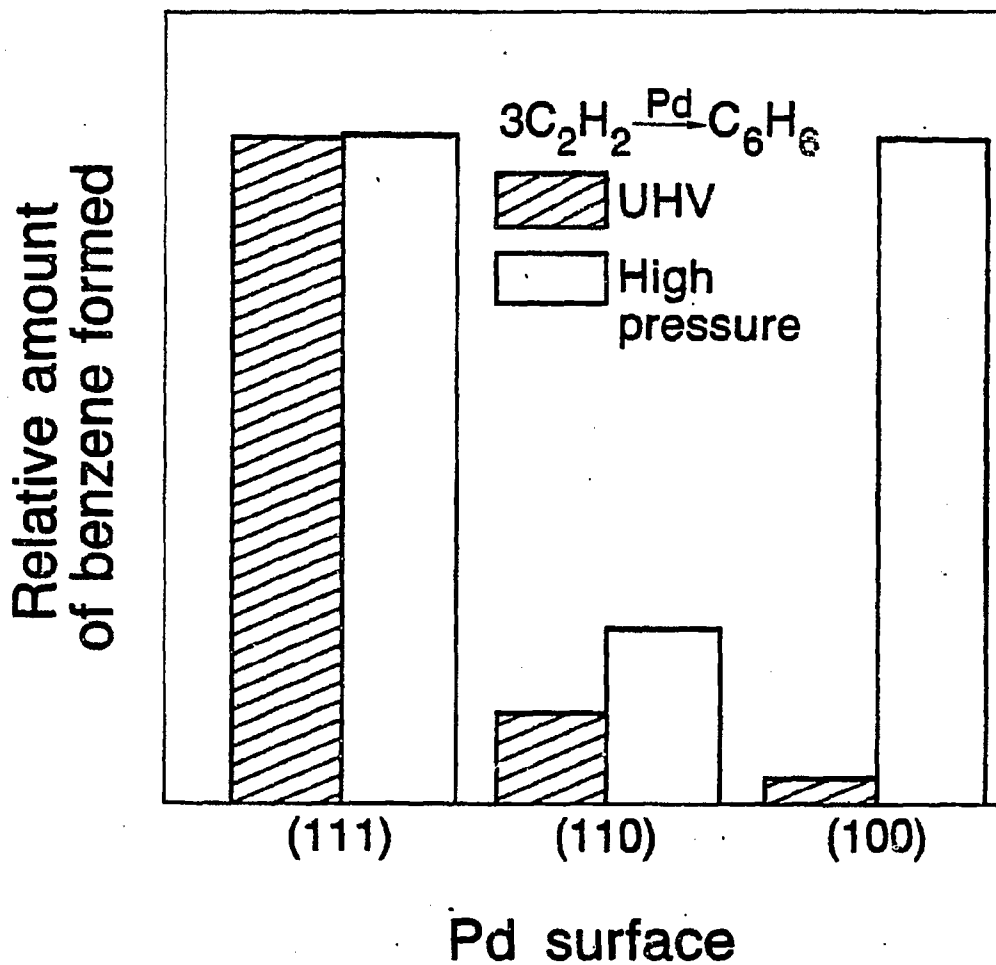


Fig. 7.13. The structure sensitivity for both atmospheric (high) and UHV studies for the conversion of acetylene to benzene over Pd(111), (110) and (100) surfaces is shown.

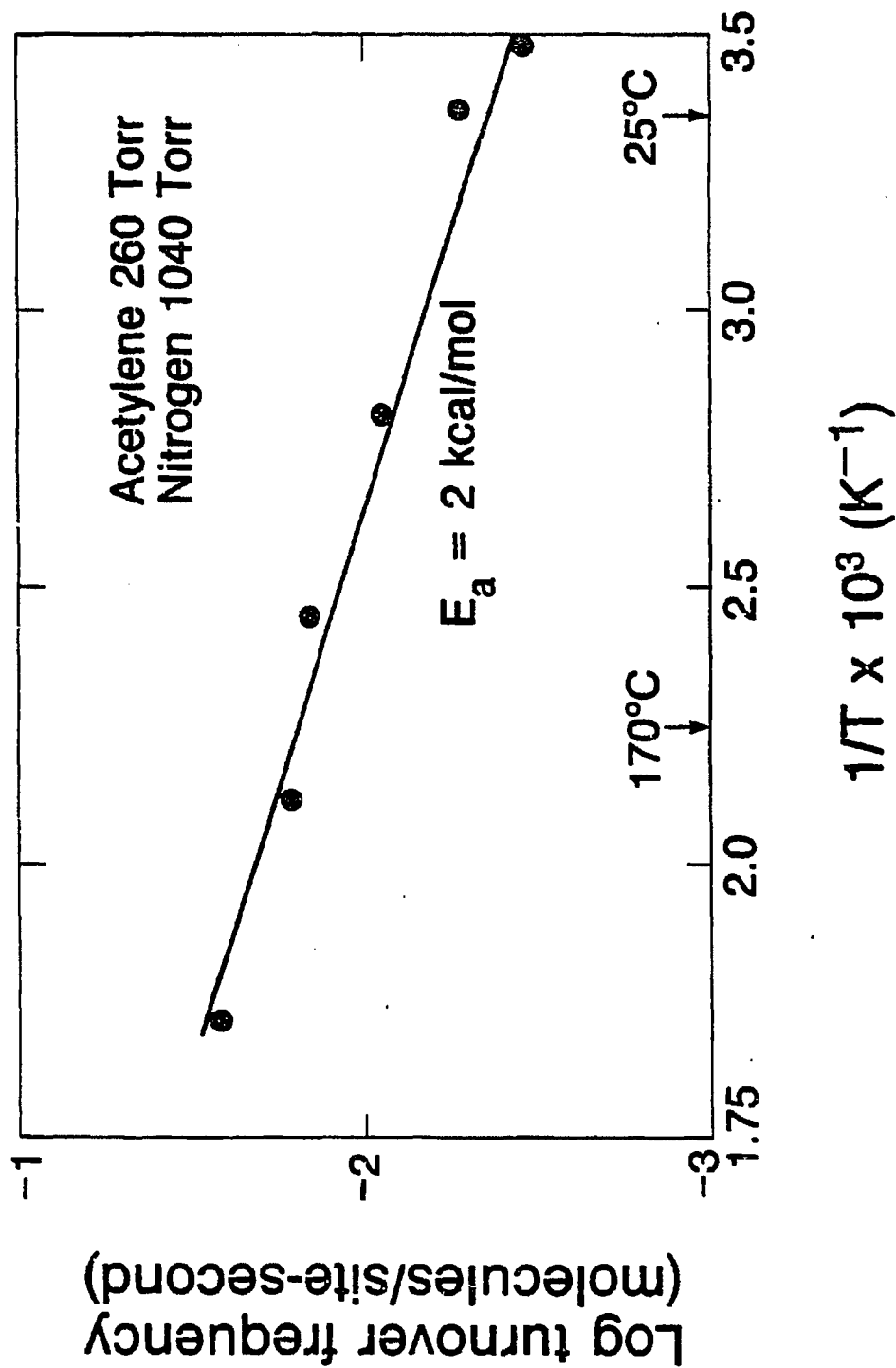


Fig. 7.14. The activation energy for the conversion of acetylene to benzene is determined by varying the reaction temperature at constant pressure.

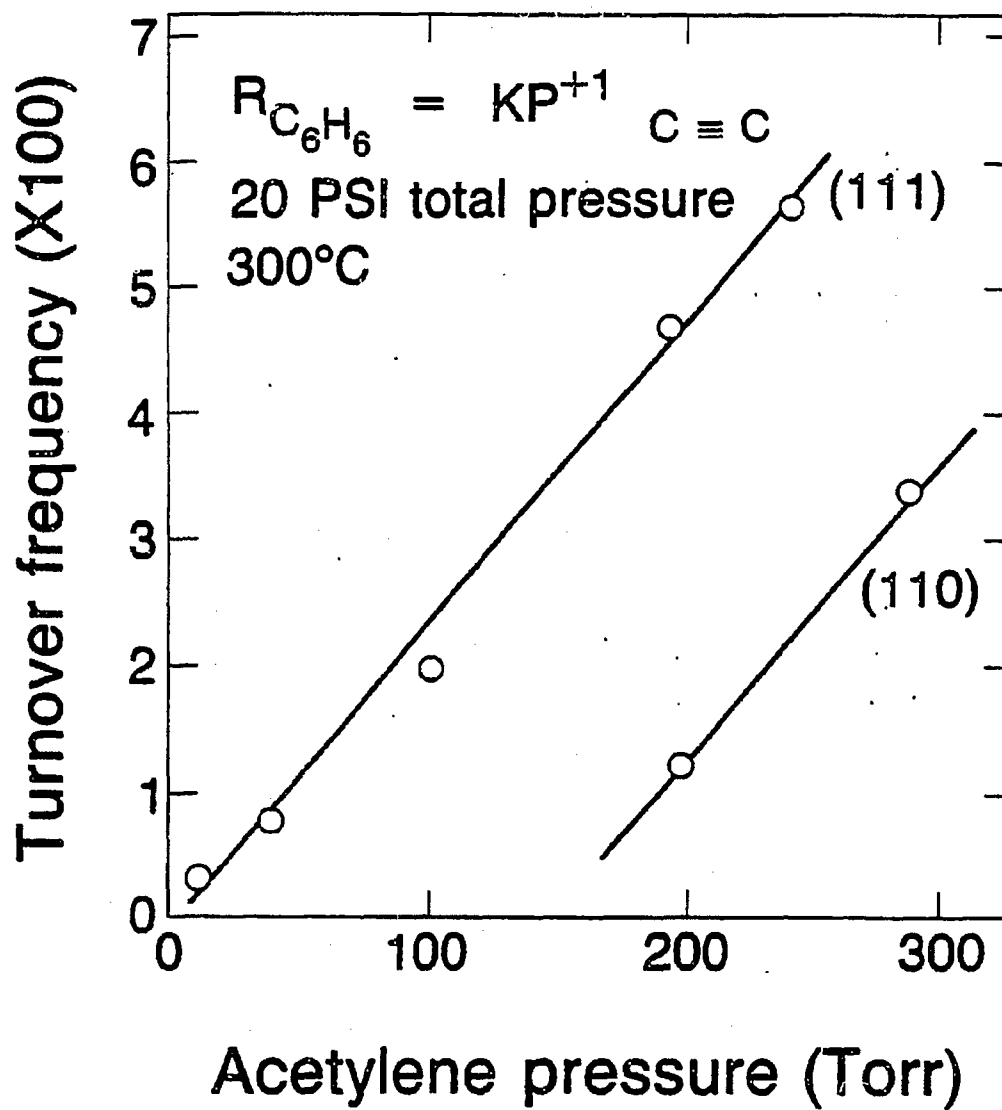


Fig. 7.15. The pressure dependence plot for the conversion of acetylene to benzene over Pd(111), (100) and (110) at high pressures. The plot is made by varying the partial pressure of acetylene at a constant total pressure and temperature.

Analysis by AES and CO titration after the reaction, found a partially carbon-covered surface. After heating the crystal to 650 K and exposing it to 1×10^{-6} Torr of H_2 , the surface remained carbon-covered, suggesting a stable graphitic overlayer. The CO titration technique determines the percentage of bare metal sites, as CO does not adsorb on carbon overlayers at low pressures. After the trimerization reaction (200 Torr acetylene, 850 Torr N_2 or Ar at 570 K for 3 h), it was found that 5-79% of the Pd(111) surface and 12-15% of the Pd(100) were composed of bare metal sites. The least active surface, Pd(110), contained less than 2% bare metal sites.

From TPD studies, it was determined that CO binds more tightly to the partially carbon covered metal than does $C \equiv C$. In order to determine if the reaction proceeded on the bare metal or carbonaceous overlayer, 200 Torr of CO was added into a room temperature reaction mixture 3 h after the start of the reaction. The reaction rate immediately decreased to ~ 0.00 T.F. Subsequent heating of the crystal to 485 K, which is above the desorption temperature of CO, restored the reaction rate to within 15% of its original value. This shows that the reaction proceeds on the bare palladium atoms. At lower reaction temperatures, the poisoning rate decreased.

Ethylene, as the reactant gas, instead of acetylene, produced small quantities of benzene (50 times less than did acetylene); and ethane, as the reactant gas, showed no activity for the formation of benzene. A mixture of methyl acetylene and acetylene produced only benzene.

Section 7.11: Effect of Adatoms on Cyclotrimerization at High Pressures: Introduction

High pressure catalytic studies were carried out over three Pd surfaces ((111), (100) and (110)) to determine the effect of adatoms on the cyclotrimerization of acetylene to form benzene. Reactions were, in general, carried out between 290 and 620 K at an acetylene pressure of 200 Torr. Reaction rates were calculated by assuming that each Pd surface atom was one reaction site, and no correction was made when adatoms were deposited on the surface. This leads us to report conservative values for the reaction rates. The products observed from all reactions were benzene and very small amounts of C₄ hydrocarbons. Small amounts of ethylene (<5% of the benzene formed) were not detectable by gas chromatography due to the large acetylene reactant gas peak tail.

Section 7.12: Effect of Adatoms on Cyclotrimerization at High Pressures: Pd(111) and Pd(100)

The initial rate of production of benzene over clean Pd(111) and Pd(100) at 570 K with 200 Torr of acetylene was found to be 0.05 molecules of benzene produced per Pd surface atom per second⁶. Potassium was observed to have the greatest positive effect on the rate of production of benzene over Pd(111) (see Fig. 7.16). With ~ 0.25 ML of K (200 Torr acetylene, 850 Torr N₂ at 570 K) the rate doubled to 0.10 molecule/site · sec. When K was present on the surface, less graphitic carbon appeared in AES (due to the decomposition reaction) and the rate of poisoning of the reaction was reduced, relative to reaction over the clean surface. The activation energy and pressure dependence for benzene formation on additive-covered surfaces did not appear to change from the values obtained on clean surfaces, being constant at ~ 2.1 kcal/mol and $\text{Rate}_{\text{C}_6\text{H}_6} = kP_{\text{C}}^{+1}$. Silicon also had a positive effect on the reaction rate of benzene formation. For example, at a coverage of ~ 0.33 ML the rate was increased by 35%. Similarly, relative to the reaction over clean Pd(111), the amount of graphitic carbon deposition was reduced with Si present on the surface.

Phosphorus had a negative effect on the reaction rate. The reaction rate decreased with coverage of P (see Fig. 7.16). For example, at $\theta_{\text{P}} = 0.33$ ML, the rate of production of benzene was reduced by 37%. With P present, the graphitic carbon deposition rate and the poisoning rate were similar to that found over clean Pd(111).

Sulfur and chlorine had a large negative effect on the reaction rate. For coverages of greater than 0.20 ML, no benzene production could be detected. Reactions on chlorinated surfaces were carried out at room

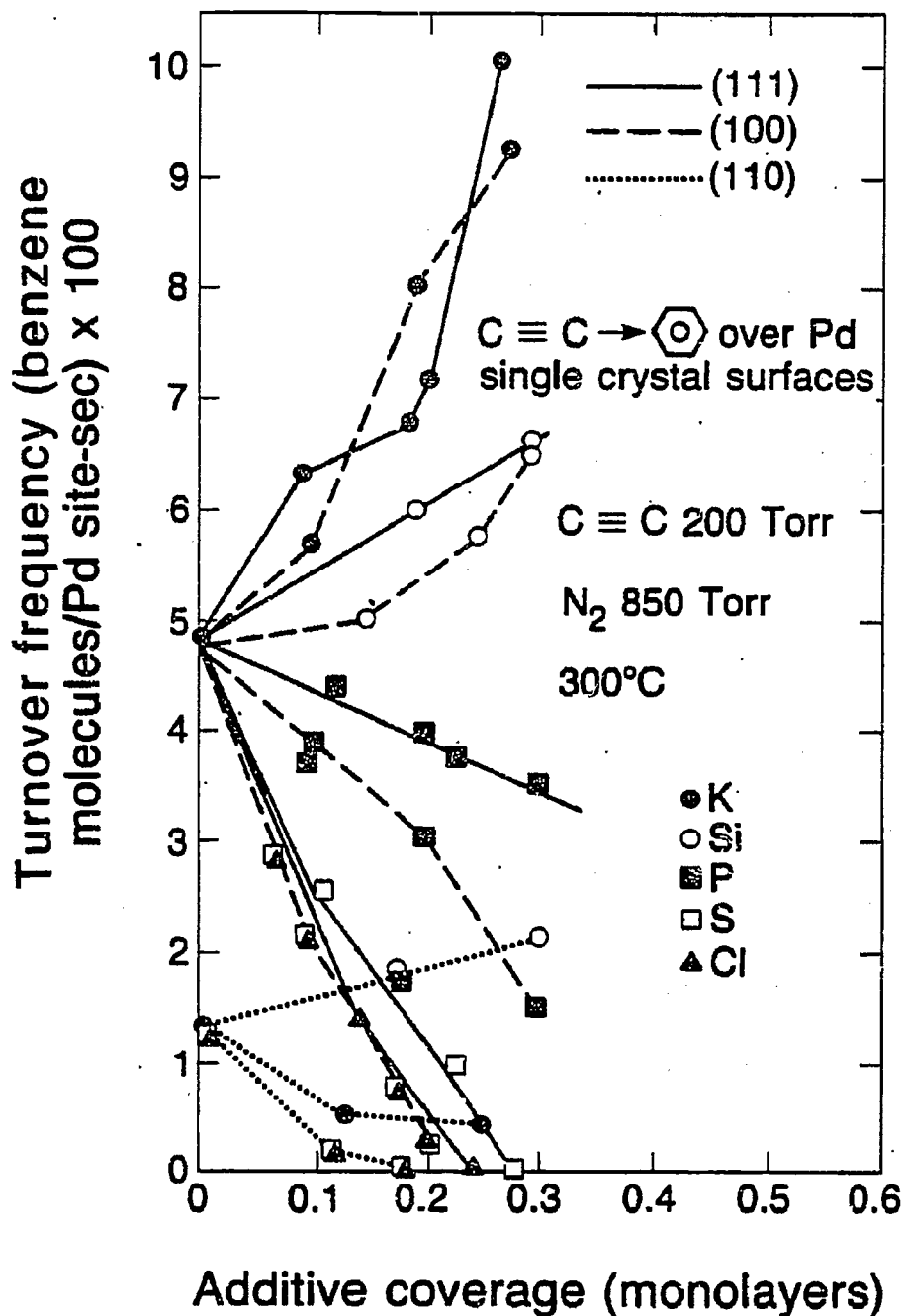


Fig. 7.16. The effect of additives at different coverages over Pd(111), Pd(100) and Pd(110) on the rate of benzene formation at high pressures (200 Torr acetylene, 850 Torr N₂ and 300 K) is shown. Pd(111) and Pd(100) appear to be affected similarly by the different additives. Potassium and Si enhance the rate of benzene formation, while P, S and Cl decrease the rate of benzene formation. On Pd(110), S and P increase the rate, while addition of K, S and Cl decrease the rate.

temperature, due to the low desorption temperature of chlorine from Pd surfaces. The rate of formation of benzene from chlorinated surfaces was very low, even for coverages as low as 0.1 ML, and for coverages over ~ 0.2 ML, no benzene formation was observed.

Section 7.13: Effect of Adatoms on Cyclotrimerization at High Pressures: Pd(110)

The rate of formation of benzene over clean Pd(110) was found to be $\sim 1/5$ that of Pd(111) for the same reaction conditions. Additives had less effect over the (110) surface. In contrast with K-doping of the (100) and (111) surfaces, adsorption of K on the (110) surface decreased the rate of benzene formation (see Fig. 7.16).

Silicon and phosphorus both enhanced the rate of benzene formation to the same extent. As on Pd(111) and Pd(100), sulfur and chlorine depressed the rate of benzene formation on the Pd(110) surface. It was also noted that the rate of poisoning was increased, at comparable coverages, as adatoms were changed from K to Cl.

Section 7.14: Discussion of UHV and High Pressure Studies on Clean Pd Single Crystal Surfaces: Introduction

The cyclotrimerization reaction of acetylene over clean Pd catalysts to form benzene proceeds readily in pressures ranging from 1×10^{-12} –1 atm and on a variety of surfaces (single crystals, films and supported on alumina). The reaction is structure-sensitive at both low and high pressures. In UHV the stoichiometric reaction over the (111) face is the most active. The (110) face is one-fourth as active, and the (100) is one-twentieth as active. At high pressures, the (111) and (100) surfaces show similar catalytic rates and the (110) face is four times less active (see Fig. 7.16).

The high activity at low pressures over Pd(111) has been attributed to a template effect¹, in which three acetylene molecules are oriented, in the six-fold symmetry of the Pd(111) surface in the Kekule benzene structure.

In addition to the cyclotrimerization reaction, hydrogenation, reversible molecular desorption and decomposition reactions are also detected³¹ at all pressures. At high pressures the reaction has an apparent activation energy of 2 kcal/mol and is first order in acetylene pressure (Rate = kP_C^{+1} \equiv C).

Section 7.15: Discussion of UHV and High Pressure Studies on Clean Pd Single Crystal Surfaces

In UHV, benzene desorbs with two maxima at 250 and 450 K, on the Pd(111) when formed from acetylene. When the surface was dosed with benzene, there were desorption maxima at the same temperatures, suggesting that benzene formation is desorption rate-limited rather than formation rate-limited. Similar thermal desorption traces of H₂ from the C \equiv C and C₆H₆ doses further substantiate this proposition. In both cases, hydrogen desorbs in a broad high temperature peak centered around 450-540 K. These similarities between benzene desorption traces exist on the other two surfaces (see Table 7.2). The low and high temperature maxima in the benzene desorption show that benzene forms readily and also that some benzene formed decomposes on the metal surface.

Using Redhead's method⁵⁵ of calculating activation energies (E_A) for UHV reactions from desorption maxima, the activation energies for benzene formation are 15 and 30 kcal/mol for the low (260 K) and high (520 K) temperature peaks, respectively, on the (111) surface. Contrasting these values with those from high pressure studies, shows large differences in E_A . At high pressure the trimerization reaction has an E_A of 2 kcal/mol. For a high pressure reaction this is an extremely low value. For comparison, the formation of methane from CO and H₂, a facile reaction on Fe, has an E_A of 24 kcal/mol and hydrogen exchange on Pt has 8 kcal/mol activation energy^{40,56}. This low energy could suggest formation of benzene on an overlayer of ethylidyne or other carbonaceous fragments, onto which it would be loosely bound.

From CO titrations, it can be seen that the reaction rate is dependent on the number of metal sites available. As mentioned previously, on the

Table 7.2. Relative catalytic rates, according to open active sites.

Crystal Face	Turnover Frequency ^a	Percentage of Open Sites	Catalytic Rates
(111)	0.048	7	0.96-0.68
(100)	0.048	12-15	0.40-0.32
(110)	0.014	~ 2	0.7

^aunits of molecules/site • sec

(111) and (100) surfaces, approximately 5-7% and 12-15%, respectively, of the surface was bare after 1 h of reaction and on the least active (110) surface only 1-4% of the surface was bare. The differences in bare metal sites on the (111) and (100) surfaces which have similar turnover frequencies are most likely due to different poisoning rates. Also, when CO was added to the room temperature reaction 3 h after the start of the reaction, the rate decreased to almost zero. Subsequent heating to 485 K, which is above the desorption of CO, restored the rate to within 15% of its original value. Carbon monoxide binds only to the metal surface and since it binds more strongly than acetylene, it displaces acetylene. The CO titrations, CO poisoning experiments and structure sensitivity show that the bare metal atom is the active site for the reacting at high pressure.

The (110) surface, the least active face, is the roughest surface and leads to the highest decomposition rate of both acetylene and benzene as seen by the low percentage of bare Pd atoms. Therefore, the amount of irreversibly-bound carbon in the catalytic steady state reaction limits the rate by blocking sites.

If the percent of open or active surface sites is taken into account, the reaction still exhibits structure sensitivity (see Table 7.2). The (111) surface is still the most active, followed by the (110) and then the (100) face. This is the same activity ordering as seen in UHV. The relative values of the activity differ; however, this may be due to the inability to determine perfectly the percentage of open sites with CO titrations.

The product distribution at low and high pressure are different. In UHV, in addition to benzene formation, approximately 20% as much ethylene

forms. At high pressure on single crystals, less than 5% ethylene forms, which is the detection limit of our gas chromatograph. Hydrogen could not be detected at high pressures.

The low activation energy for this reaction can be explained by incorporating an adsorption equilibrium constant into the rate law. The apparent activation energy, which is determined from the slope of the $\ln(K_{\text{exp}})$ versus $1/T$ plot, then equals the combination of the surface process activation energy and the heat of chemisorption. We were unable to extend the experimental parameters to regions of high acetylene coverage to test this hypothesis.

The most difficult question to address is that of possible mechanisms for the cyclotrimerization reaction. It is possible that at high and low pressures two or more mechanisms exist. Since benzene is detected in all pressure regions investigated, there may be a gradual transition from one path to another.

There are a few possible mechanisms which could occur on the surface. One scheme involves the concerted reaction of three acetylene molecules simultaneously joining^{11,31}. Another mechanism involves formation of a cyclobutadiene ring on the surface, which is bound roughly parallel to the surface¹¹. This ring would not be tightly bound to the surface, since no C_4 products were detected either at low or high pressure, thus this type of mechanism seems improbable. This type of mechanism has been ruled out in the homogeneously catalyzed reaction^{10,12}. The third mechanistic scheme involves a metallacyclopentadiene as an intermediate¹². In organometallic chemistry, numerous studies have investigated possible schemes for [2+2+2] cycloadditions¹². Spectroscopic evidence (NMR, IR) suggest that two acetylenes sequentially displace two ligands to form a

metallacyclopentadiene intermediate. This is followed by the insertion of another acetylene to form a metallacycloheptane or a Diels-Alder type addition to form benzene. The first portion of the scheme has been proven, but the addition of the final acetylene is very rapid and the pathway has not been determined.

Analysis of product distribution and yields did not give enough information to propose a mechanism. Current electron energy loss spectroscopy studies will shed some light on this intriguing problem.

Section 7.16: Discussion of UHV and High Pressure Studies on Promoted Pd Single Crystal Catalysts: Introduction

The cyclotrimerization of acetylene has been observed over promoted (111), (100) and (110) single crystal surfaces of palladium at both high and low pressures. The difference in benzene yield at low pressures, relative to the rate of production of benzene at high pressures, was quite dramatic over the different promoted surfaces. Potassium was found to eliminate virtually all benzene formation at low pressures, whereas at high pressures, it was found to be the best promoter studied for the formation of benzene. Sulfur and chlorine, on the other hand, slightly enhanced the low pressure formation of benzene, while at higher pressures, even very low coverages (<0.1 ML) of S or Cl poisoned the reaction, and above ~ 0.25 ML, no benzene formation was observed.

The effects of the different additives will be discussed in terms of steric and electronic interactions with surfaces and the cyclotrimerization of acetylene. Also, the high pressure catalytic results will be compared and contrasted to the low pressure stoichiometric results.

Section 7.17: Discussion of UHV and High Pressure Studies on Promoted Pd Single Crystal Catalysts: Adatom Properties

To facilitate understanding of the results presented in this study, some of the important properties of the adatoms are considered first.

The four adatoms (Si, P, S and Cl) decrease slightly in atomic radius^{35a} (see Table 7.3) with increasing atomic number, from 1.32 Å for Si to 0.90 Å for Cl. The atomic radius of Cl, however, ranges from 0.90 Å for the neutral Cl atom to 1.80 Å for Cl⁻. The ionic radius of K is 1.33 Å. Palladium is slightly larger, with an atomic radius of 1.38 Å. Although structural data is not available for these adatoms on Pd surfaces, there is some structural data for S and Cl on Ni(111) and Pt(111)²⁵. These studies show adatoms to reside generally in threefold hollow sites. Therefore we expected that Si, P, S and Cl would also chemisorb in the threefold sites of the close-packed Pd(111) surface. Due to insufficient data for the Pd(100) and Pd(110) surfaces, no conclusions can be drawn on the nature of the binding sites for the adatoms, but it is known that S on Ni(100) resides in the highest coordination site³⁰.

Electronegativity is another empirical parameter that differs significantly for the adatoms used in this study. To observe how the surface electronegativity changes with the addition of different adatoms to the surface, we performed work function measurements on Pd(100) (see Fig. 17). The change in work function varies linearly with the coverage of each additive. The decrease in work function is greatest for K, indicating that it donates the most electron density to the surface per unit coverage, followed by Si and then P. Conversely, S increases the work function, implying that it withdraws electron density from the surface.

Table 7.1. Pauling electronegativity^{35a} and atomic radius^{35a} of each adatom, palladium and hydrogen.

Element	Pauling Electronegativity	Atomic Radius (Å)
H	2.1	0.37
K	0.8	1.33 ^a
Si	1.8	1.32
P	2.1	1.28
S	2.5	1.27
Cl	3.0	0.90
Pd	2.2	1.37

^aionic radius

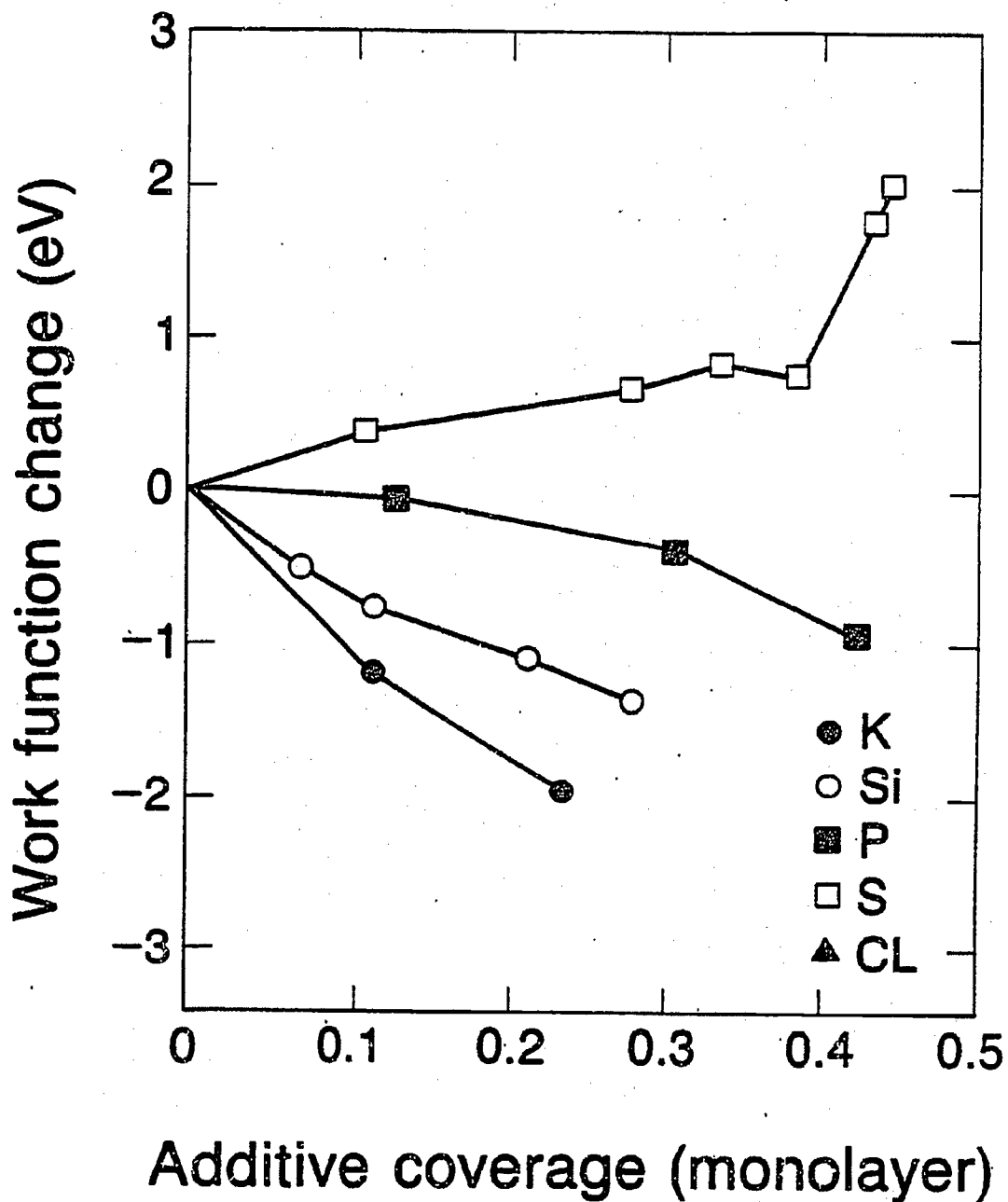


Fig. 7.17. The change in work function, $\Delta\phi$, is plotted vs. the coverage of different adatoms on Pd(100). Sulfur withdraws electron density from the surface, $\Delta\phi \sim 1$ eV at 0.33 ML of S, whereas P, Si and K donate electron density to the surface, $\Delta\phi \sim -1.5$ eV at 0.25 ML of Si.

While the atomic radii of the adatoms vary only slightly, there is a large difference in electronegativity (see Table 7.3) for the additives. Therefore we expect that electronic interactions will have the greatest influence on the surface chemistry. The work function changes observed in our study fit with the electronegativity data very well and will be used to explain the results of the cyclotrimerization reaction studies.

Adatoms on all metal surfaces, under conditions of low pressure, have several effects on surface reactions - the additives can (1) donate or withdraw electron density from the surface, (2) form islands on the surface, (3) form surface compounds and (4) block certain reaction pathways. Studies have found K to be uniformly dispersed on metal surfaces^{32,33} (except at higher monolayer coverages), and to donate electrons to the surface¹⁹. Sulfur and chlorine are known to form ordered islands at low coverages³⁰ and withdraw electron density from the surface³⁴. From our work function measurements, we found P and Si to be electron donors, but not to the same extent as K (see Fig. 18). Phosphorus and silicon were found to form ordered LEED structures over some metal surfaces. For example, K forms a $\sqrt{7} \times \sqrt{7} R17^\circ$ over Pd(111). Also, structures have been observed over C_g and Si³⁰. Phosphorus and silicon are known to form stable compounds with many metals (Pd₂Si, PdSi, Ni₂Si, Ni₂P and Ni₅P₂)^{35a,b,36}.

Both acetylene and benzene are known³⁷⁻³⁹ to donate electrons to metal surfaces. Acetylene has a low-lying antibonding orbital which is partially filled in the presence of electron donors on the metal surface, such as K³⁸, destabilizing the carbon-carbon bond. Benzene's antibonding orbitals have lower binding energy and thus are not filled even in the presence of K, as evidenced by the TPD and EELS work of this group^{40,41}.

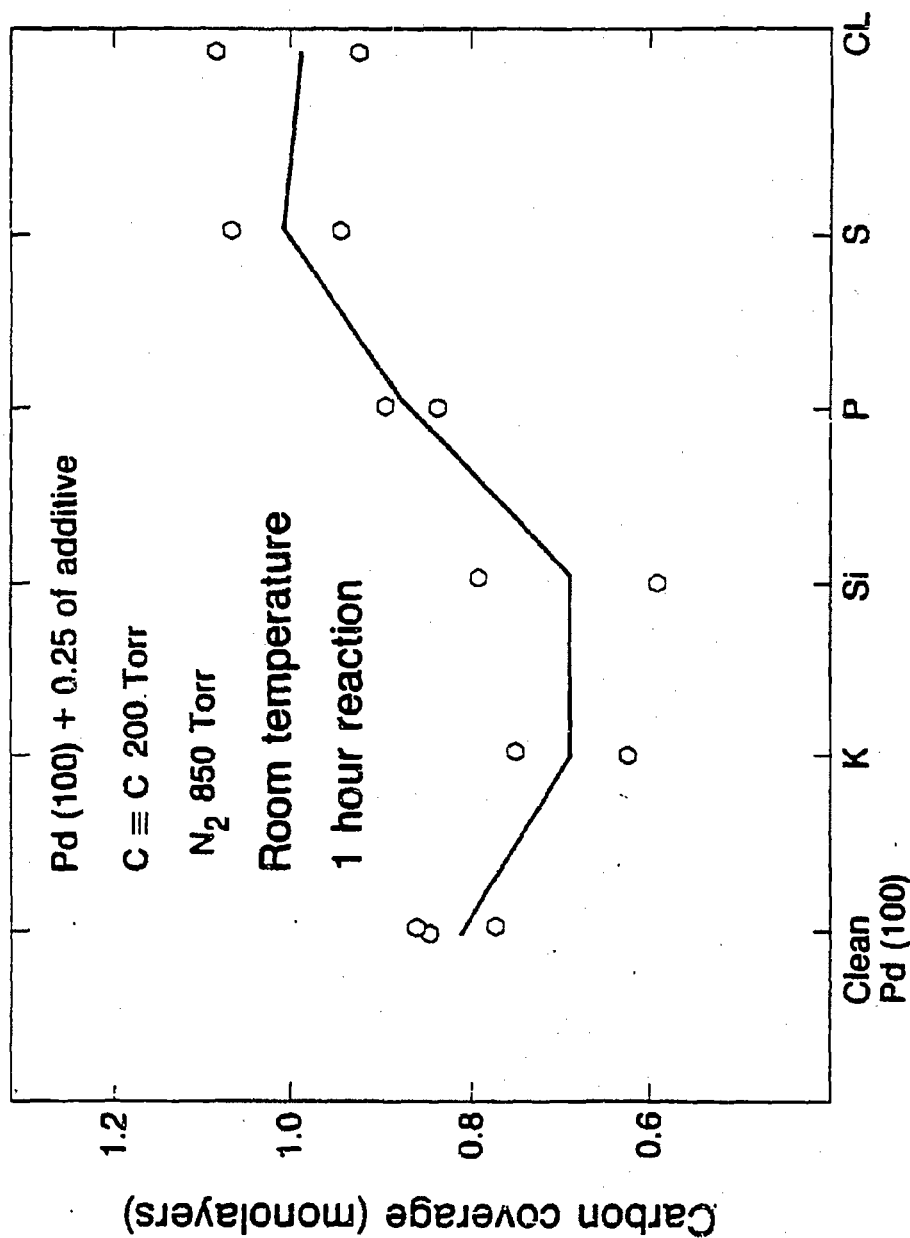


Fig. 7.18. The effect of additives on Pd(100) on final carbon coverage. Electron-donating additives (K, Si) appear to keep the palladium surface cleaner than starting with an initially clean Pd surface. Electron-withdrawing additives on Pd(100) have higher carbon levels and faster rates of poisoning relative to clean Pd(100).

From the theoretical work of Anderson^{37,38} on Ni, Pt and Ag surfaces, S and Cl would be expected to poison the surface toward acetylene chemisorption. No other work has been completed on the effects of Si and P on the bonding of acetylene and benzene to metal surfaces, so no comparisons can be made at this time.

Section 7.18: Discussion of High Pressure Studies on Promoted Pd Single Crystal Catalysts: Introduction

The effect of promoters at atmospheric pressures on the reaction of acetylene over single crystals of palladium has been investigated. We have previously published⁶ the rate (Turnover frequency=0.05 molecules benzene/site • sec, 200 Torr acetylene, 850 Torr N₂, 570 K on Pd(111)), pressure dependence (rate of benzene= $kP_C \cong C^{+1}$) and activation energy ($E_A \cong 2$ kcal/mol) for the formation of benzene from acetylene over Pd single crystals. In these earlier studies, we found Pd(111) and Pd(100) surfaces to have the same rate of benzene production, but on the Pd(110) surface the rate was about 25% of the rate on the (111) and (100) surfaces.

Section 7.19: Discussion of High Pressure Studies on Promoted Pd Single Crystal Catalysts: Pd(111) and Pd(100)

The additives investigated had the same effect on each of these two surfaces. Electron-donating additives were observed to enhance the rate of formation of benzene. As can be seen from Fig. 7.16, the electron-donating additives, K and Si, had a large positive effect on the rate of formation of benzene. Electron-withdrawing additives decreased the rate of production of benzene and increased the amount of carbon present on the surface after each reaction. We found that the activation energy and pressure dependence for the formation of benzene did not change, from the clean surface values, for all the modified surfaces studied.

The difference in rate of benzene formation for the different modified surfaces may be caused by the amount of open Pd surface area. The surface formed an equilibrium amount of carbon, which appeared to block reaction sites. This surface carbon could be in the form of graphite or a polymer of acetylene. It is possible that the electron-withdrawing additives enhance the polymerization process, by acidifying the metal surface⁵¹, thereby decreasing the rate of benzene formation. Figure 7.18 shows the amount of carbon present on the (100) surface after flashing the modified surface to 520 K in UHV. Electron-donating additives appear to keep the surface cleaner, and the rate of poisoning for surfaces modified with electron-donating additives was much slower than for the surfaces modified with electron-withdrawing additives.

Phosphorus did not fit the trend of electron donors acting to enhance the rate of benzene formation. It appears to have slightly more carbon at equilibrium than the clean Pd(100) surface, so the electron-donating power of P is not enough to stop either polymerization or decomposition.

Section 7.20: Discussion of High Pressure Studies on Promoted Pd Single Crystal Catalysts: Pd(110)

The clean Pd(110) surface was shown to have only ~ 2% open surface at equilibrium, which was used to explain the diminished rate of benzene production. The (110) surface of fcc metals can be thought of as a monotonically-stepped surface. This high density of steps is expected to be more reactive towards decomposition of acetylene. High carbon coverages on the surface under reaction conditions are therefore expected.

Additives on Pd(110) had less effect on the rate of formation of benzene than on Pd(111) and Pd(100). Potassium was found to inhibit the reaction rate and P enhanced the rate as much as Si. One explanation for K decreasing the rate of formation of benzene is that K on Pd plus acetylene induces faceting on the surface. Alkali metals are known to induce a 2 X 1 reconstruction in Ag(110) surfaces^{43,44}. If K or K + acetylene, induces a reconstruction in Pd(110) then K would be expected to sit in a deeper trough and therefore have less effect on the surface reaction, possibly just acting to block reaction sites.

Section 7.21: Discussion of UHV Studies on Promoted Pd Single Crystal Catalysts: Pd(100), Pd(111) and Pd(110)

Low pressure results for additive-covered surfaces can be explained by a combination of surface structure and electronic interactions. Potassium-covered Pd surfaces produced less benzene and less decomposition products than Si-, P-, S- and Cl-covered surfaces. Potassium is the least likely of the additives studied to form islands on the surface. At low coverages, K is known to be disordered on metal surfaces and only at coverages approaching saturation does a LEED pattern form³⁰. If the adsorbate interaction is short range, then well-dispersed adatoms will produce a greater overall effect than adatoms with a clustering tendency. Less metal sites would be covered by additives such as Si, P, S and Cl, which form islands on compounds on the surface. This would help explain our results, since acetylene was not found to chemisorb to multilayers on K, due possibly to K atoms blocking sites. With dispersed K on the surface, three acetylene molecules would be less likely to be close enough together on the surface to form benzene. Our results seem to indicate that the electronic effect, as correlated to the change in work function, is not the major promoter function for K under UHV.

Ultra-high vacuum studies are summarized in Fig. 7.19, which shows the effect of each additive on the benzene yield on each surface, at a coverage of 0.25 ML. The most pronounced effect observed was that of Si on Pd(100), where at a coverage of 0.38 ML, the yield of benzene increased twenty-fold.

Significant effects on the formation of benzene from acetylene were observed from Si on Pd(100) surface and P on the Pd(111) surface. The greatly increased benzene formation over these two surfaces may be attributed

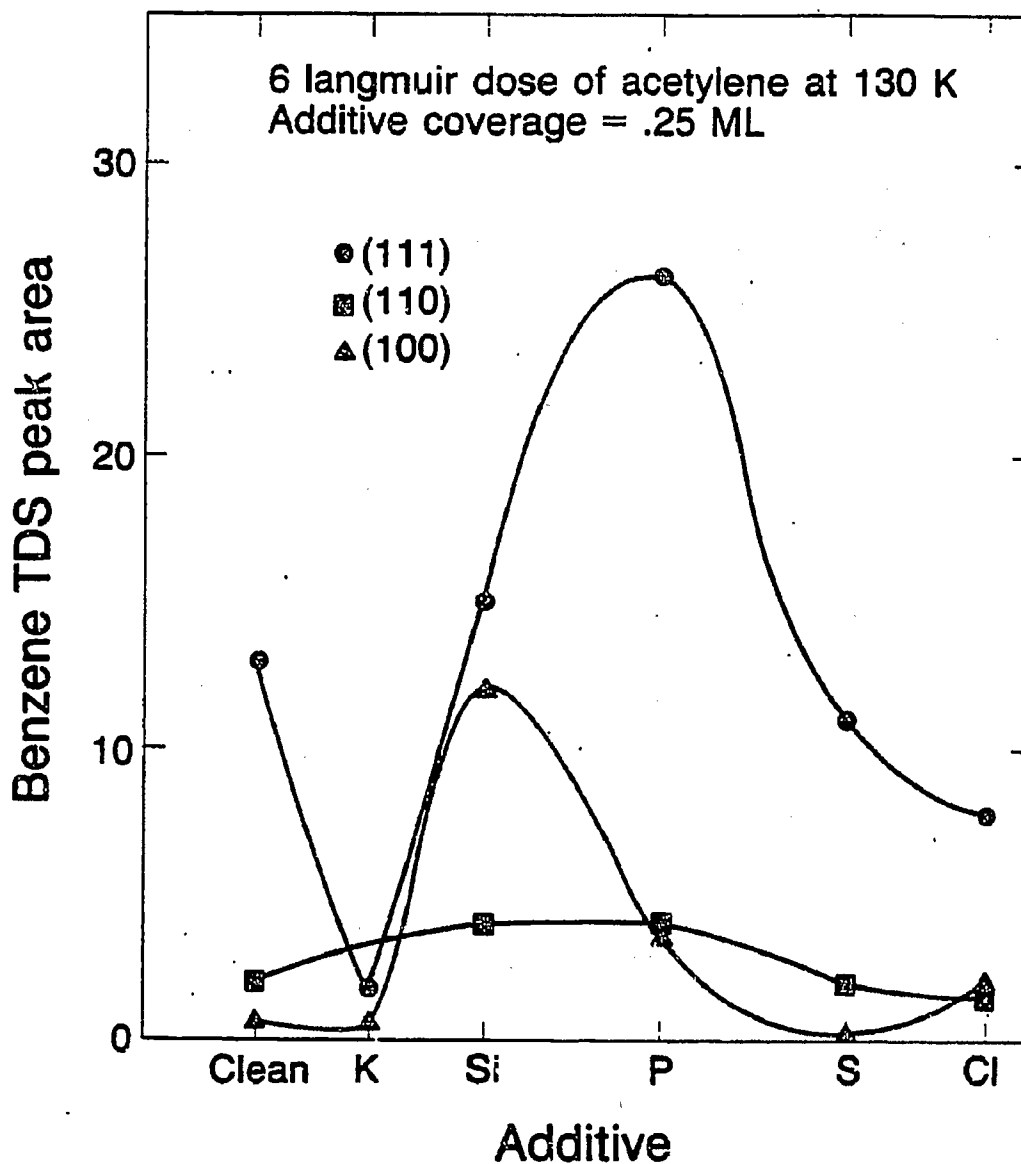


Fig. 7.19. The effect on the rate of benzene formation by additives at constant 0.25 ML coverages on different Pd single crystal surfaces is displayed. Benzene TPD spectra were recorded after a 6L dose of acetylene at 130 K. Phosphorus on Pd(111) and Si on Pd(100) have the greatest enhancement on benzene formation.

to the formation of surface compounds. The PdSi compound is known to be stable³⁵, and although no palladium phosphides are known, they are well known for nickel³⁵ (Ni_2P , melting point of 1385 K; and Ni_5P_2 , melting point of 1458 K). Figure 7.20 shows evidence for the formation of a surface palladium silicide. As the temperature of the Si-covered Pd(100) surface is raised, the work function shifts dramatically, indicating a reversal of dipole moments. This shift corresponds to Si dissolution, as also shown by the slight change of the AES Si signal (no Si desorption was observed). This work function shift has been shown to indicate surface compound formation^{26,45-51}.

Phosphorus on Pd(111) was found to have similar changes in the work function, showing a change upon annealing the crystal. These changes were not observed for any of the other additives on any other Pd surface. In general, the work function versus coverage plot was reversible with annealing/flashing of the crystal to desorb some of the additive. Future work is planned to test the hypothesis of surface compound formation with Si and P on Pd(111) and (100).

Sulfur on Pd suppressed the decomposition reaction. Relative to the three clean surfaces, only ~5-10% as much H_2 and ethylene were observed (see Figs. 7.11) in the TPD experiment. As noted previously, Anderson and coworkers^{37,38} predicted electron-withdrawing additives would block most acetylene adsorption and weaken the acetylene-metal bond. The weakened acetylene-Pd surface bond can account for the large decrease in decomposition observed. Benzene formation remained approximately unchanged and molecular desorption was enhanced somewhat (see Fig. 7.2,4,9). It appears that S selectively blocks hydrogenation, as has been seen previously for S on Mo in the hydrogenation of CO (see Chapter 5), as well as dehydrogenation reactions.^{14,52}

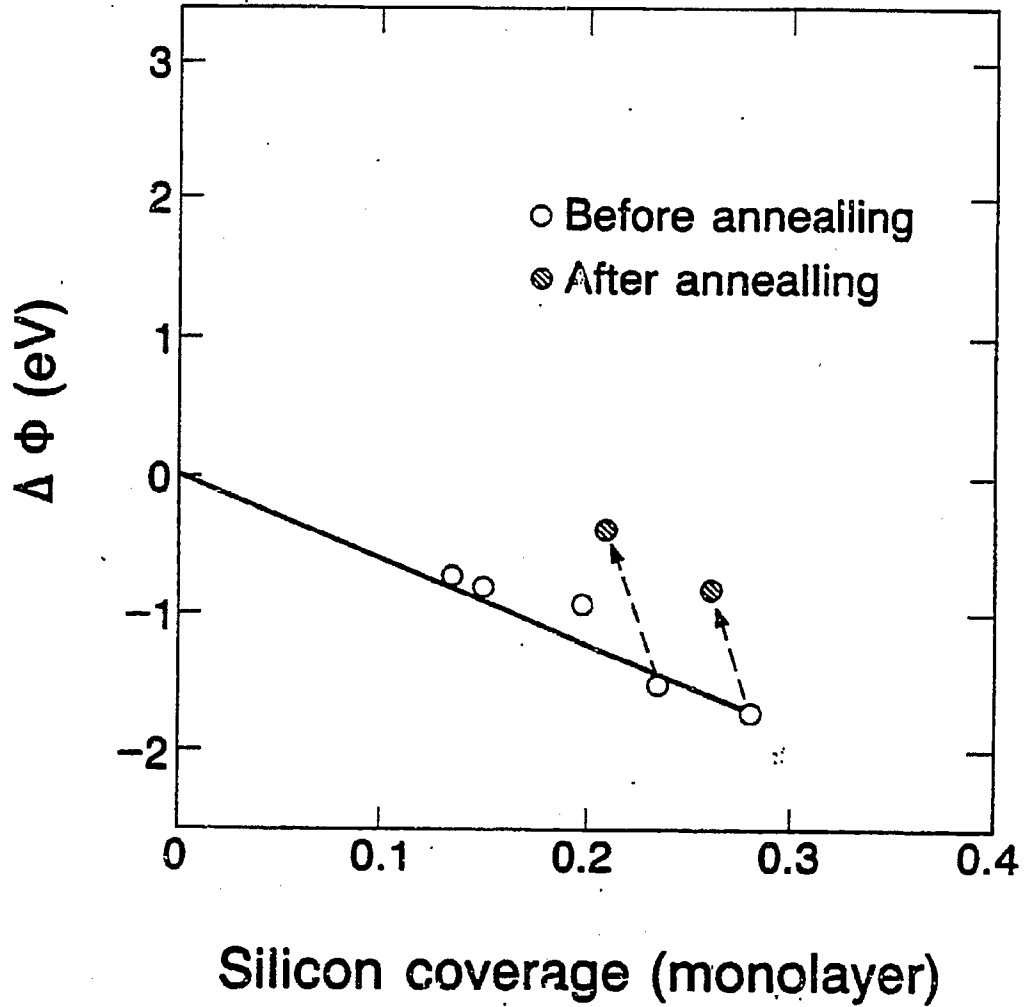


Fig. 7.20. The effect of annealing the Si-covered Pd(100) surface is displayed. Upon annealing at 700 K for 3 min., the work function shifts 0.75 - 1.25 eV, while the Si surfaces coverage remains almost constant (as measured by AES).

Chlorine also reduced the amount of acetylene decomposition, but not to the same extent as does S. Molecular desorption of acetylene was enhanced. Benzene formation was enhanced slightly on Pd(100) while it declined slightly on Pd(111) and Pd(110). Chlorine should act very much like S, because additives withdraw electron density from the surface and become enlarged as electron density is removed from the metal. Both Cl and S are known to form ordered structures at low coverages, indicating island formation. It is interesting that for similar coverages of S and Cl 2-10 times more hydrogen was formed on the chlorinated surfaces. In general, the trend from K → Si → P → S → Cl seems to indicate that increasingly electron-withdrawing additives lead to decreasing decomposition, but the most electron-withdrawing additive, Cl, breaks this trend.

The site blocking contribution to the surface reaction appears to be greatest for K and decreases as the additive atoms become more electronegative. The electron interactions increase as the additives become more electronegative.

Section 7.22: Comparison of Results of UHV and High Pressure Studies on Promoted Pd Single Crystal Surfaces

Our results for additive effects on the conversion of acetylene to benzene are quite different at high and low pressures. The high pressure catalytic results appear to depend on the amount of bare palladium exposed. At high pressures, the surface is saturated with acetylene and the formation of benzene competes with the decomposition and polymerization reactions which poison catalytic sites. Additives which keep the surface cleaner, such as K and Si, enhance the rate of benzene formation; but, S and Cl appear to enhance to polymerization or decomposition reactions, poisoning the catalytically active sites. The low pressure stoichiometric results correlate with site-blocking for electropositive additives and shifting to more of an electronic interaction for electronegative additives.

Section 7.23: References

1. Tysoe, W.T., Nyberg, G.L., and Lambert, R.M., *J. Chem. Soc. Chem. Commun.*, 623 (1983).
2. Tysoe, W.T., Nyberg, G.L., and Lambert, R.M., *Surf. Sci.* 135, 128 (1983).
3. Gentle, T.M., and Muettterties, E.L., *J. Phys. Chem.* 87, 2469 (1983).
4. Sesselmann, W., Woratschek, B., Ertl, G., and Kuppers, J., *Surf. Sci.* 130, 245 (1983).
5. Gentle, T.M., Grassian, V.H., Klarup, D.G. and Muettterties, E.L., *J. Am. Chem. Soc.* 105, 6766 (1983).
6. Rucker, T, Logan, M.A., Gentle, T.M., Muettterties, E.L., and Somorjai, G.A., to be published.
7. Gates, J.A., and Kesmodel, L.L., *J. Chem. Phys.* 76, 4281 (1982).
8. Gates, J.A., Kesmodel, L.L., *Surf. Sci.* 124, 68 (1983).
9. Kesmodel, L.L., Laddell, G.D., and Gates, J.A., *Surf. Sci.* 138, 464 (1984).
10. Parshall, G.W., "Homogeneous Catalysts." Wiley, New York 1980, p. 165.
11. Maitlis, P.M., *Acct. of Chem. Research* 9, 93 (1976).
12. Vollhardt, K.P.C., *Angewandte Chem.* 23 (8), 539 (1984).
13. Broden, G., Gafner, G., and Bonzel, H.P., *Surf. Sci.* 84, 295 (1979).
14. Logan, M.A., Gellman, A.J., and Somorjai, G.A., *J. Catal.*, 94, 60 (1985).
15. Ertl, G., Lee, S.B., and Weiss, M., *Surf. Sci.* 114, 527 (1982).
16. Kiskinova, M.P., *Surf. Sci.* 111, 584 (1981).
17. Campbell, C.T., and Goodman, D.W., *Surf. Sci.* 123, 413 (1982).
18. Luftman, H.S., and White, T.M., *Surf. Sci.* 139, 369 (1984).
19. Nieuwenhays, B.E., *Surf. Sci.* 105, 505 (1981).
20. Erley, W., *Surf. Sci.* 94, 281 (1980).
21. Fischer, T.E., and Kelemen, S.R., *Surf. Sci.* 74, 47 (1978).
22. Norskov, J.K., Holloway, S., and Lang, N.D., *Surf. Sci.* 137, 65 (1984).
23. Lang, N.D., Holloway, S., and Norskov, J.K., *Surf. Sci.* 150, 24 (1985).

24. Kiskinova, M., and Goodman, D.W., Surf. Sci. 108, 64 (1981).
25. Bartholmew, C.H., Agrawal, P.K., and Katzer, J.R., Adv. Catal. 31, 135 (1982).
26. Ertl, G., and Koppers, J., "Low Energy Electrons and Surface Chemistry." Verlag Chemie, Weinheim 1974, p. 175.
27. Cabrera, A.L., Spencer, N.D., Kozak, E., and Davies, P.W., Rev. Sci. Instrum. 53 (12), 1893 (1982).
28. (a) Palmberg, P.W., Riach, G.E., Weber, R.E., and MacDonald, N.C., "Handbook of Auger Electron Spectroscopy." Physical Electronics Inc. 1972.
(b) Mroczkowski, Lichtman, Surf. Sci. 131, 159 (1983).
29. Davis, S.M., Zaera, F., and Somorjai, G.A., J. Amer. Chem. Soc. 104, 7453 (1982).
30. Somorjai, G.A., "Chemistry in Two Dimension: Surfaces." Cornell University Press, New York 1981.
31. Gentle, T.M., Ph.D. Thesis, Univ. Calif. Berk. 1984.
32. Pirug, G., Bonzel, H.P., and Broden, G., Surf. Sci. 122, 1 (1982).
33. Garfunkel, E.L., and Somorjai, G.A., Surf. Sci. 115, 441 (1982).
34. Maurice, V., Peralta, L., Bertlier, Ouden, J., Surf. Sci. 148, 623 (1984).
35. (a) "Handbook of Chemistry and Physics." 64th ed., CRC Press 1983.
(b) Dubois, L.H., Nuzzo, R.G., J. Am. Chem. Soc. 105, 365 (1983).
36. Calandra, C. Bisi, O., and Ottaviani, G., Surf. Sci. 4, 271 (1985).
37. a) Mehandru, S.P., and Anderson, A.B., to be published.
b) Anderson, A.B., McDevitt, M.R., and Urbach, F.L., to be published.
38. Anderson, A.B., J. Catal. 67, 129 (1981).
39. Somorjai, G.A., "Chemistry in Two Dimensions: Surfaces." Cornell University Press, New York 1981, p. 248.
40. Garfunkel, E.L., Ph.D. Thesis, Univ. Calif. Berk. 1983.
41. Crowell, J., Ph.D. Thesis, Univ. Calif. Berk. 1982.
42. Satherfield, C.N., "Heterogeneous Catalysis in Practice." Ch. 7, McGraw-Hill, New York 1980.

43. Heyden, B.E., Prince, N.C., Davies, P.J., Paolucci, G., and Bradshaw, A.M., *Solid State Commun.* 48, 325 (1983).
44. Francis, S.M., and Richardson, N.V., *Surf. Sci.* 152/153, 63 (1985).
45. Bauer, E., Poppa, H., and Viswanath, V., *Surf. Sci.* 58, 517 (1976).
46. Kramer, H.M., and Bauer, E., *Surf. Sci.* 92, 53 (1980); 93, 407 (1980).
47. Zingermann, Y.P., and Ishchuk, V.A., *Fiz. Tver. Tela.* 9, 2529 (1967).
48. Holloway, P.H., and Hudson, J.B., *Surf. Sci.* 43, 123 (1974).
49. Demuth, J.E., and Rhodin, T.N., *Surf. Sci.* 45, 249 (1974).
50. Akimoto, K., Sakisaka, Y., Nishijma, M., and Onichi, M., *Surf. Sci.* 82, 349 (1979).
51. Papageorgopoulos, C.A., and Chen, J.M., *Surf. Sci.* 52, 40 (1975).
52. Godbey, D.J., personal communication.
53. Berthelot, M., *C.R. Acad. Sci.* 62, 905 (1866).
54. Reppe, W., and Schweckendieck, W.J., *Liebigs Ann. Chem.* 560, 104 (1948).
55. Redhead, R.A., *Vacuum* 12, 203 (1962).
56. Zaera, F., Ph.D. Thesis, Univ. Calif. Berk. (1984).

CHAPTER EIGHT: CONCLUSIONS

Section 8.1: Overview

The effect of additives on catalysts for the hydrogenation of carbon monoxide and the cyclotrimerization of acetylene has been investigated using both low pressure surface science techniques and high pressure reaction studies. Additives were found to have relatively complicated catalytic behavior, which could be explained with the aid of surface analytical tools such as AES, XPS, TPD, and LEED. Potassium was found to have the greatest effect on both the hydrogenation of CO and the cyclotrimerization of acetylene over all metal catalysts.

Section 8.2: Hydrogenation of Carbon Monoxide

Hydrogenation of carbon monoxide was carried out over Mo, Rh, mixed oxides of Rh and 3d transition metal perovskites.

The hydrogenation of CO on Mo surfaces in the pressure range 1-10 atm and temperature range 520-670 K, primarily produces methane, ethene and propene. The reaction rate exhibits positive order in CO pressure for CH₄ formation unlike other methanation catalysts. The reaction also produces a large fraction of ethene and propene instead of saturated hydrocarbons as observed for other transition metal catalysts (Fe, Re). The addition of K to the surface, at low coverages, causes an increase in the overall rate and a shift in selectivity toward unsaturated products. This has been explained in terms of an electronic effect by which K induces back-donation of electrons into the CO 2 π* orbital, increasing the amount of CO dissociation on the surface. The addition of S to the surface, on the other hand, causes a decrease in the overall rate, but again, an increase in the fraction of unsaturated products. This has been explained in terms of selective adsorption site blocking, preferentially reducing the amount of hydrogen on the surface.

For hydrogenation of CO over Rh polycrystalline foil catalysts, a large equilibrium deuterium isotope effect is observed. The activation energy for the reaction is similar to other methanation catalysts. Also, the pressure dependence of the reaction obeys the rate law:

$$\text{Rate}_{\text{CH}_4} = K P_{\text{H}_2}^{+1} P_{\text{CO}}^{-1}$$

These observations lead to the conclusion that one of the final hydrogenation steps in the reaction mechanism is rate-limiting.

Over oxides of Rh and La perovskites, the products of the hydrogenation of CO were found to be very dependent on the oxidation state of the transition metal catalysts. The activity is lower for the oxide catalysts relative to clean metal catalysts with the same active metal center. For the transition metal perovskites, the overall activity increases from left to right on the periodic table, from Cr to Co.

Section 8.3: Cyclotrimerization of Acetylene

Acetylene cyclotrimerization over additive-covered Pd(111), (100) and (110) single crystal surfaces at both high (~ 1 atm) and low ($\sim 10^{-12}$ atm) pressures has been studied.

At low pressures the reaction was found to have a high degree of structure sensitivity for the formation of benzene, Pd(111) > Pd(110) > Pd(100). At low pressures, additives had large effects on the amount of benzene formed. On Pd(111), addition of P to the surface (0.25 ML) doubled the amount of benzene formed, while K (0.25 ML) greatly reduced the amount of benzene relative to the clean surface (see Fig. 7.19). Benzene formation on Pd(100) increased 15 fold, relative to clean Pd(100), with the addition of 0.25 ML of Si, possibly due to formation of a Pd silicide. The effect of additives on the low pressure stoichiometric reaction can be explained by a combination of surface structure and electronic interactions.

The effect of additives on the high pressure catalytic conversion of acetylene to benzene was much different than in the low pressure stoichiometric reaction. At high pressures, the dominant factor in the rate of benzene formation appeared to be the number of active sites on the surface. The amount of graphite or polyacetylenic carbon on the surface decreased with electron-donating additives (K, Si) on the surface, relative to clean Pd (see Fig. 7.18), and increased with electron-withdrawing additives (S, Cl). The structure sensitivity at high pressures for additive-covered surfaces was found to be in the same order as at low pressures, Pd(111) > Pd(110) > Pd(100), when only the active surface (free of carbon) is taken into account. Much less difference in the overall rate of benzene formation over the three surfaces is observed at high pressures.

APPENDIX: CYLINDRICAL MIRROR ANALYZER SCHEMATICS AND PHOTOGRAPHS

Section A.1: Materials and Suppliers

Schematics for the double pass cylindrical mirror analyzer (CMA) used in the studies discussed in this thesis are shown in Figs. A.1 - A.37 and Photographs A.38 - A.53. Not shown are schematics for the field terminating plates, which were purchased from the vacuum division of Physical Electronics. The Mu metal shields, shown in Figs. A.19 - A.22 and Photographs A.38,39, were purchased from

Mu Shield Company
121 Madison St.
Malden, MA 02148
(617) 321-4410.

Vacuum feedthroughs were purchased from Varian (Rotary-Varian 954-5151, 10 pin-Varian 954-5033). The channeltron used was purchased from Gallileo (5800 series, high voltage model). The wire meshes used were tungsten 100 X 100 with 0.001 in. wire and 50 X 50 with 0.002 in. wire and purchased from

Unique Wire Weaving
762 Ramsey Ave.
Hillsdale, WI.

All ceramic components are composed of 100% Al_2O_3 and were built in the ceramic shop at LBL by Will Lawrence and Bill Wilkie. All measurements shown in the figures are in units of inches.

Section A.2: Overview of Schematics

Figs. A.1 - A.12 are the schematics for the double pass CMA.

Figs. A.13 - A.18 are schematics for the pivoting aperture for switching from Auger to XPS mode.

Figs. A.19 - A.22 are schematics for the outer Mu metal shielding for the CMA.

Figs. A.23 - A.37 are schematics for the internal electron gun which is used for Auger electron spectroscopy.

Section A.3: Abbreviations Used in Schematics

Be-Cu = Berrilium-Copper

CL = center line

CCF = conflat flange

FH = flat head screw

HEX = hexagonal head screw

IC = inner cylinder

ID = inside diameter

OC = outer cylinder

OD = outside diameter

OFHC = oxygen-free high purity copper

R = radius

SH = socket head

304SST = 304 stainless steel

Vac = vacuum

Section A.4: Figs. A.1 - A.12

The main body of the double pass CMA is shown in Figs. A.1 - A.12. Photographs A.40 - A.43 and A.47 - A.52 show the CMA being disassembled piece by piece.

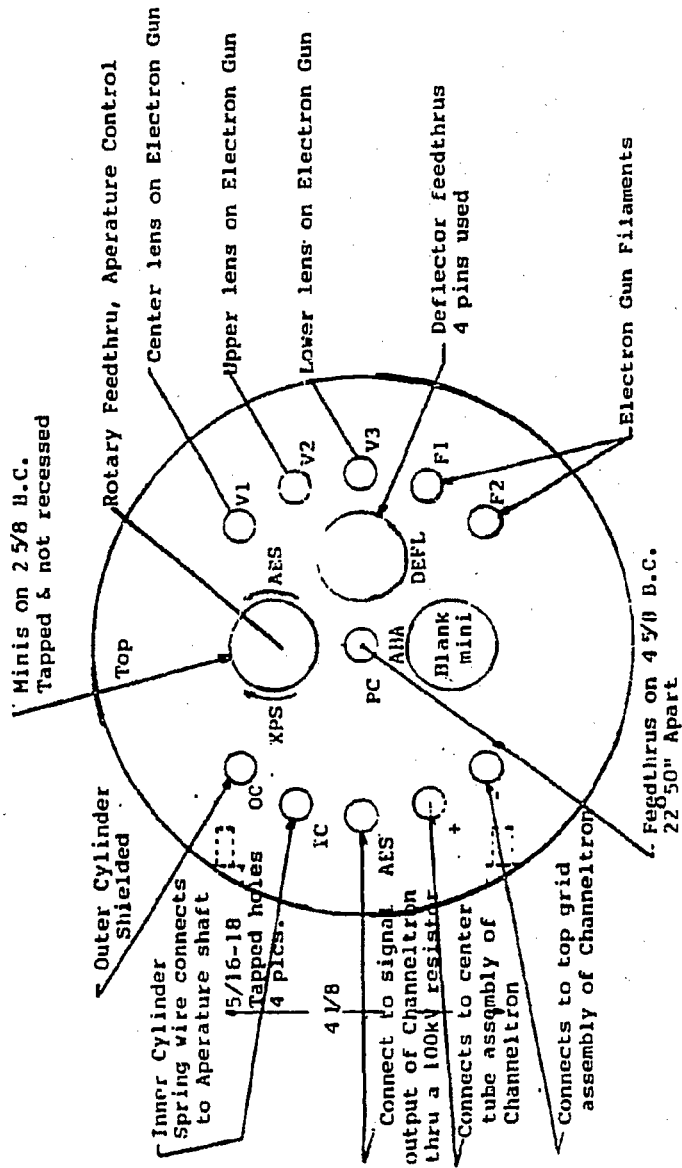


Fig. A.1. 8-in. conflat flange for mounting the CMA to the vacuum chamber has a 10 pin feedthrough mounted on a mini flange, a rotary feedthrough to move the pivoting aperatures (see Fig. A.13 - A.18), and 11 high voltage feedthroughs.

Attachment Plate-Top from Vac Side
 Material-Aluminum
 OD=5 3/8 ID= 3 3/4 Thickness= 1/4

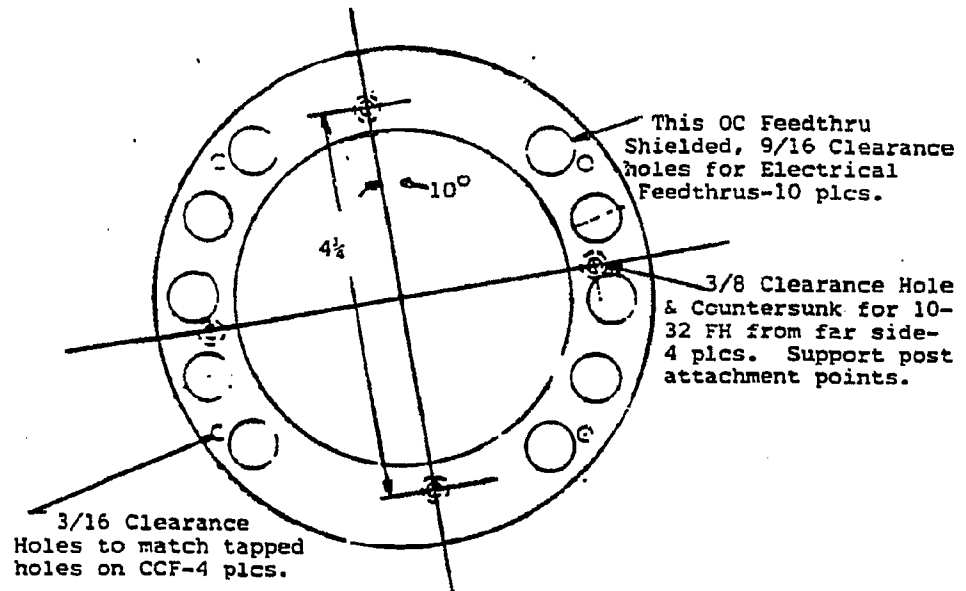


Fig. A.2. The aluminum attachment plate for the support posts is also the attachment point for the OC shielding (see Photograph A.49).

Back-up Plate for Bottom Field
Terminator Support (Copper)
304SST-1/16 Thick

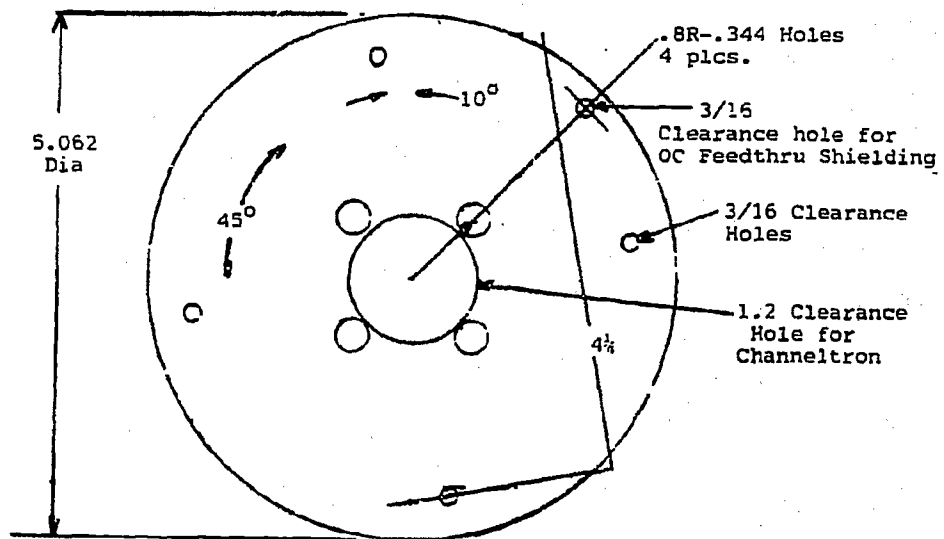


Fig. A.3. The back up plate for the final field terminator support is held above the channeltron by four support posts (see Photograph A.48).

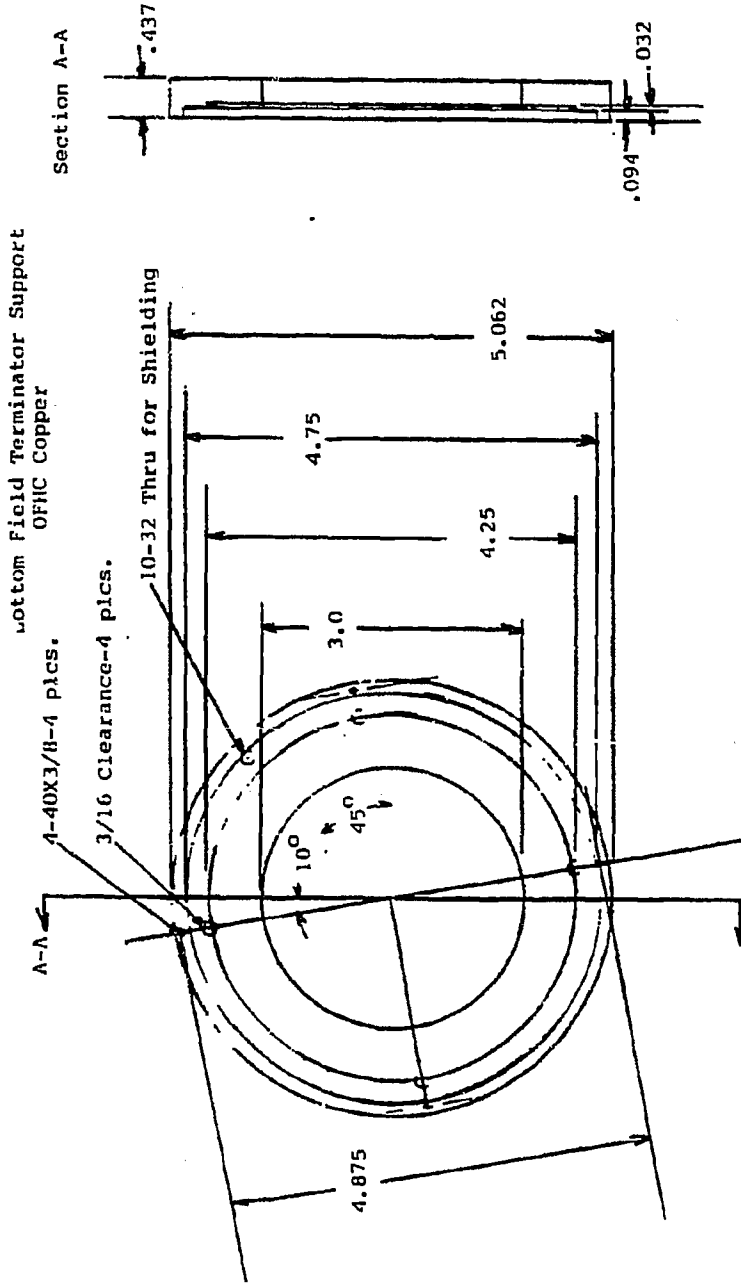


Fig. A.4. The bottom copper field terminator support is attached to the back up plate (see FIG. A.3, Photograph A.48).

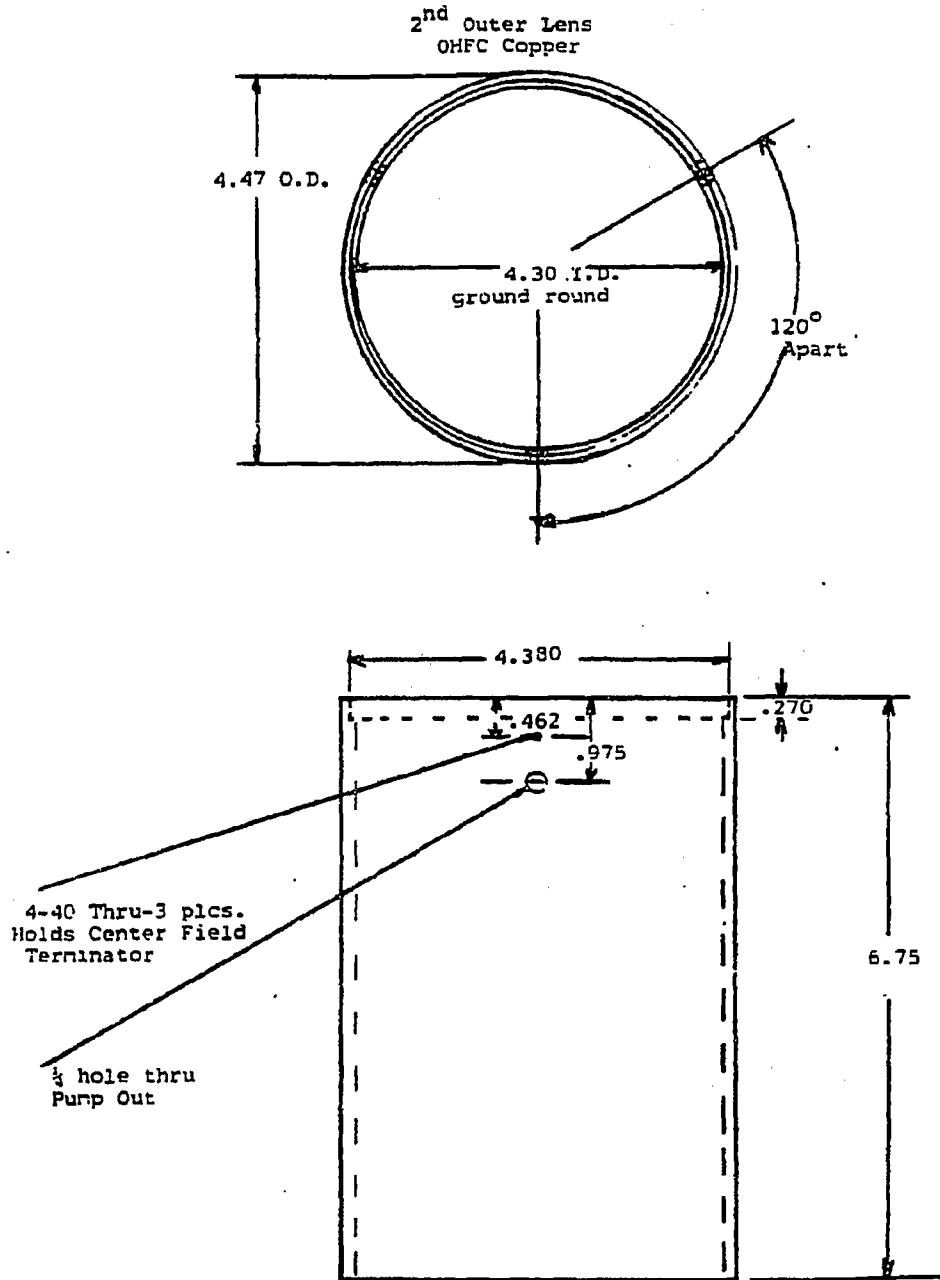
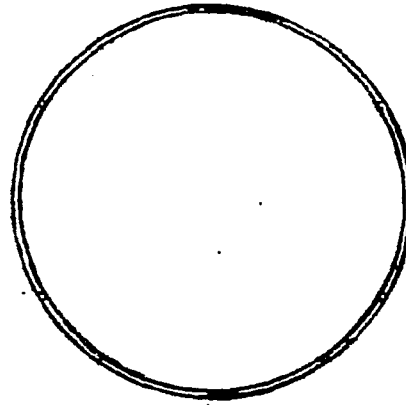


Fig. A.5. The lower oxygen free copper outer cylinder (see Photograph A.41).
The middle field terminator is held by three 4-40 allen head screws.

1st Outer Lens
OHFC Copper



1/16 slot- Equally spaced
60° Apart-6 plcs.

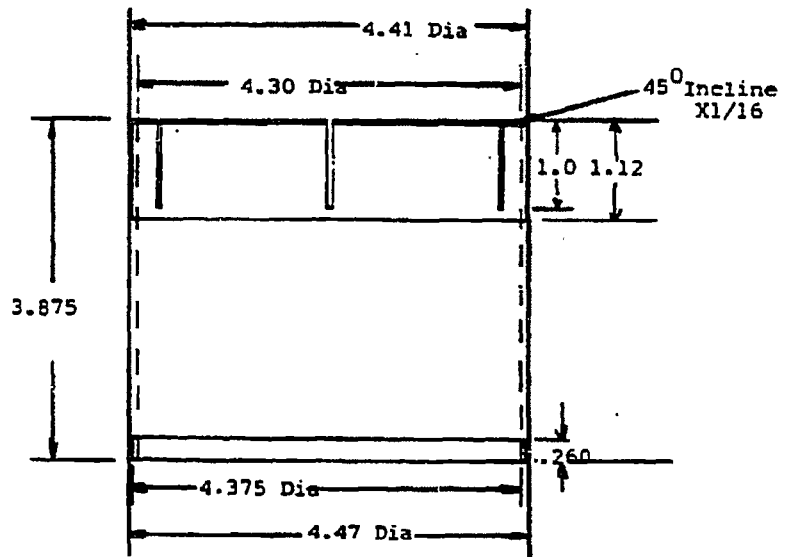
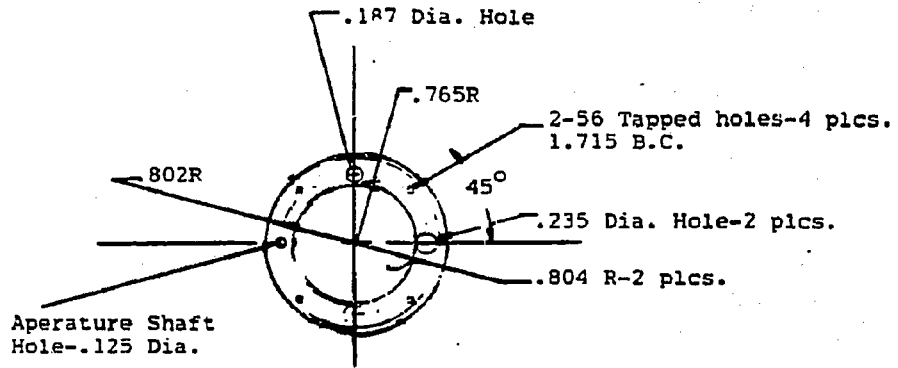


Fig. A.6. The upper oxygen free copper cylinder. The bottom interlocks into the bottom outer cylinder and the top field terminator rests on the slotted top (see Photograph A.40).



2nd Inner Lens Be-Cu Grid Dimensions=.002 wire X .020 sq. sections

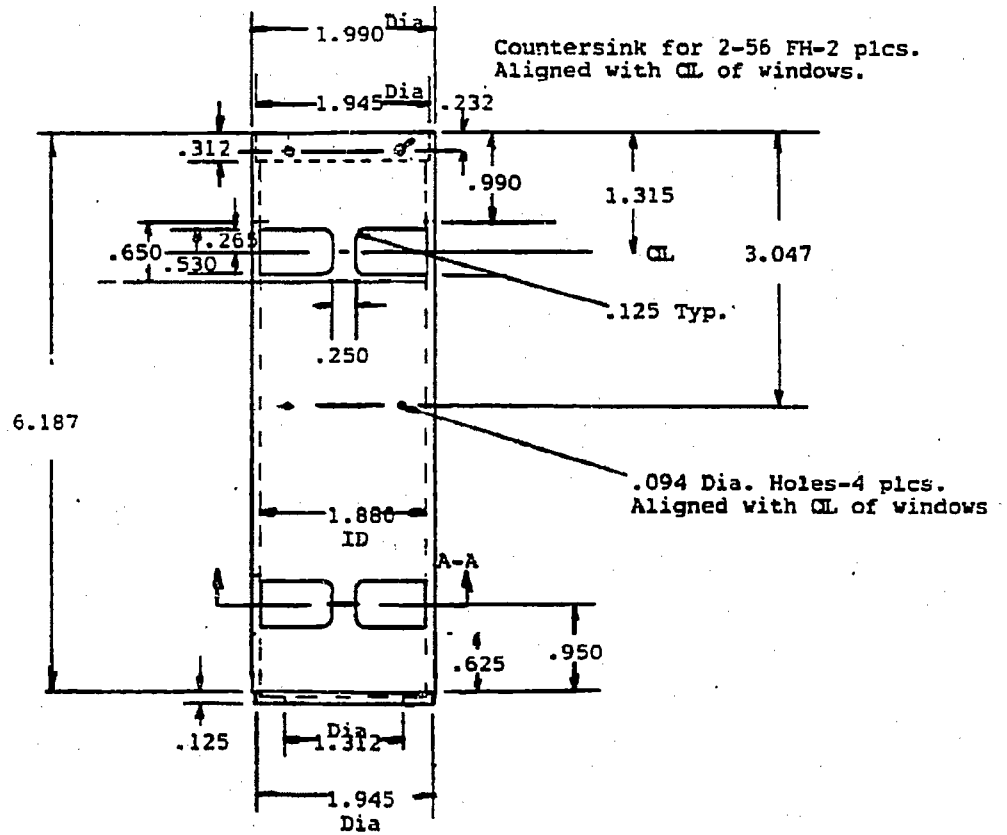


Fig. A.7. The lower Be-Cu inner cylinder with tungsten mesh-covered electron windows (see Fig. A.9). The middle field terminator sits on top of this cylinder and is held in place by the upper inner lens (see Fig. A.8, Photographs A.42,43).

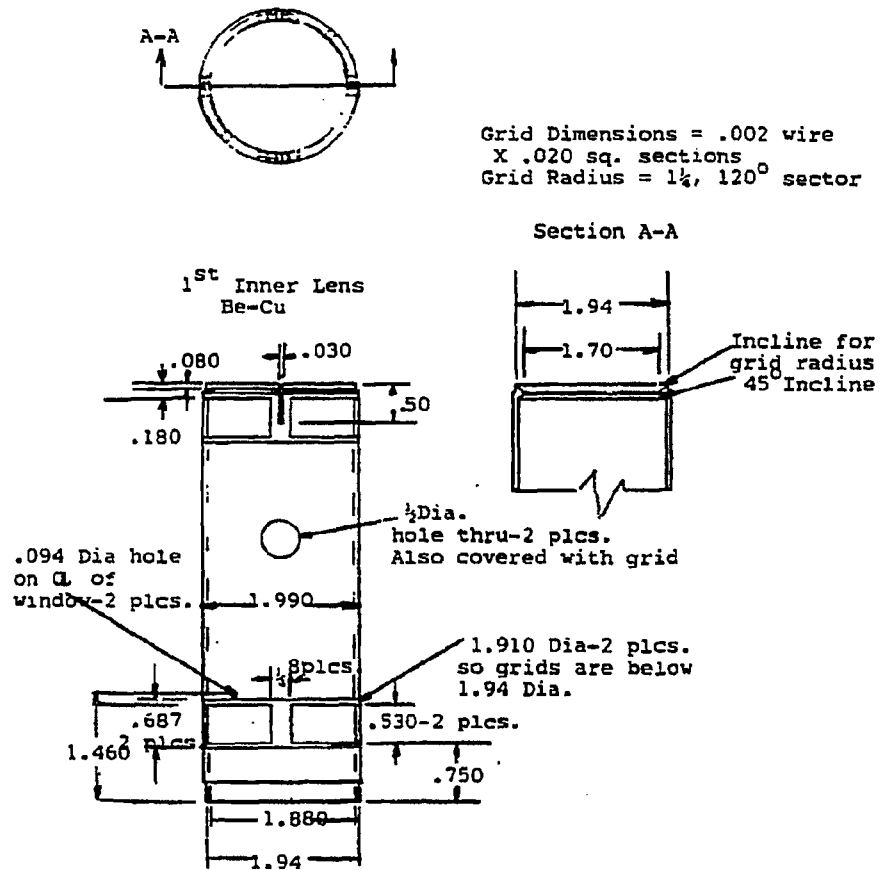
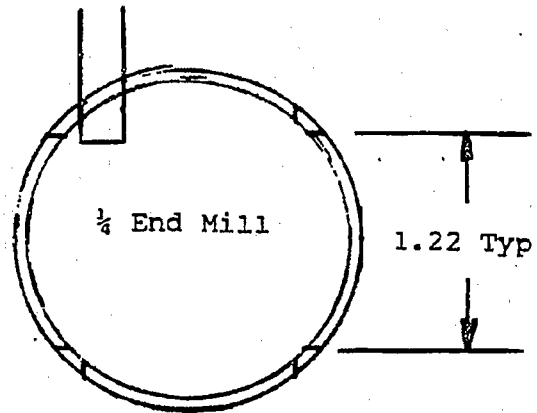


Fig. A.8. The upper Be-Cu inner cylinder. The middle field terminator is held by the long shoulder on the bottom of this inner cylinder (see Photograph A.51). The top field terminator rests on the top of the cylinder and the electron gun sits between the grid-covered electron windows (see Fig. A.9).

Section A-A
Machining Detail of Windows



Window Grid Holddown Sheet
Use PT between sheet and BE-CU



Fig. A.9. Detail of the electron windows for the inner cylinder.

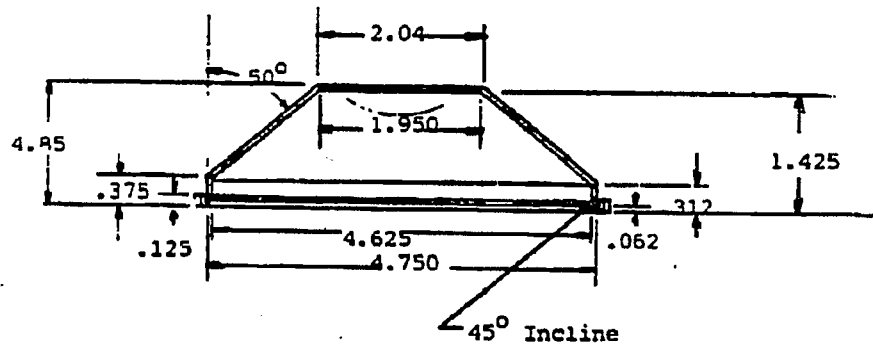
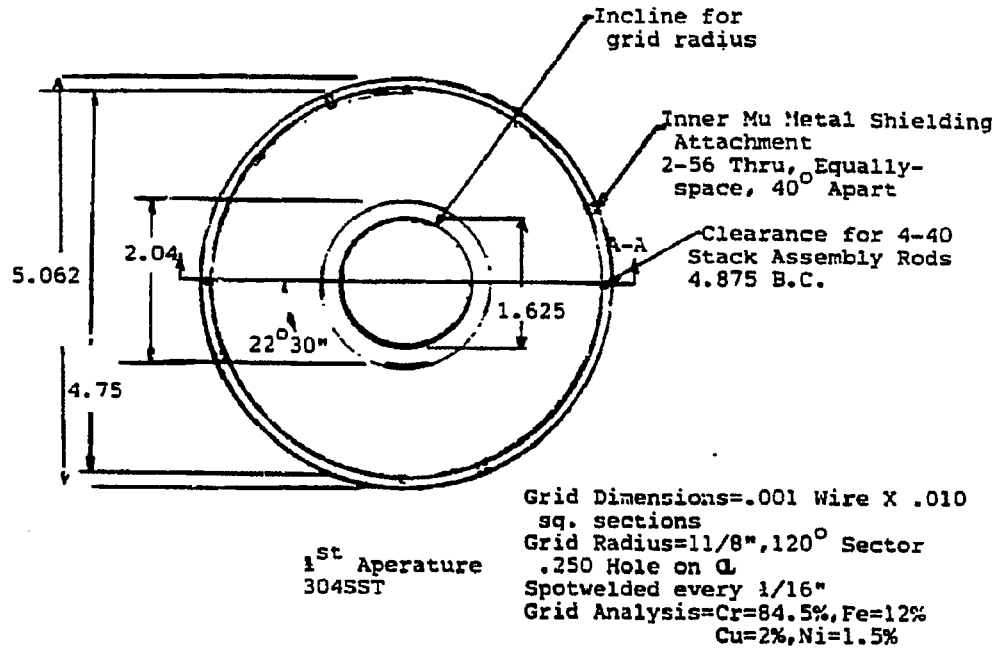


Fig. A.10. The cover shield for the CMA, with attachments for the stack assembly rods (see Fig. A.11), and inner Mu shield. The shield has a hemispherical grid spotwelded on the top (see Photograph A.50).

Stack Assembly Rods-4 pcs.
OHFC Copper

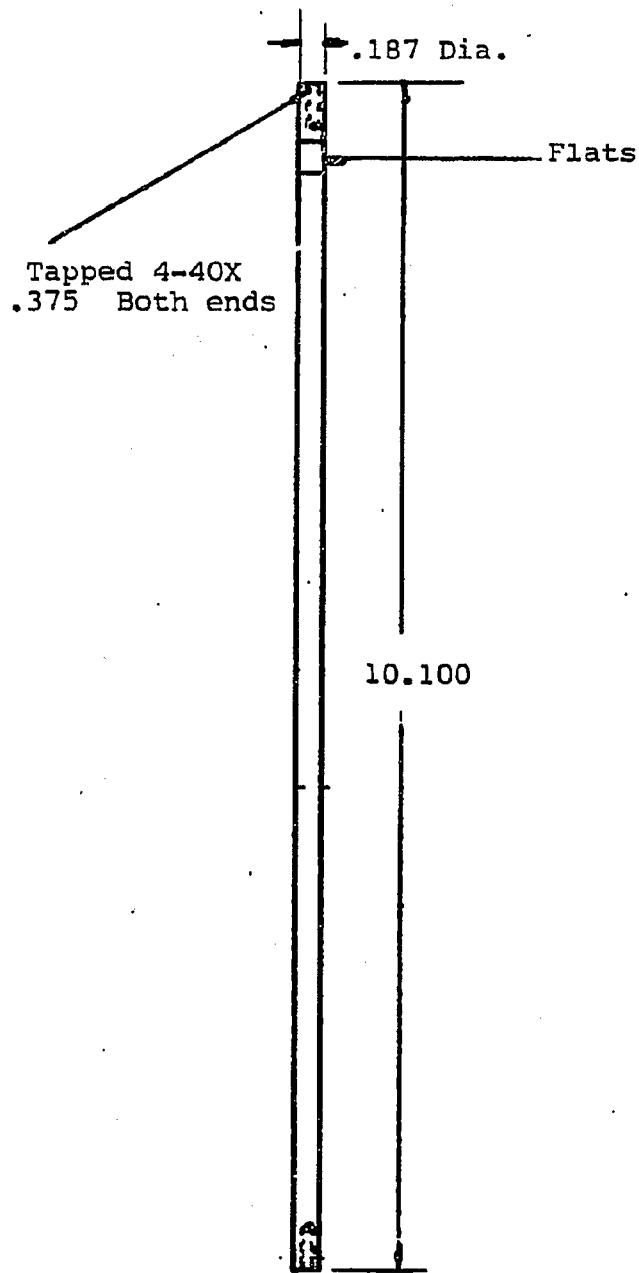


Fig. A.11. The OHFC copper stack assembly rods (see Photographs A.40,41).

Support Posts-4 pcs.
304SST 5/16 Hex

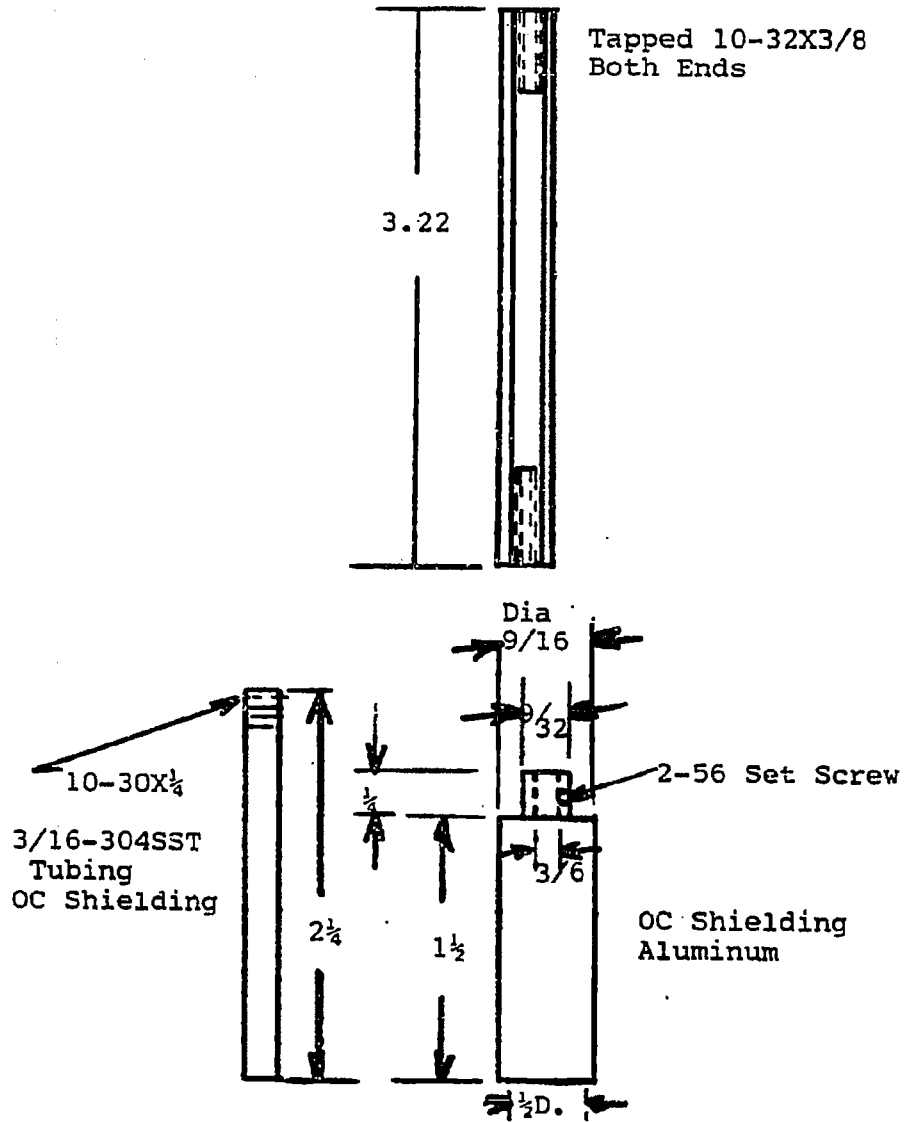


Fig. A.12. The bottom terminator support posts and outer cylinder aluminum shielding (see Photograph A.49).

Section A.5: Figs. A.13 - A.18

The pivoting aperatures are incorporated into the CMA for changing from AES to XPS mode. The electron flux for AES is much higher than that for XPS, therefore, to extend the channeltron lifetime, smaller aperatures are used in the AES mode. The pivoting aperatures are located above the channeltron and at the field terminating plate (at the apexes of the electron flux through the CMA).

Fig. A.1 shows the rotary feedthrough used to move the aperature. The aperatures are connected by a 0.125" stainless steel rod. The rod is inserted through the "aperature shaft hole" in each aperature (see Figs. A.15,16) and moved by the rotary feedthrough on the 8" CCF (see Fig. A.13) moving the pivoting aperature lever arm (see Fig. A.17). The 0.125 rod rotates 45° and is attached to the two pivoting aperatures. The 0.125 rod is attached to the 8" CCF as shown in Photographs A.47,49.

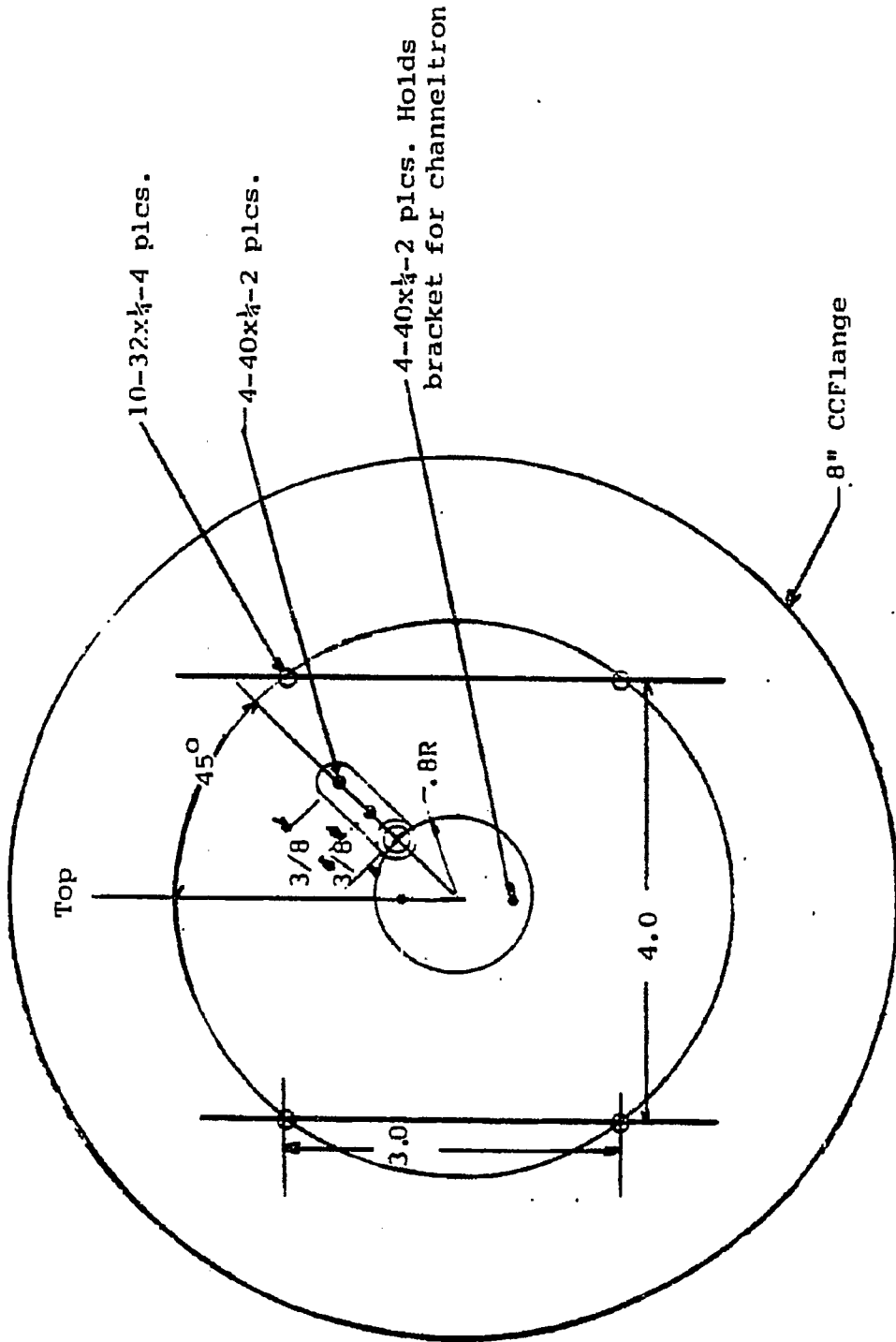


Fig. A.13. The back of the 8" CCF with the pivoting bracket (see Photographs A.47,49).

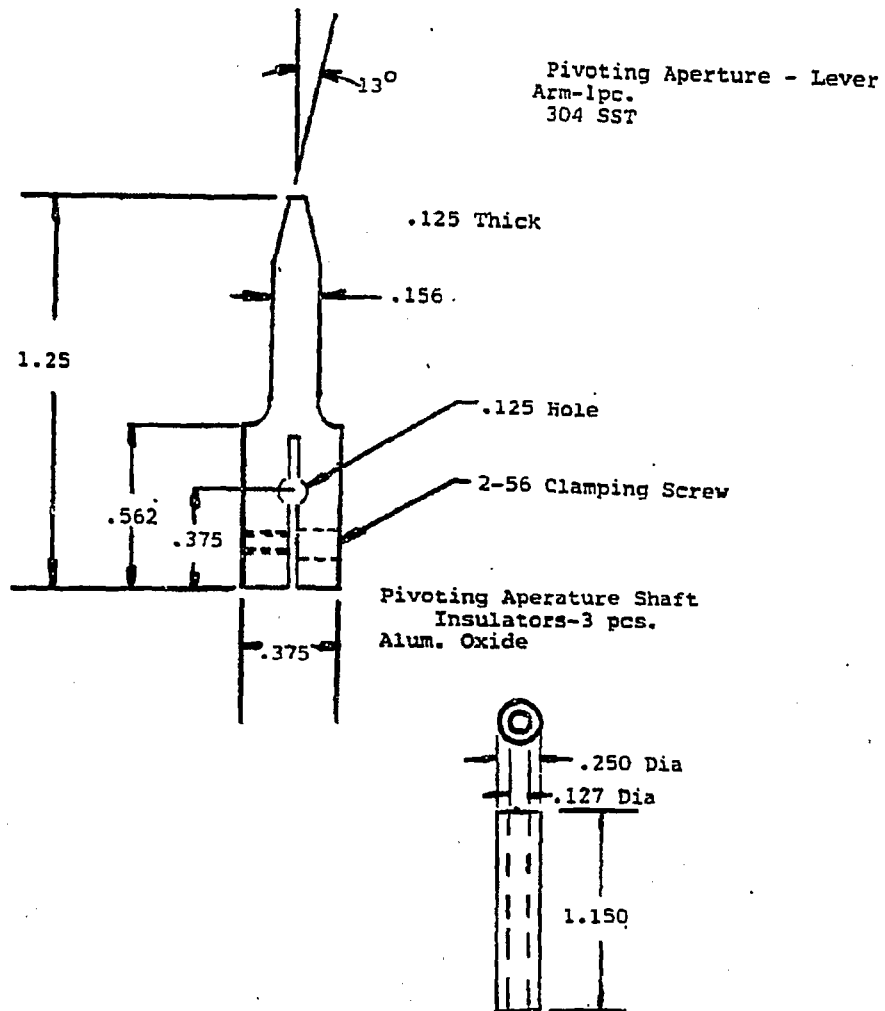
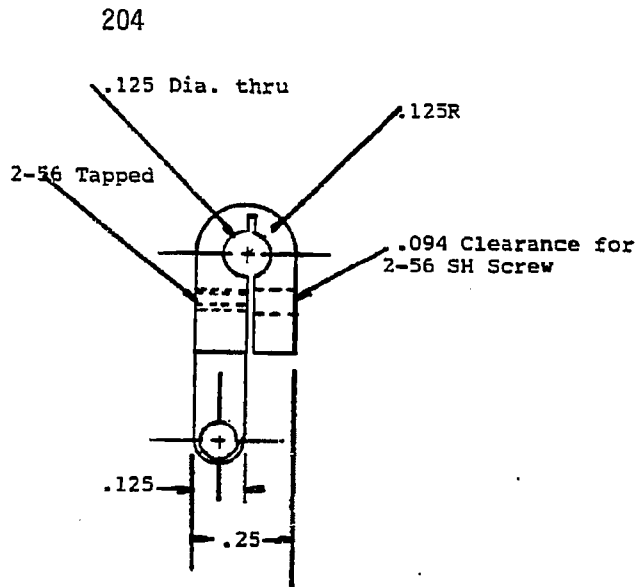
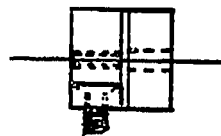


Fig. A.14. The pivoting aperture arm which is activated by the rotary feed-through. The 0.125 rod is attached with the clamping screw (see Photograph A.49) insulators for the 0.125 rod, to go inside the outer cylinder of the CMA.



Aperature Pivot Arm

BE-CU 2 pcs.

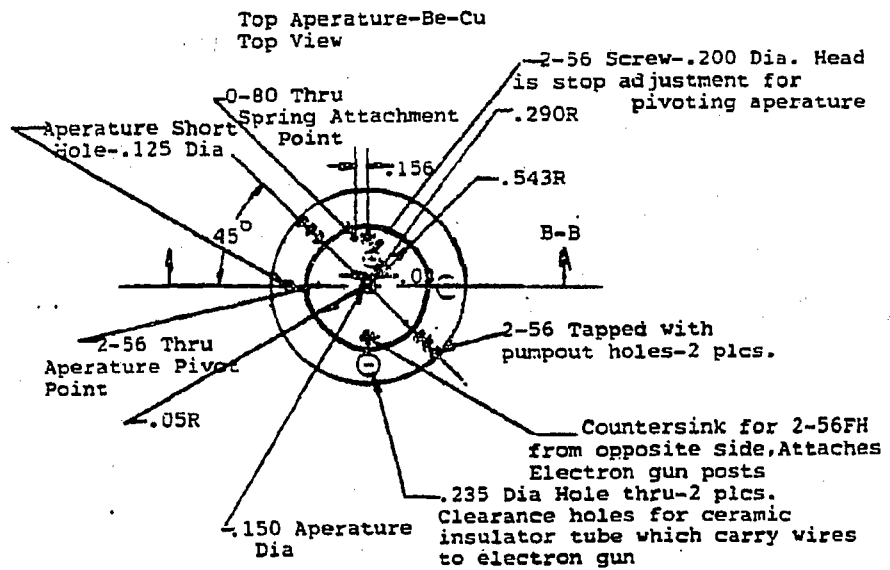


Countersink & Tap Hole for
O-80 FH Screw
Screw to stick down .180

SST-Pivoting Aperature Shaft-.125 Dia X
9.75 Long

BeCu-2 Thrust Bushing=.250 O.D. X .128 I.D. X
.125 Thk
One has 2-56 Tapped hole radially into
.127 I.D. for Set Screw

Fig. A.15. The pivot arm connected to 0.125 shaft is inserted in the oval hole of the pivoting aperature (see Photograph A.45, Fig. A.18).



Section B-B

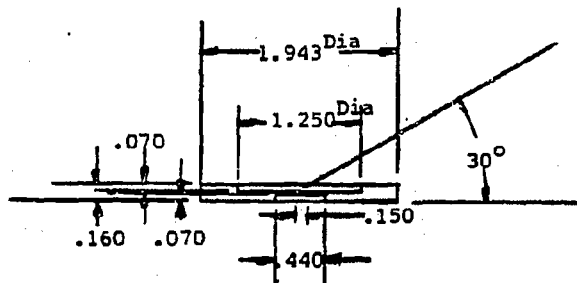
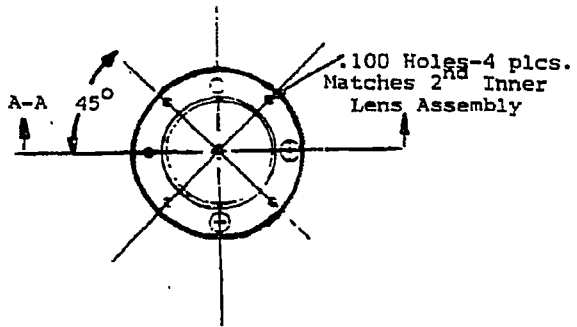


Fig. A.16,17. The top and bottom aperature each have an aperature hole, spring attachment point and stop to hold the pivoting aperature in the correct position (see Photograph A.45).

Bottom Aperature Top View
Pivoting Aperature Not Shown
Same as Top Aperature



Section A-A

Pivoting Aperature Dia=.062
Grid spotwelded to underside
Grid is .002 wire, .020 square sections

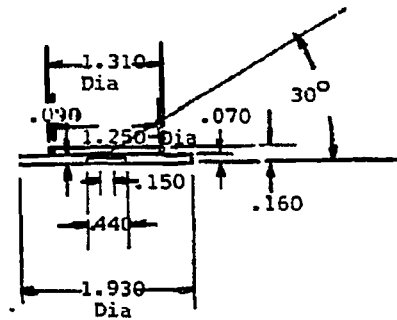


Fig. A.17. See previous figure for description.

Pivoting Aperture Details
 Top=.100 Dia
 Bottom=.062 Dia
 Spring Length Relaxed \leq .44

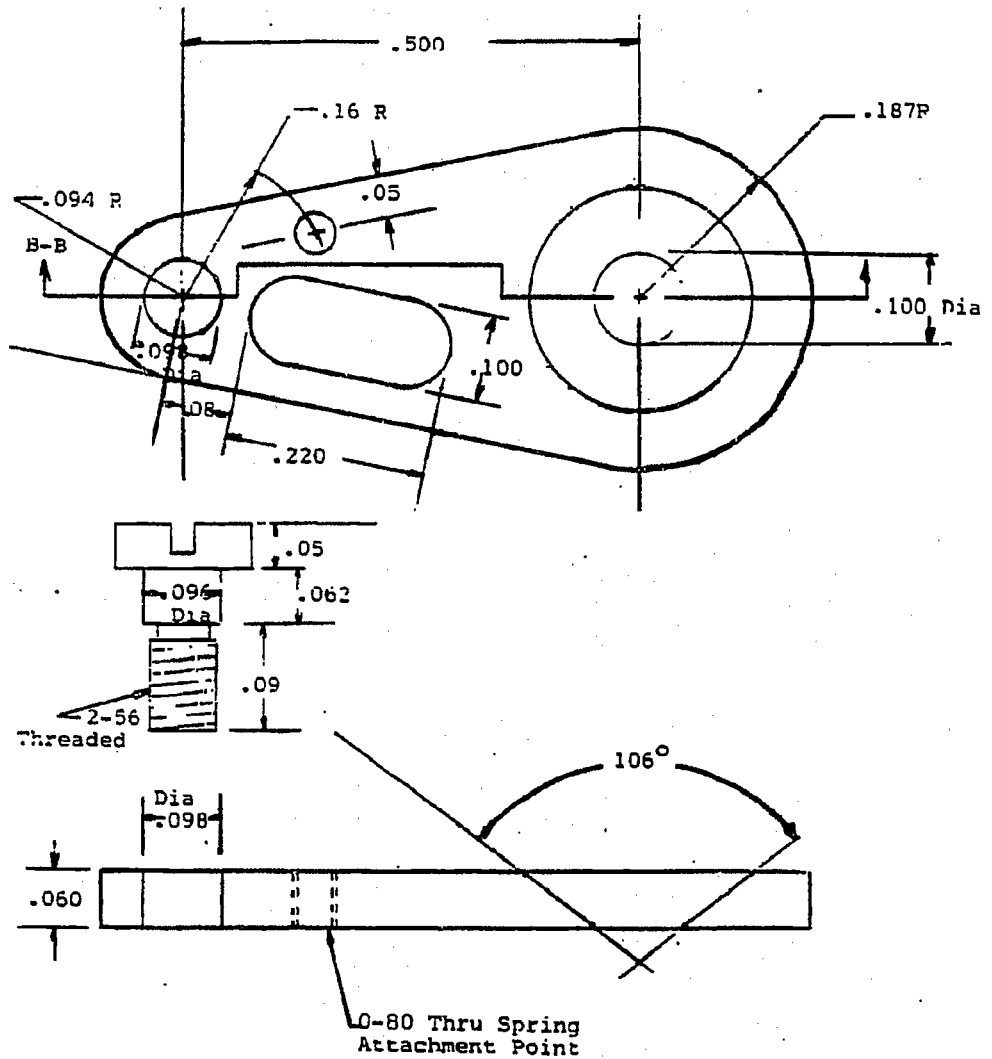


Fig. A.18. The pivoting aperture. The top aperture is 0.100 in diameter and the bottom aperture is 0.062 in diameter (see Photograph A.45).

Section A.6: Figs. A.19 - A.22.

The Mu metal shield shown in Figs. A.19 - A.22 and Photographs A.38,39 insure uniform magnetic fields inside the CMA.

Inner Mu Metal Shielding

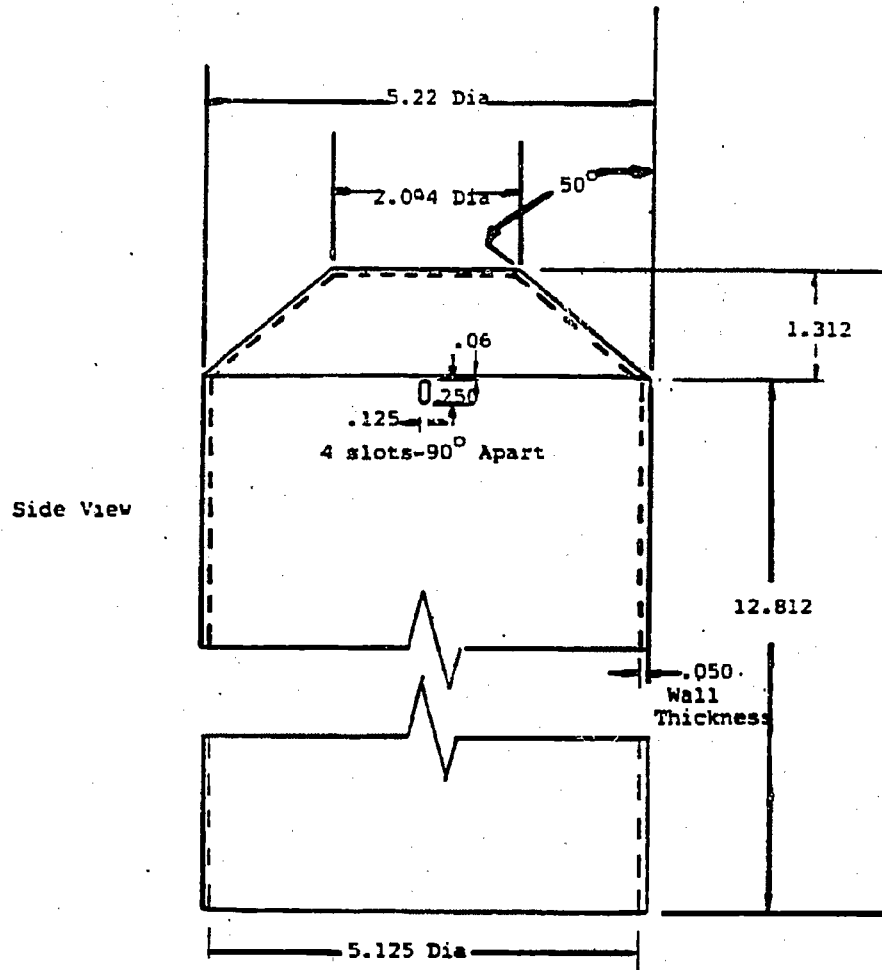


Fig. A.22. Side view of the inner Mu metal shield. The inner and outer shields are separated by 0.090 in. and are parallel with respect to the body of the CMA.

Inner Mu Metal Shielding-1 pc.

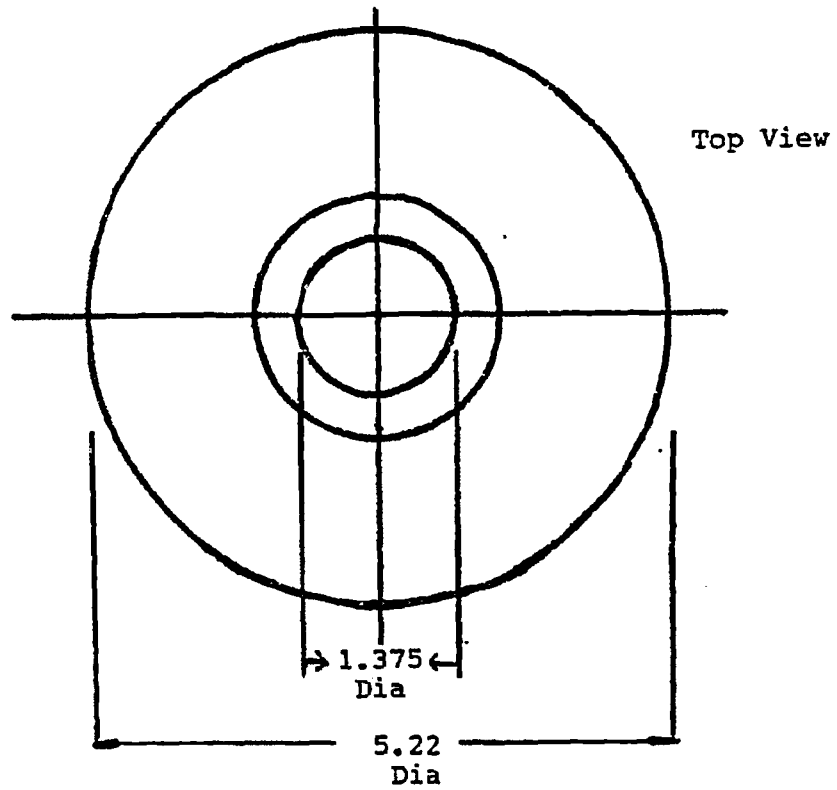


Fig. A.21. Top view of the inner Mu metal shield (see Photograph A.39).

Section A.7: Figs. A.23 - A.37

The internal electron gun is shown in Figs. A.23 - A.37. The gun is taken apart from the bottom to the top. Ceramic insulators, support rods and screws are shown in Figs. A.34 - A.37. Photographs A.44 - A.46 show the actual electron gun from two viewpoints.

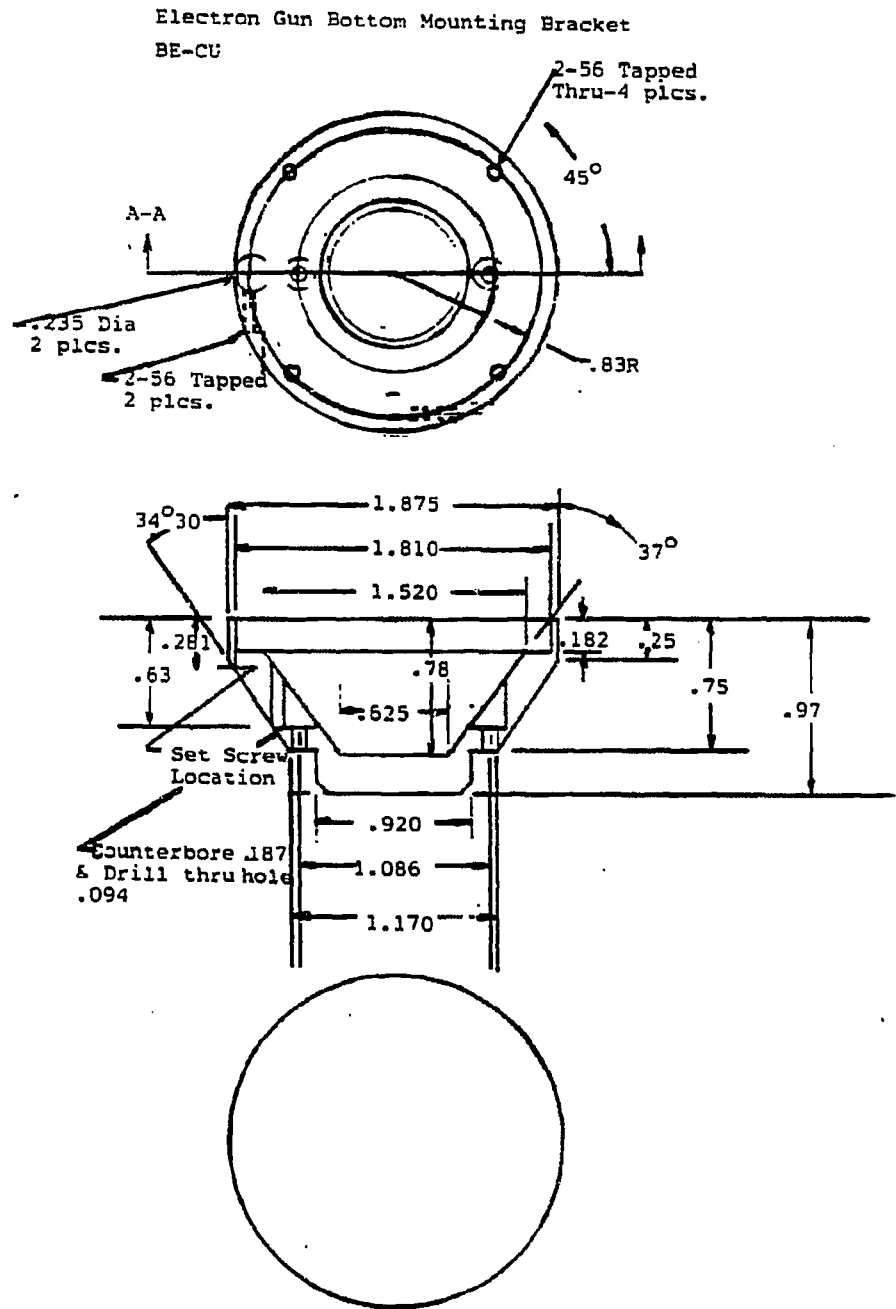


Fig. A.23. Electron gun base with four 2-56 holes tapped to hold the gun together and two counterbored holes for the gun mount on the QMA (see Fig. A.36).

Outer Mu Metal Shield

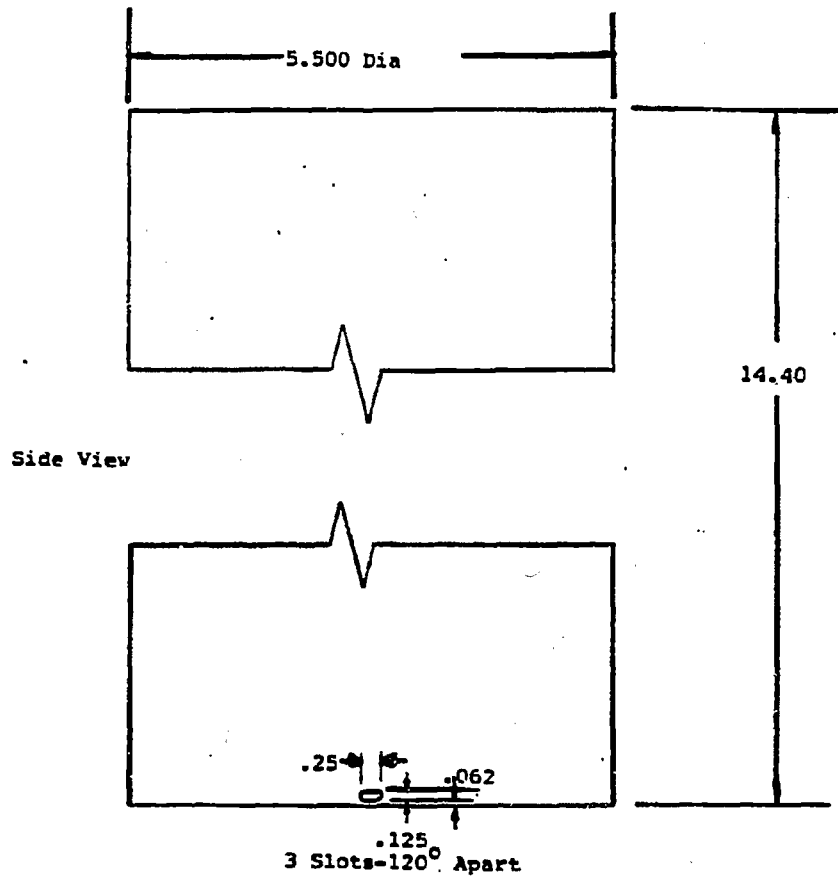


Fig. A.20. Side view of the outer Mu metal shield.

Outer Mu Metal Shielding-1 pc.

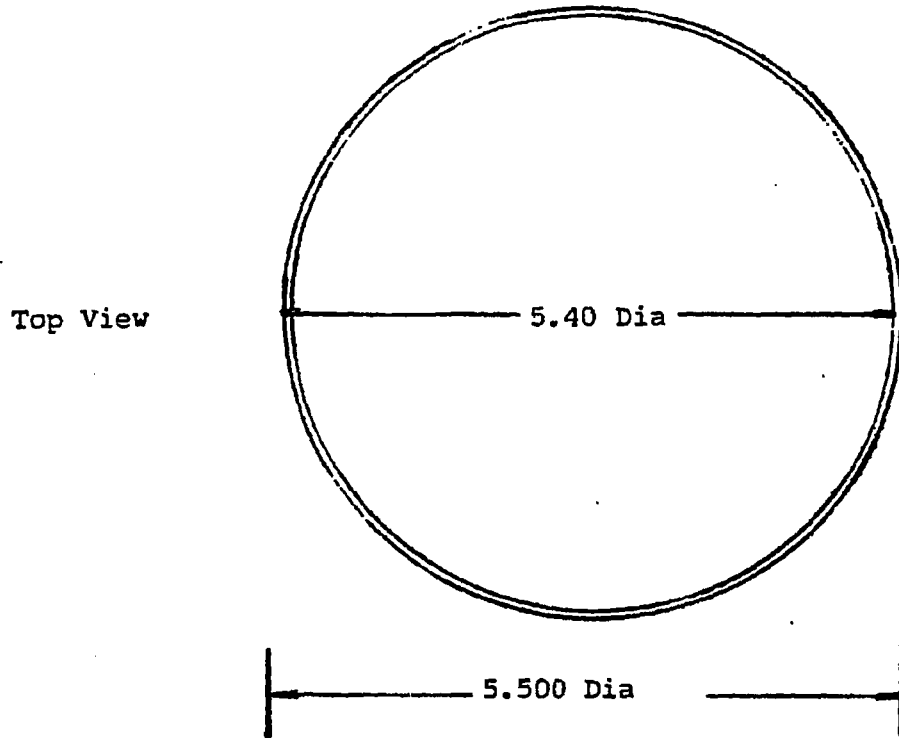


Fig. A.19. Top view of the outer Mu metal shield (see Photograph A.38).

Electron Gun-Plate
304SST

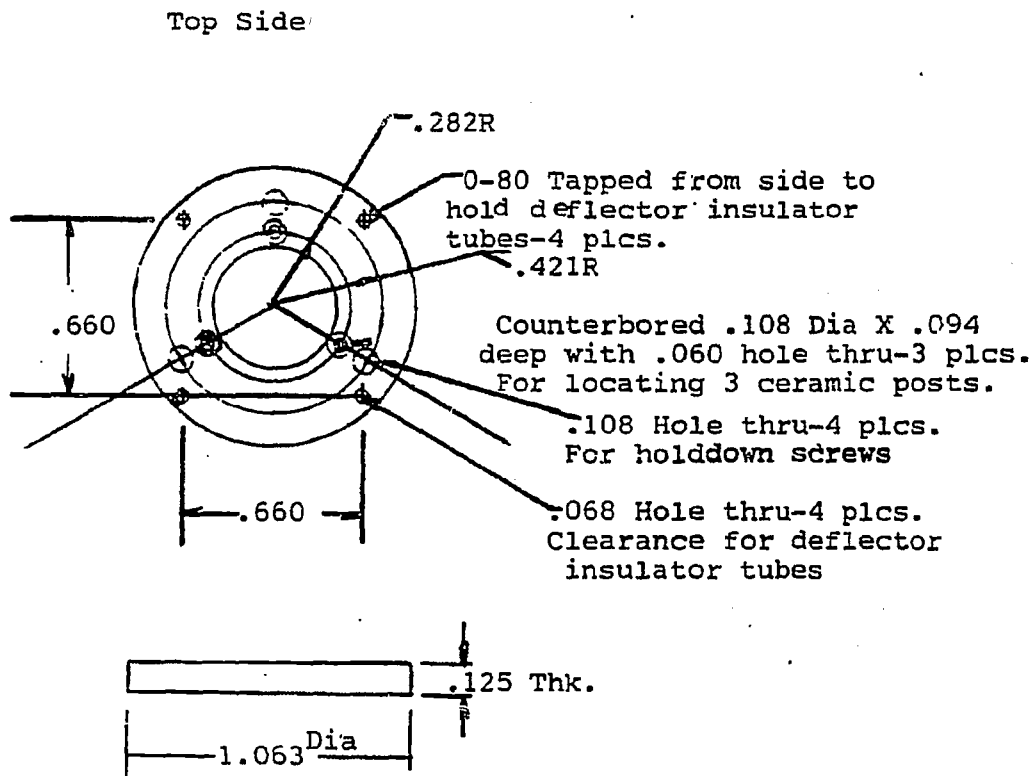
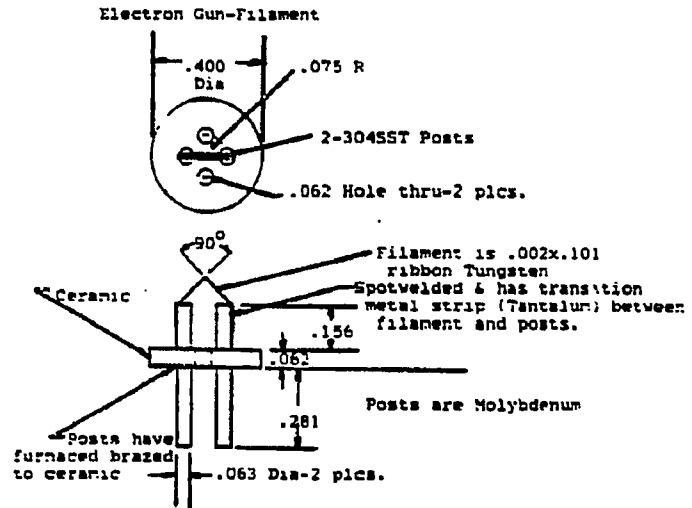


Fig. A.24. Base plate for the electron gun. The internal parts of the electron gun are bolted to this plate (see Photographs A.44 - A.46).



Electron Gun-Filament Assembly Plate-1 pc. 304SS

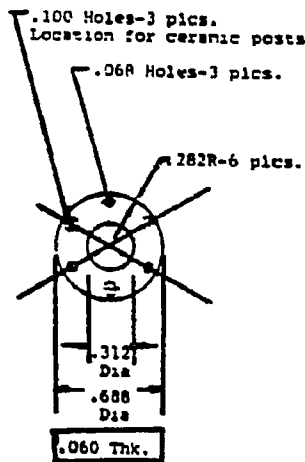


Fig. A.25. Electron gun filament. The tungsten (preferably thoriated tungsten) filament is spotwelded to the Mo support posts using a thin foil of tantalum or platinum. The height of the filament is critical to insure reasonable emission during use. The 2 Mo rods are connected to F1 and F2 on Fig. A.1.

Electron Gun-Filament Assembly Plate-1 pc.
304SST

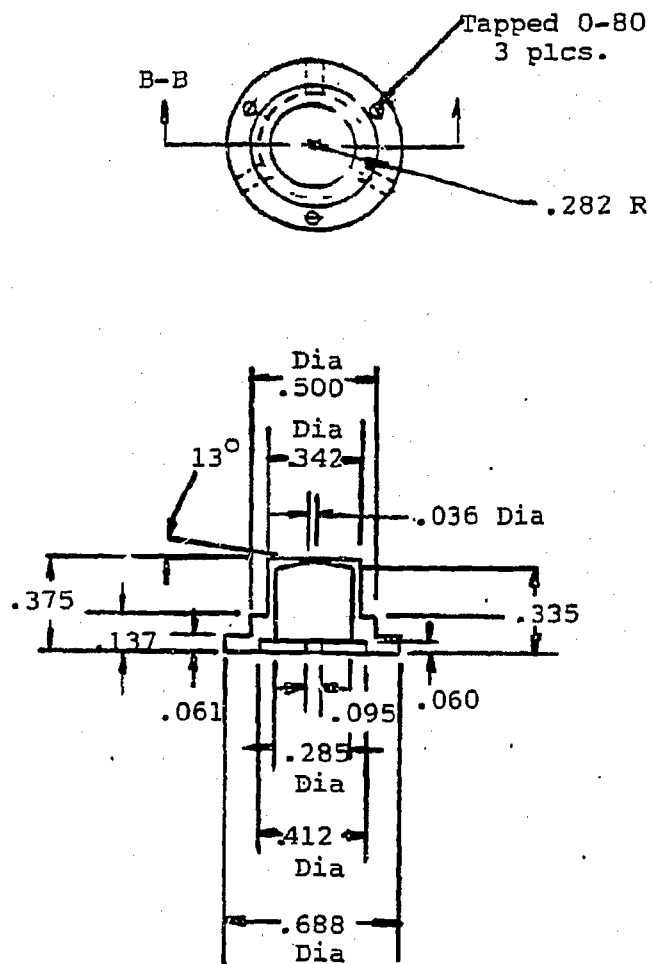


Fig. A.26. Electron filament holder. The filament assembly fits up in the holder such that the end of the filament is lined up with the 0.036 hole at the top and is ~ 0.010-0.002 in. from touching the sides of the hole. The filament holder assembly plate holds the filament in place and is wired to V1 on Fig. A.1. The plate is held away from the electron gun plate (Fig. A.26) by 3 ceramic posts (see Fig. A.37).

Electron Gun Lens
304SST

Top View

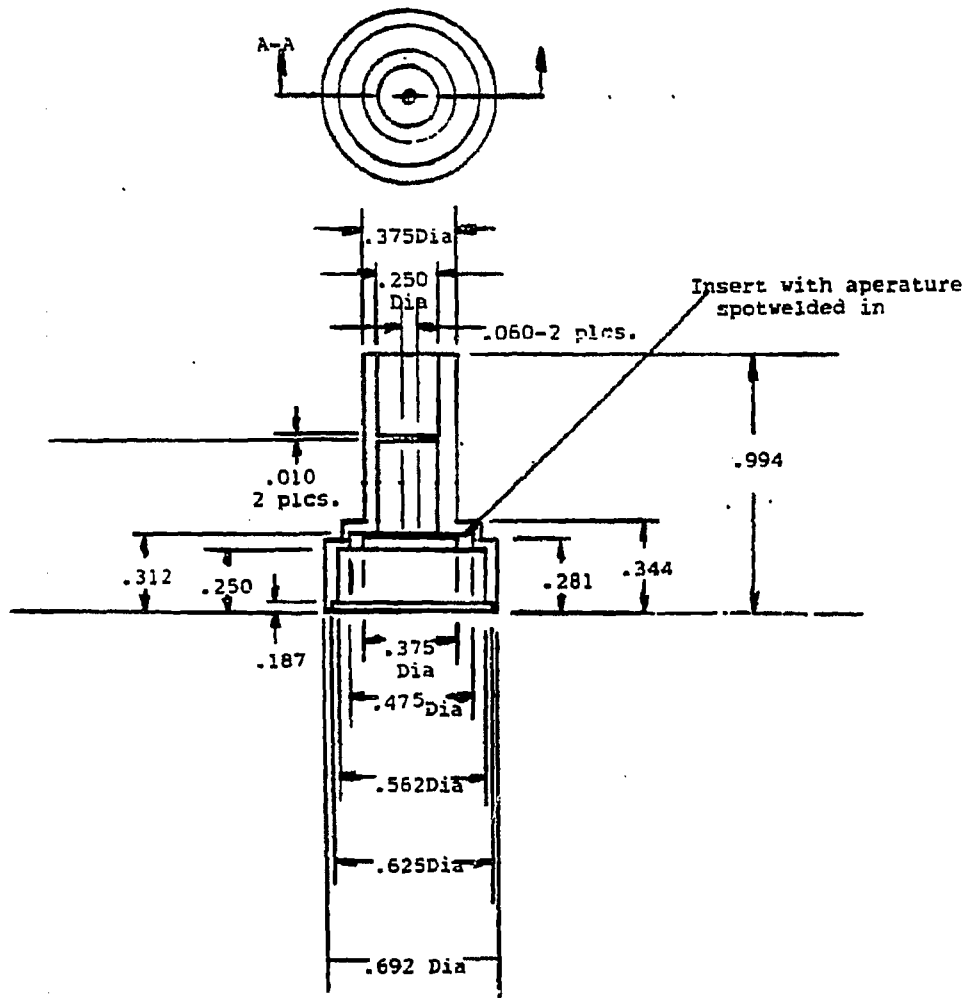


Fig. A.27. The electron beam focusing stage fits on top of the deflector lens assembly and is connected to V2.

Electron Gun-Plate
304SST

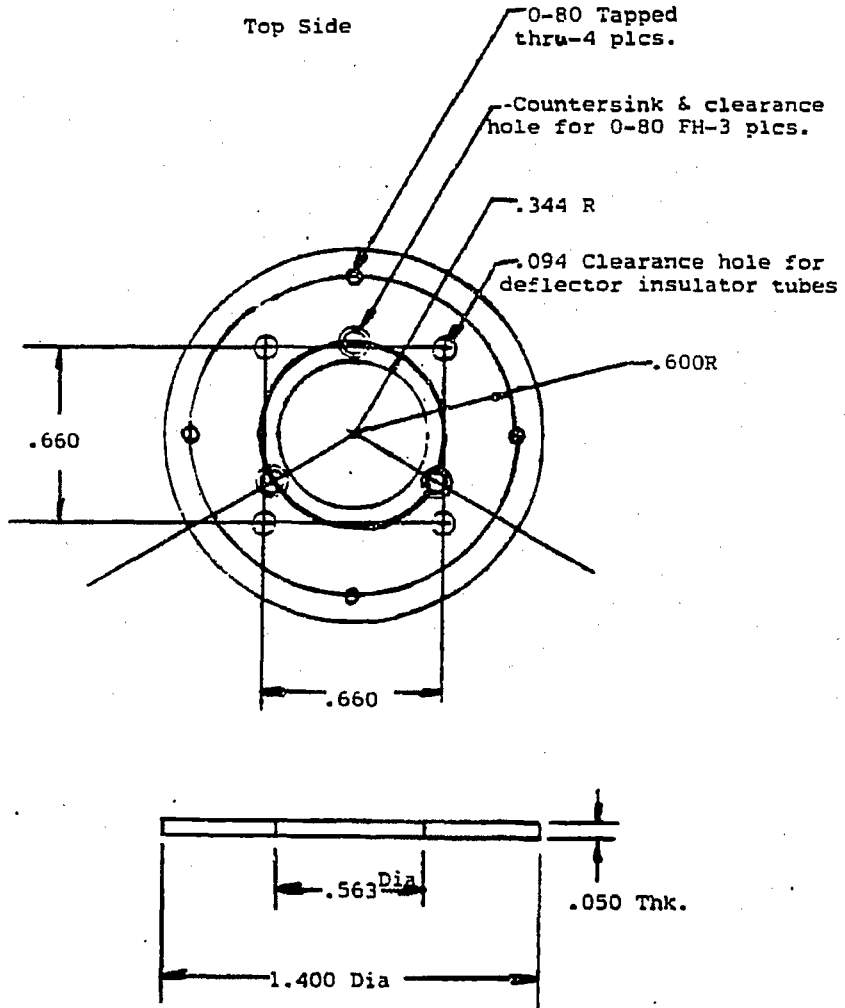
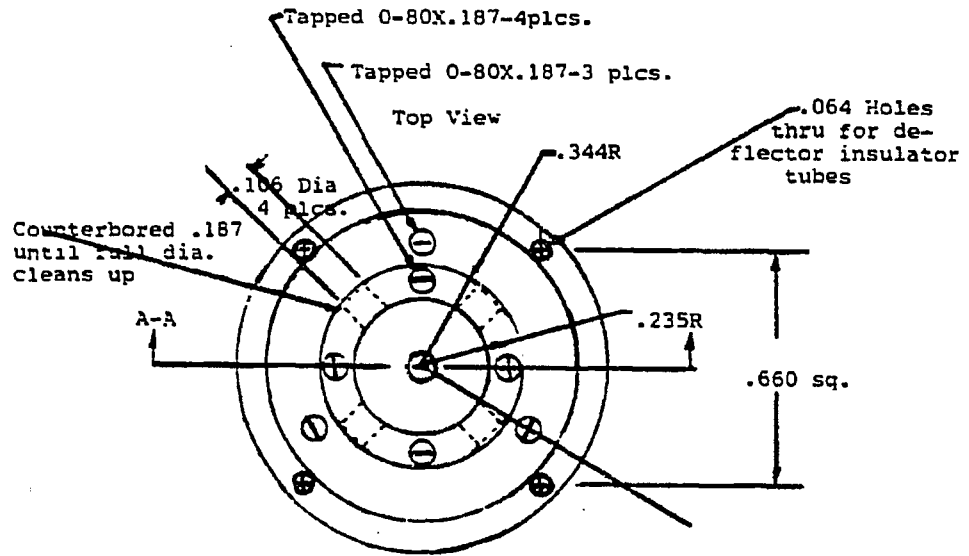


Fig. A.28. The middle plate holding the internal electron gun parts lines up the deflector lens wires and is bolted to the top electron gun plate.

Electron Gun-Deflector Lens Holder-1 pc.
304SST



Deflector Lens-4 pcs.
304SST Scale 4X

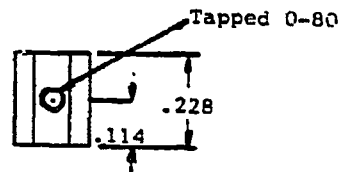
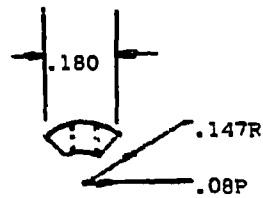


Fig. A.29. The electron gun deflector lens holder is shown from the top (Fig. A.29) and side and bottom (Fig. A.30) views. The deflector plates (see Fig. A.30) are held in place by ceramic isolated screws (see Figs. A.34,36), which are connected to the 10 pin connector in Fig. A.1.

Electron Gun Deflector Lens Holder

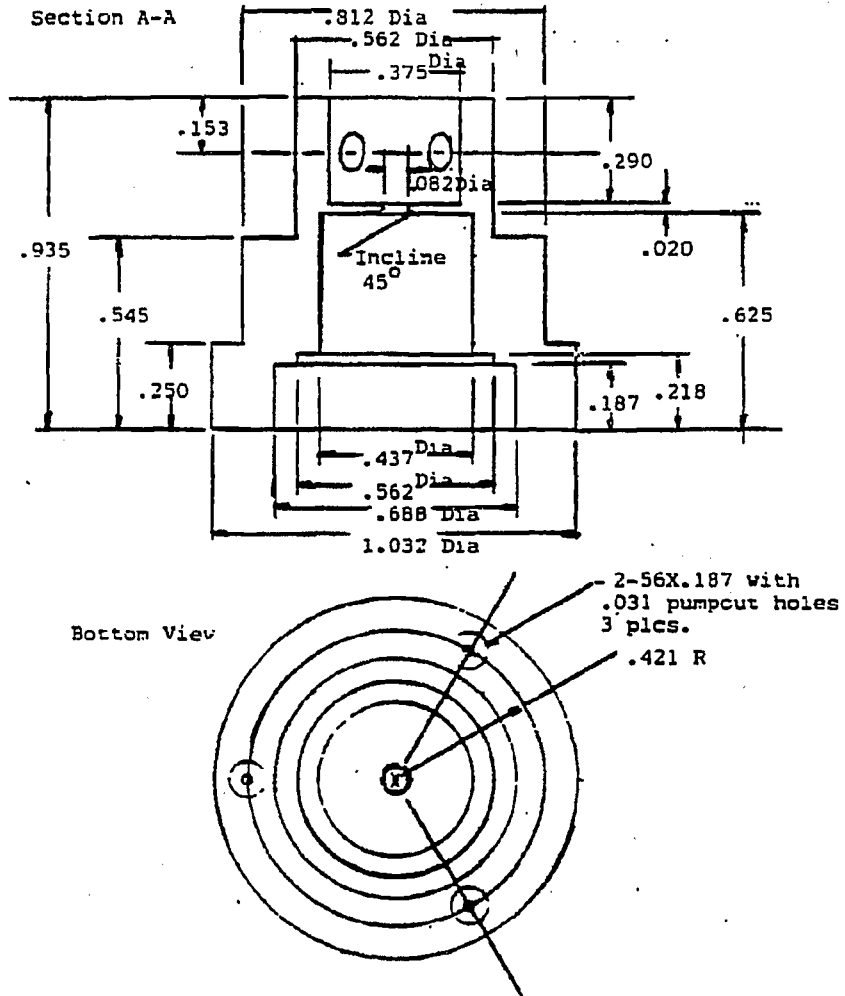


Fig. A.30. See Fig. A.29 for description.

Electron Gun-Final Aperature-i pc.
304SST

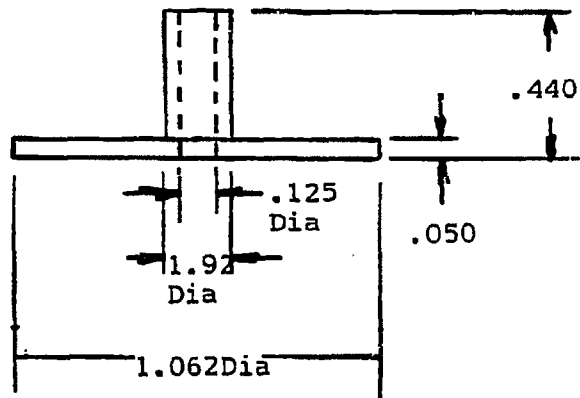
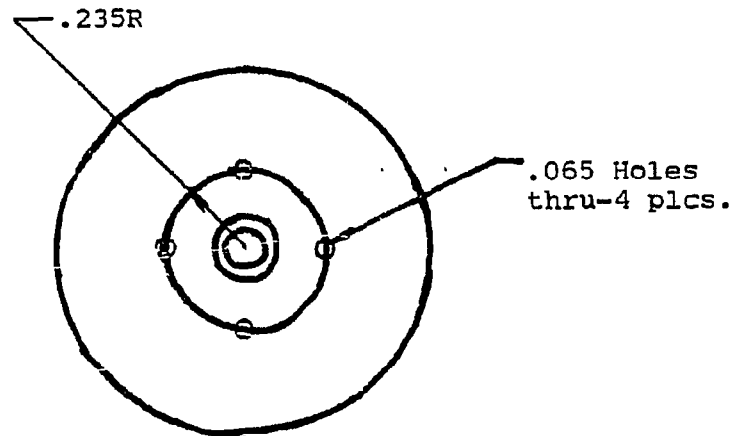


Fig. A.31. The final aperture for the electron beam is 0.125 in. diameter and 0.440 in. long, and usually at ground potential, connected to V3.

Electron Gun-Plate
304SST

Top Side

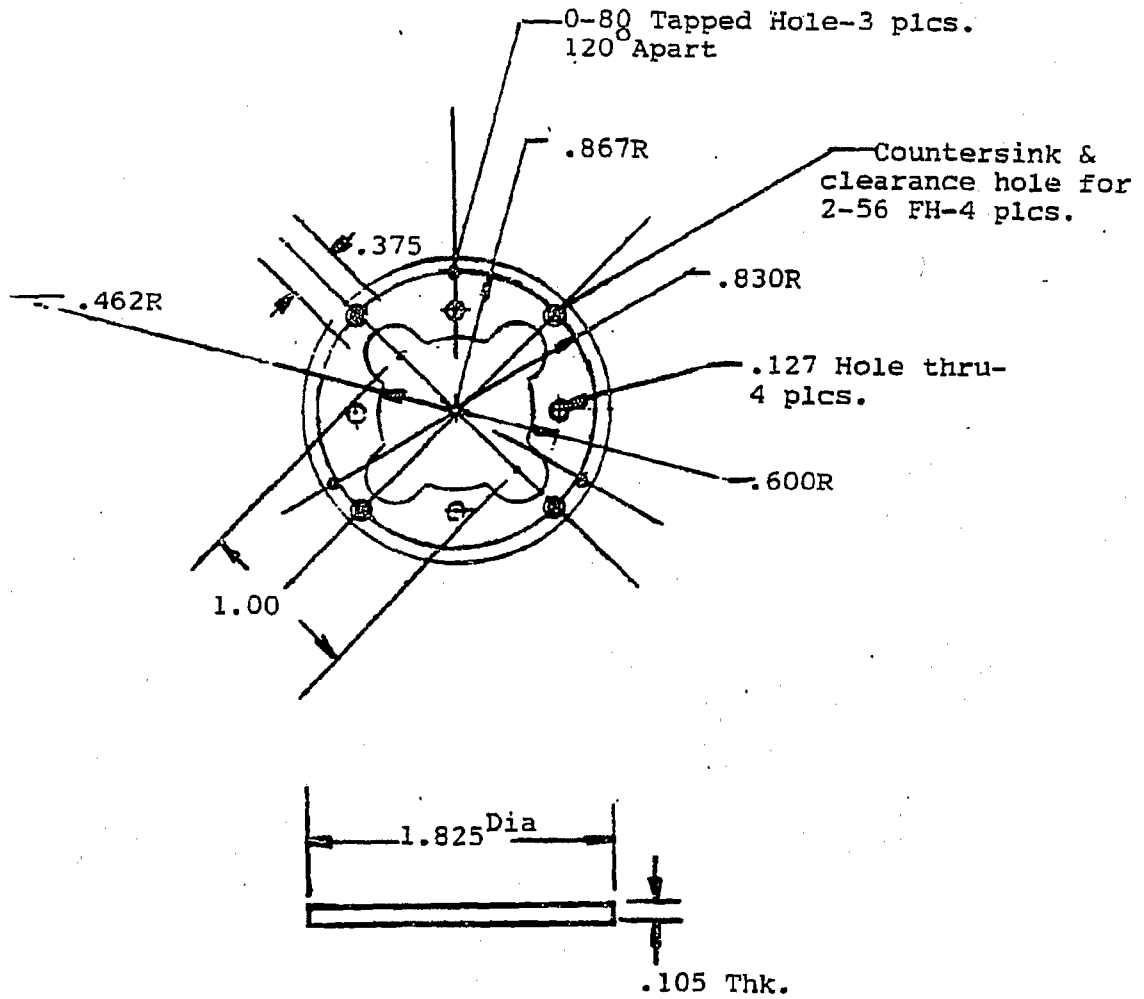


Fig. A.32. The top electron gun mounting bracket holds the electron gun in place and bolts the electron gun together with the gun support posts (see Fig. A.35).

Electron Gun-Top Shield-1 pc.
304SST

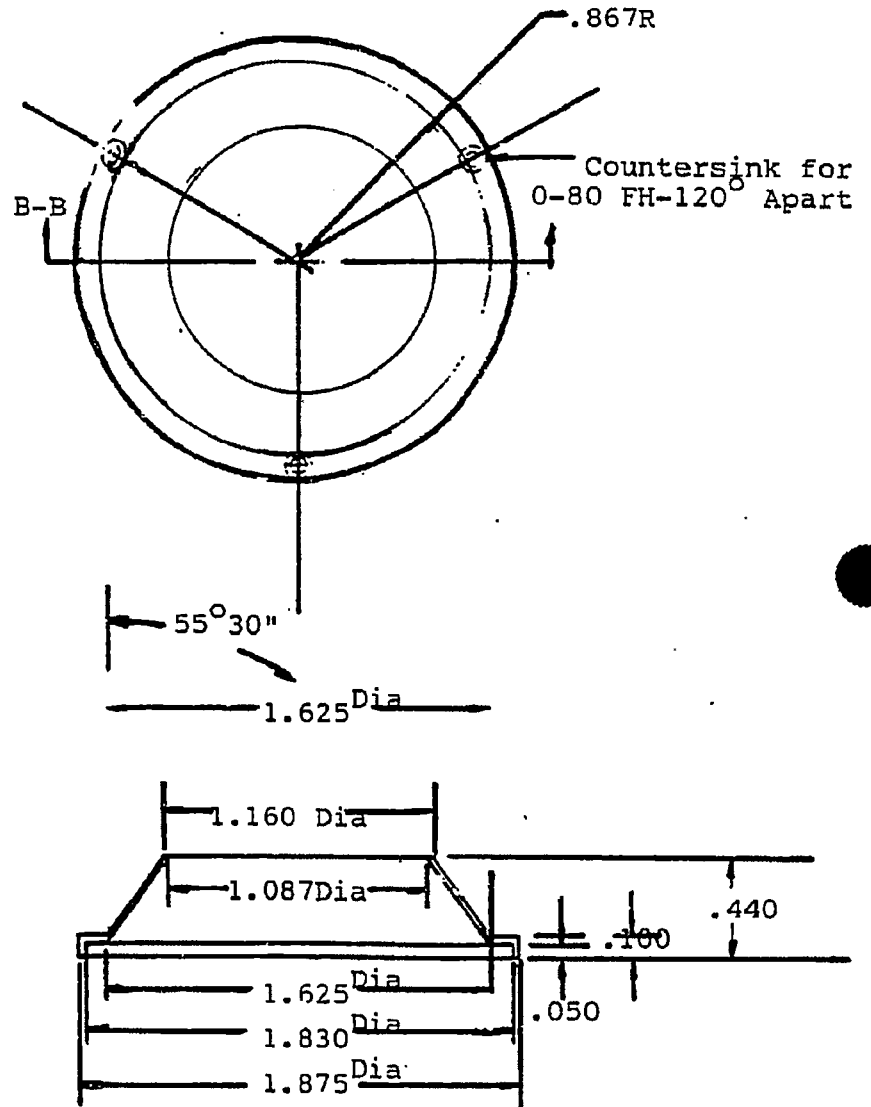
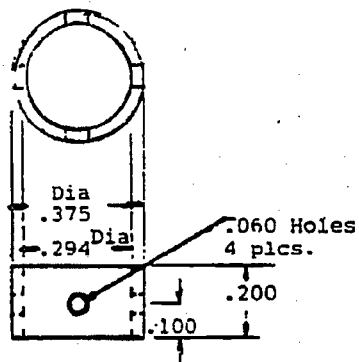
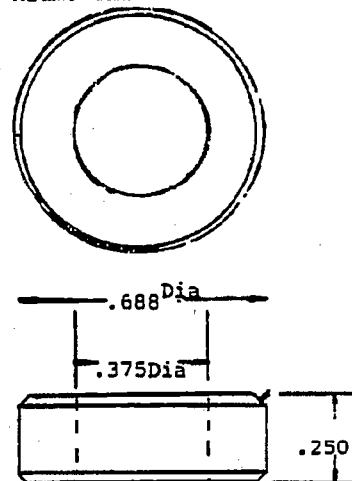


Fig. A.33. Top shield for the electron gun is bolted to the top mounting bracket with three 2-56 screws (see Fig. A.35).

Electron Gun
Deflector Lens Insulator-1pc.
Alum. Oxide



Electron Gun
Lens Insulator-1pc.
Alum. Oxide



45° Incline X .031

Electron Gun-Lens Insulators-4 each
Alum. Oxide

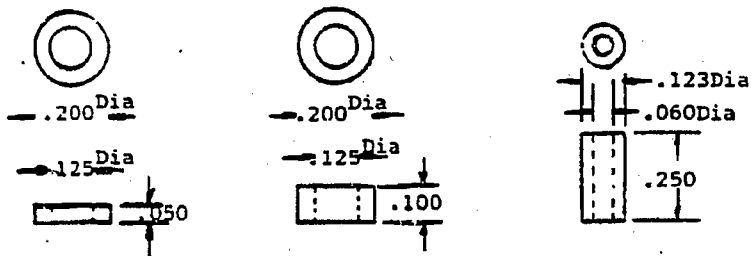
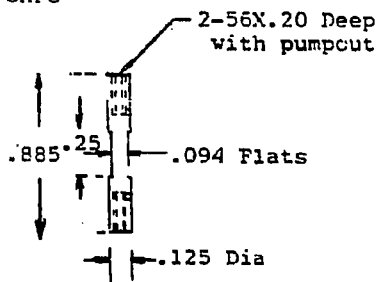


Fig. A.34 - A.37. The assorted ceramics, support posts, screws and wire insulation ceramics in detail.

Electron Gun Assembly Support
 Posts- 2 pcs.
 OHFC



Electron Gun Support Posts-4 pcs.
 304SST

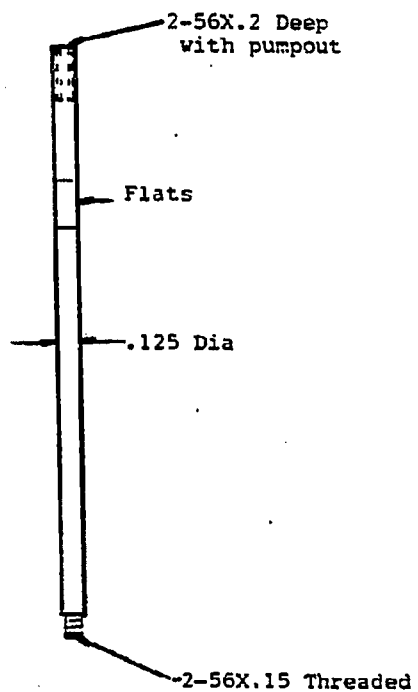
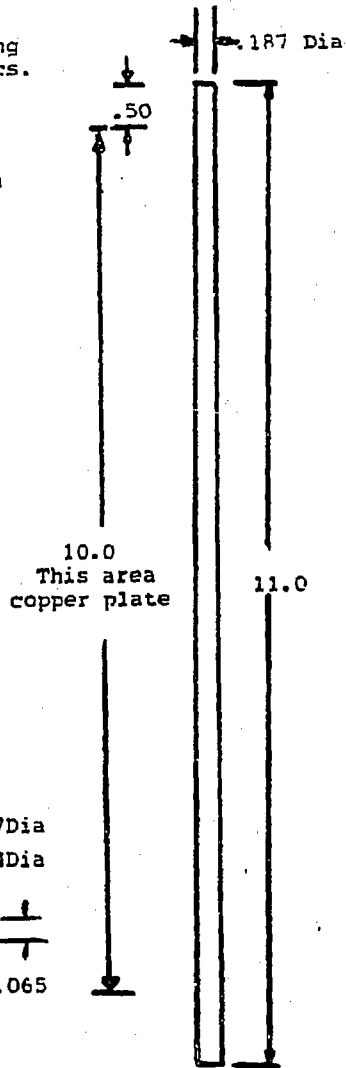
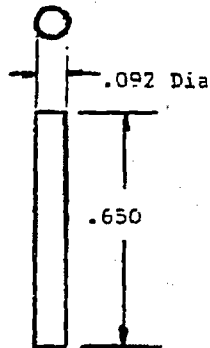


Fig. A.35.

Electron Gun Wire Insulation Tubes
 1 pc. for 4-.020 Copper Wire
 1 pc. for 5-.020 Copper Wire
 Alum. Oxide

Electron Gun-Insulating
 Mounting Posts-3 pcs.
 Alum. Oxide



Electron Gun
 Deflector Lens

Alum. Oxide

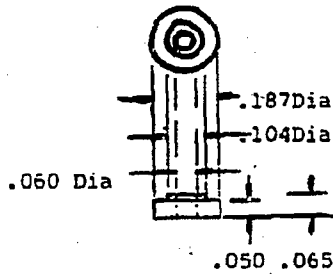


Fig. A.36.

Electron Gun Screws-3 pcs.
304SST

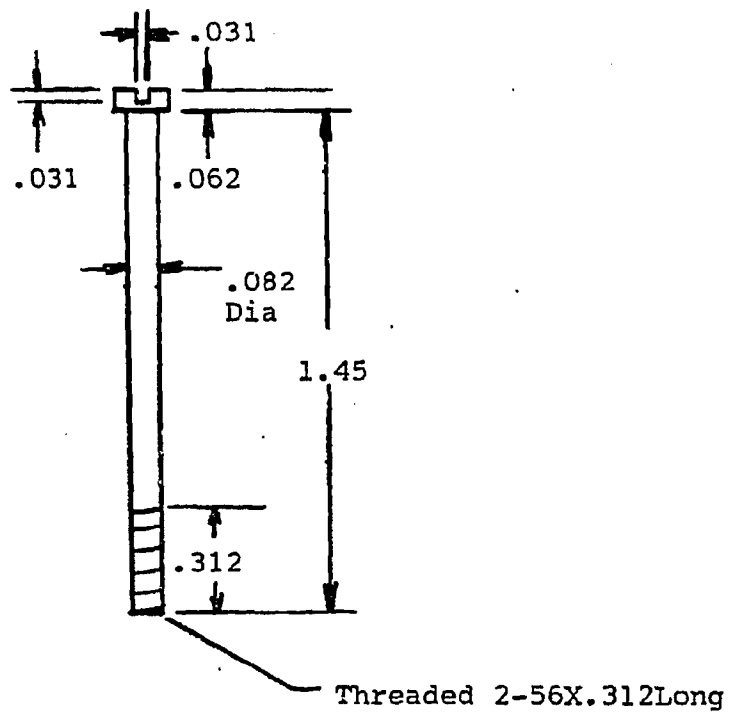


Fig. A.37.

Section A.8: Photographs A.38 - A.52

- Photograph A.38. The CMA mounted on its stand, showing the outer metal shield (see Fig. A.19,20). The cylinder is attached to the Al plate (see Fig. A.2) by four allen head screws.
- Photograph A.39. The inner metal shield (see Fig. A.21,22). The shield is attached to the first aperture (see Fig. A.10, Photograph A.50).
- Photograph A.40. The outer OF copper cylinders are held in place by the first aperture (see Fig. A.10), The bottom field terminator support (see Fig. A.4) and the stack assembly rods (see Fig. A.11).
- Photograph A.41. The lower outer cylinder. The middle field terminating plate is held by 3 set screws on the top of the cylinder.
- Photograph A.42. The top and bottom inner cylinders with the middle field terminating plate in place (in practice, the lower outer cylinder must be in place prior to putting in the middle field terminating plate).
- Photograph A.43. The upper inner cylinder and middle field terminating plate removed to exposed the internal electron gun.
- Photograph A.44. A closeup of the electron gun. The four ceramic sleeved wires in the middle are for deflection and the other set is for filament current, focusing, accelerating and grounding the various stages of the gun (see Fig. A.23 - A.37).
- Photograph A.45. Another view of the electron gun. The pivoting aperture for the top inner cylinder is also shown (see Fig. A.15 - A.18).
- Photograph A.46. A top view of the electron gun (see Fig. A.31,33).
- Photograph A.47. A closeup view of the lower portion of the CMA. The channeltron is mounted such that it can be replaced without further disassembly (see Fig. A.48). The mounting block for the 0.125 pivoting rod is also shown (see Fig. A.49). The high voltage feedthrus have copper barrel connectors on the vacuum side for easy connection and removal.
- Photograph A.48. A second closeup of the lower CMA assembly. The 10 pin feedthru for deflection is clear as well as the channeltron connection.
- Photograph A.49. A third closeup of the lower CMA assembly. The rotary feedthru and pivoting arm setup (see Fig. A.13,14) and the outer cylinder Al shielding (see Fig. A.12) are shown.

Photograph A.50. The first aperture (see Fig. A.10) with hemispherical tungsten mesh spotwelded in place.

Photograph A.51. The upper Be-Cu inner cylinder (see Fig. A.8).

Photograph A.52. The top field terminating plate.

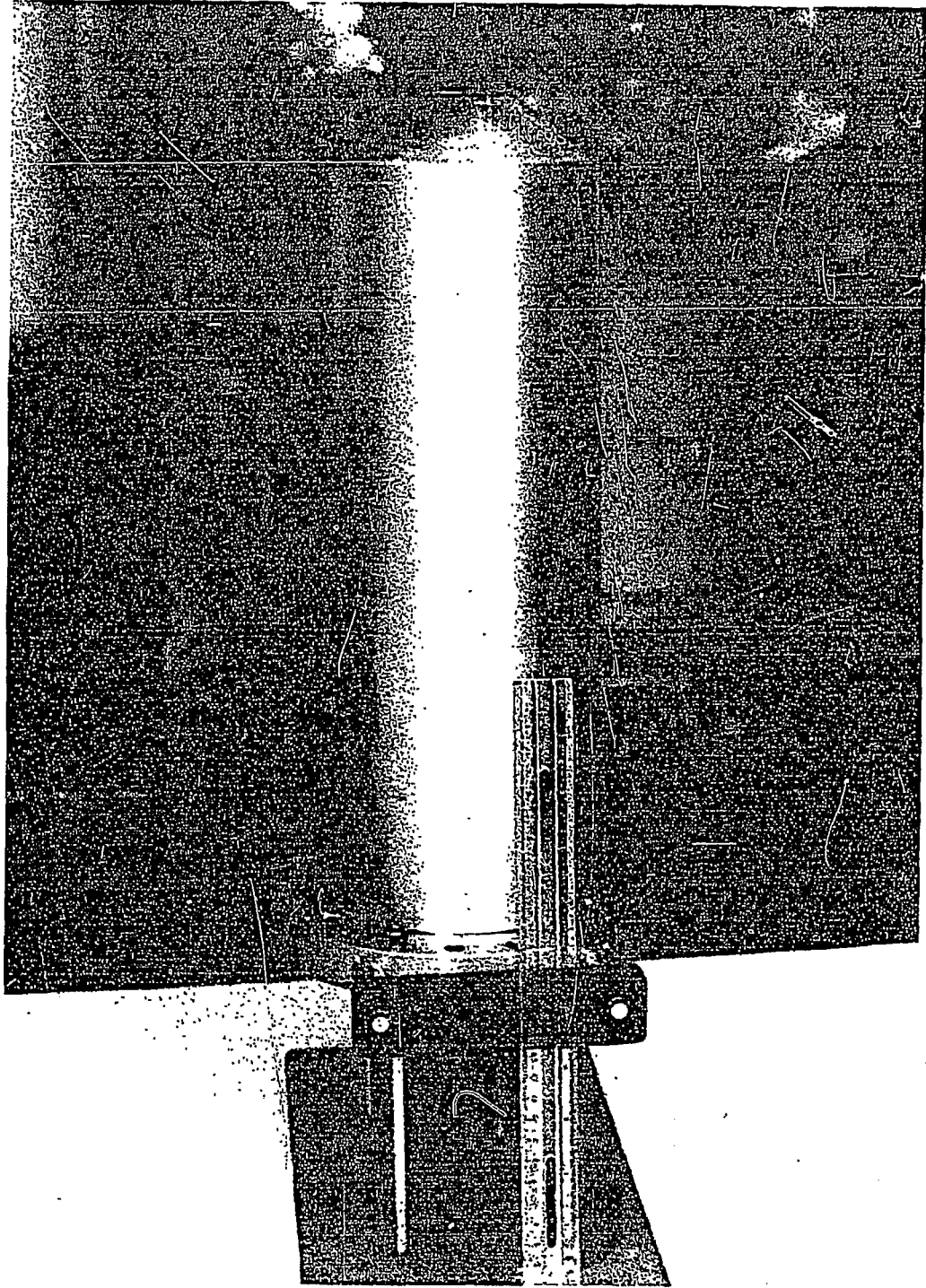


Fig. A.38

XBC 857-5522

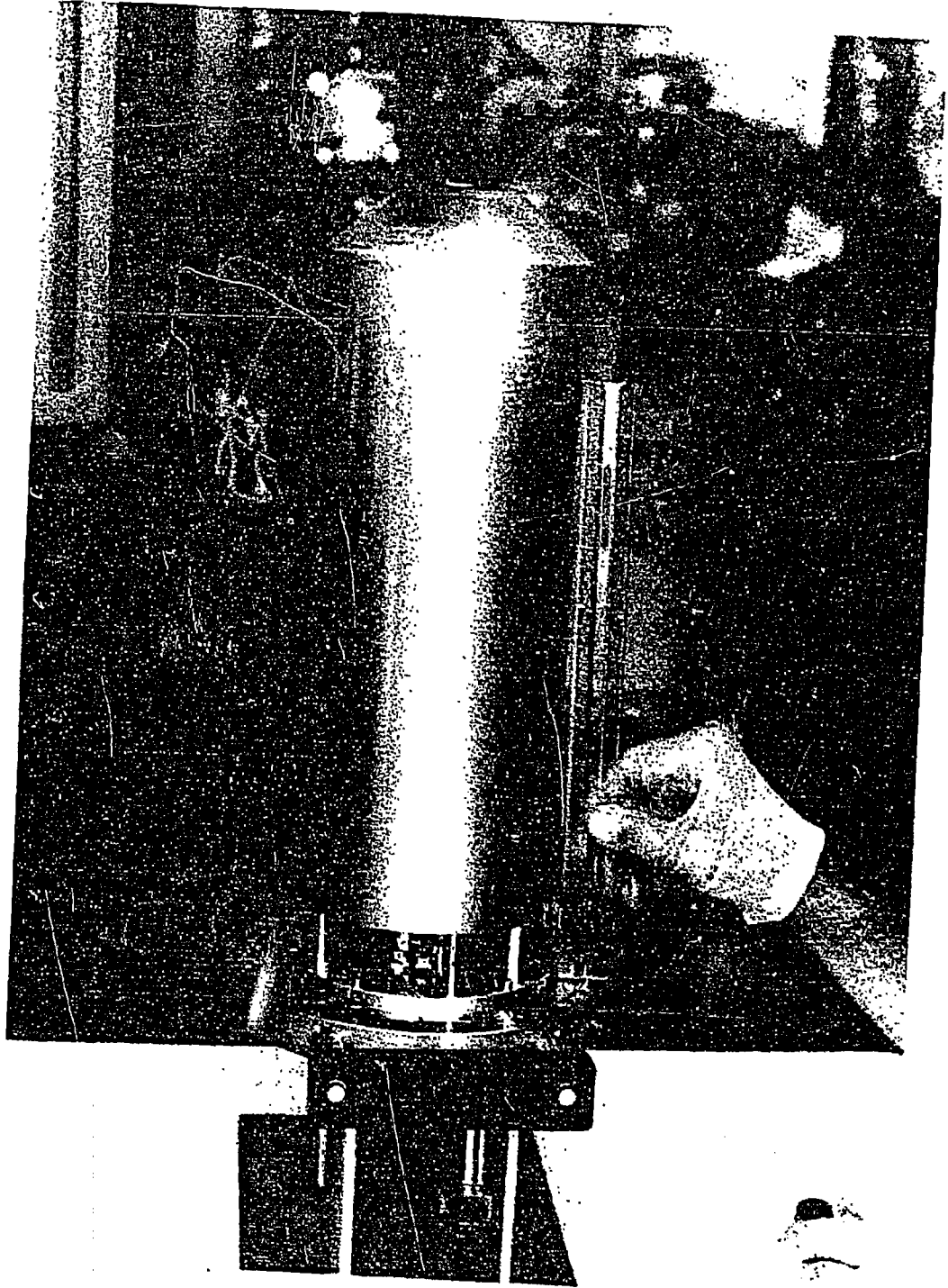


Fig. A.39

XBC 857-5523

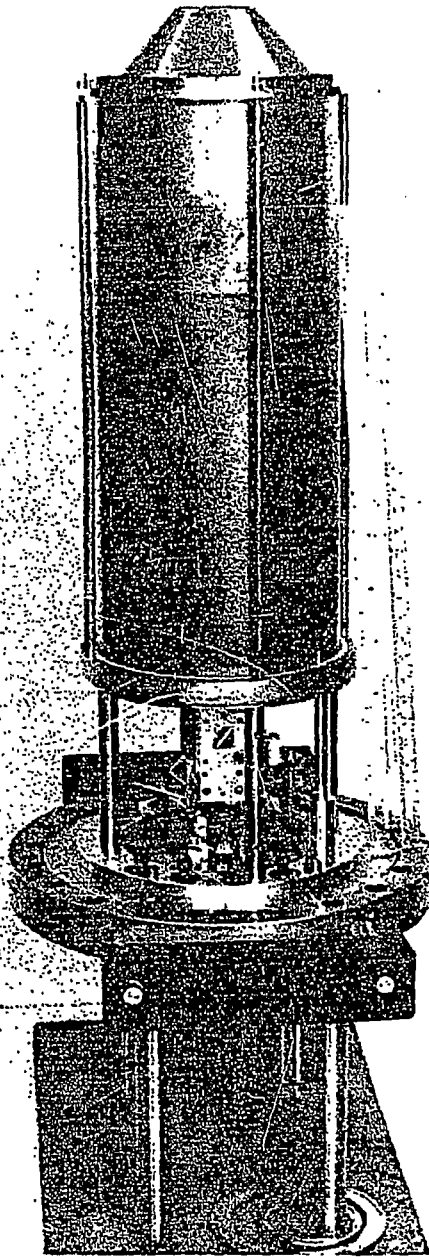


Fig. A.40

XBC 857-5524

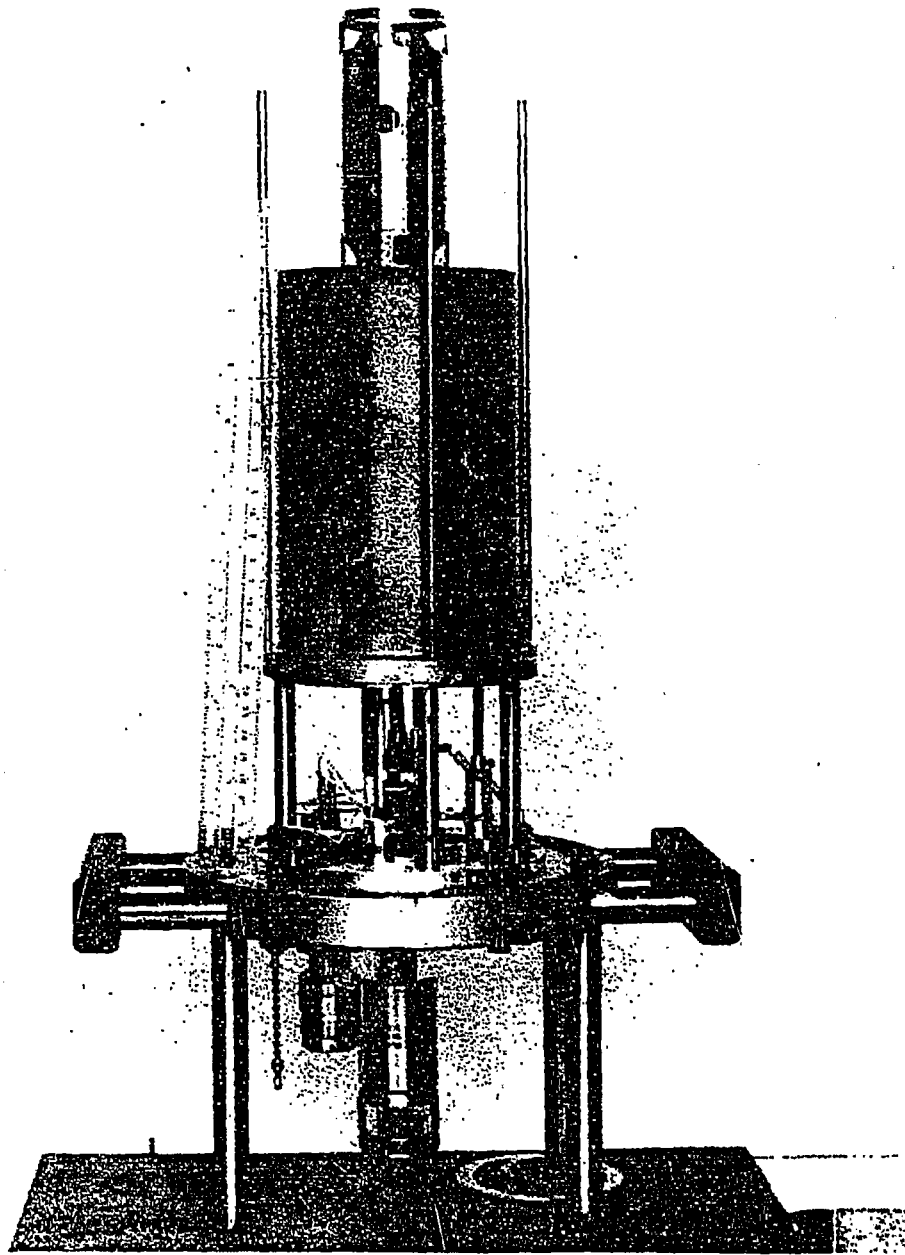


Fig. A.41

XBC 857-5527

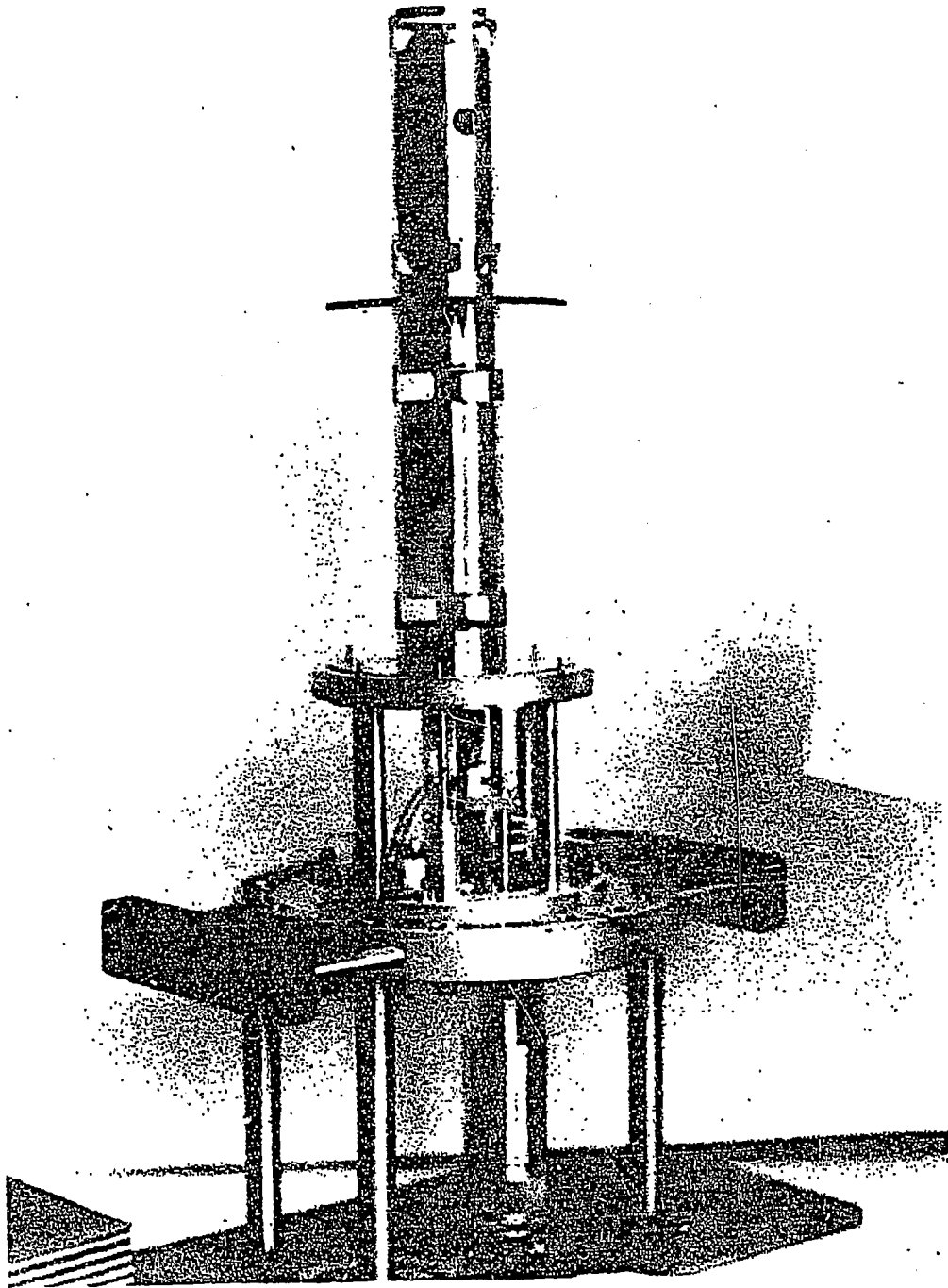


Fig. A.42

XBC 857-5521

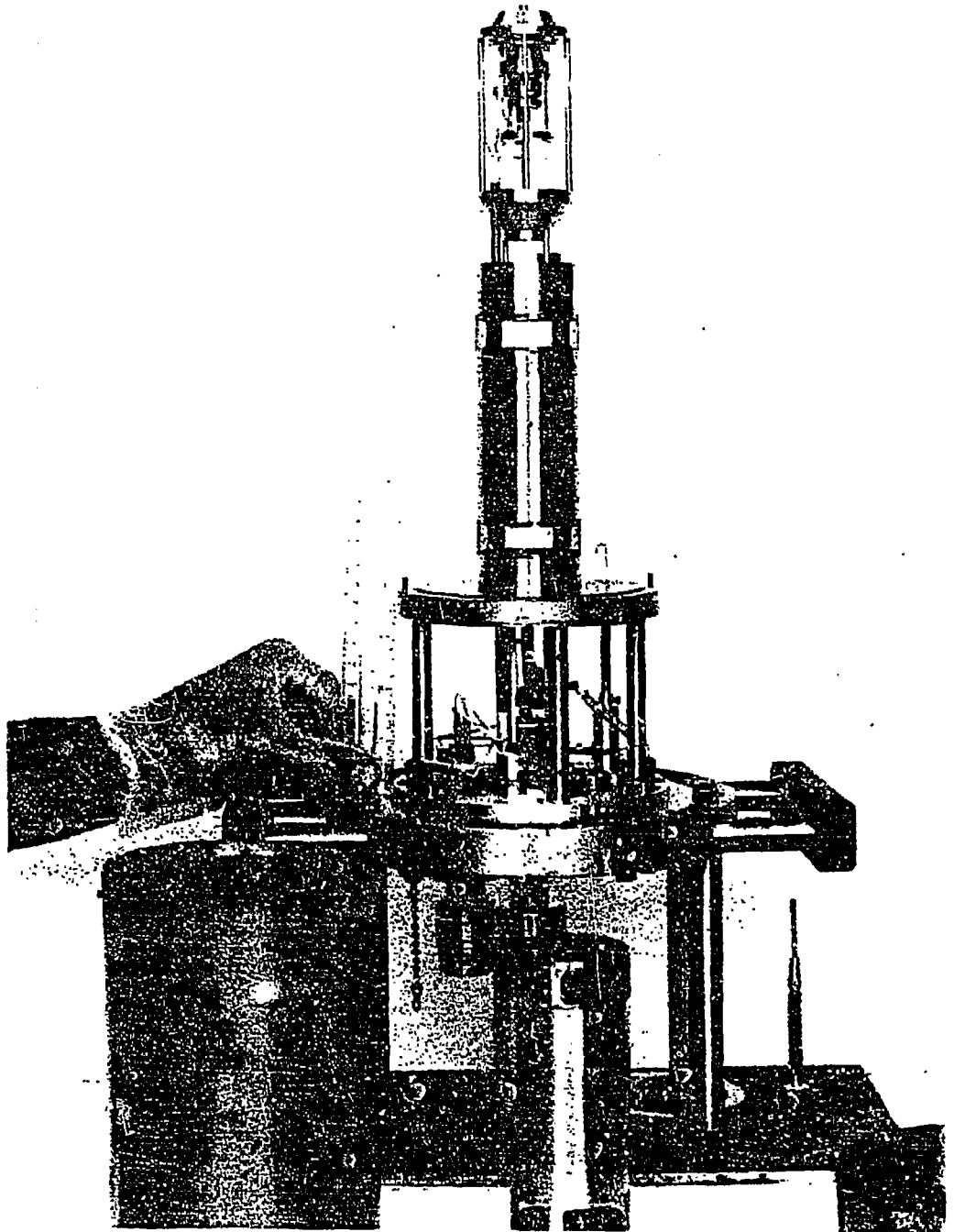


Fig. A.43

XBC 857-5528

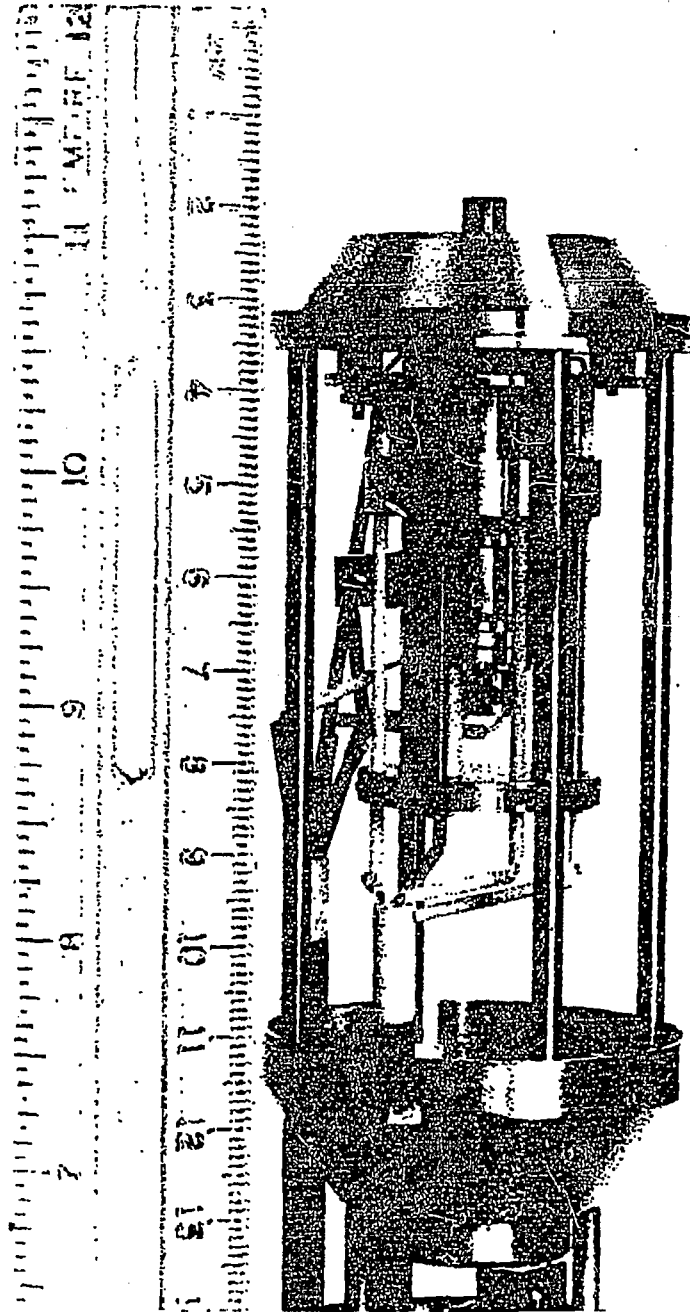


Fig. A-44

XBC 857-5529

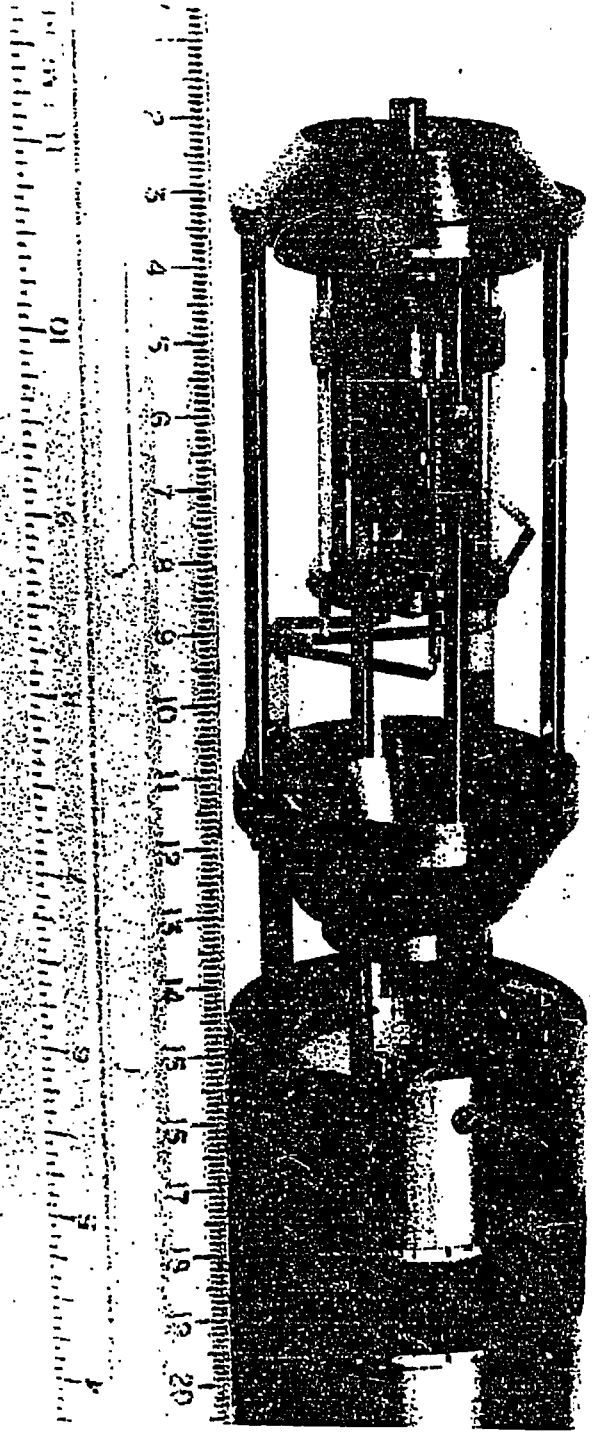


Fig. A.45

XBC 857-5531

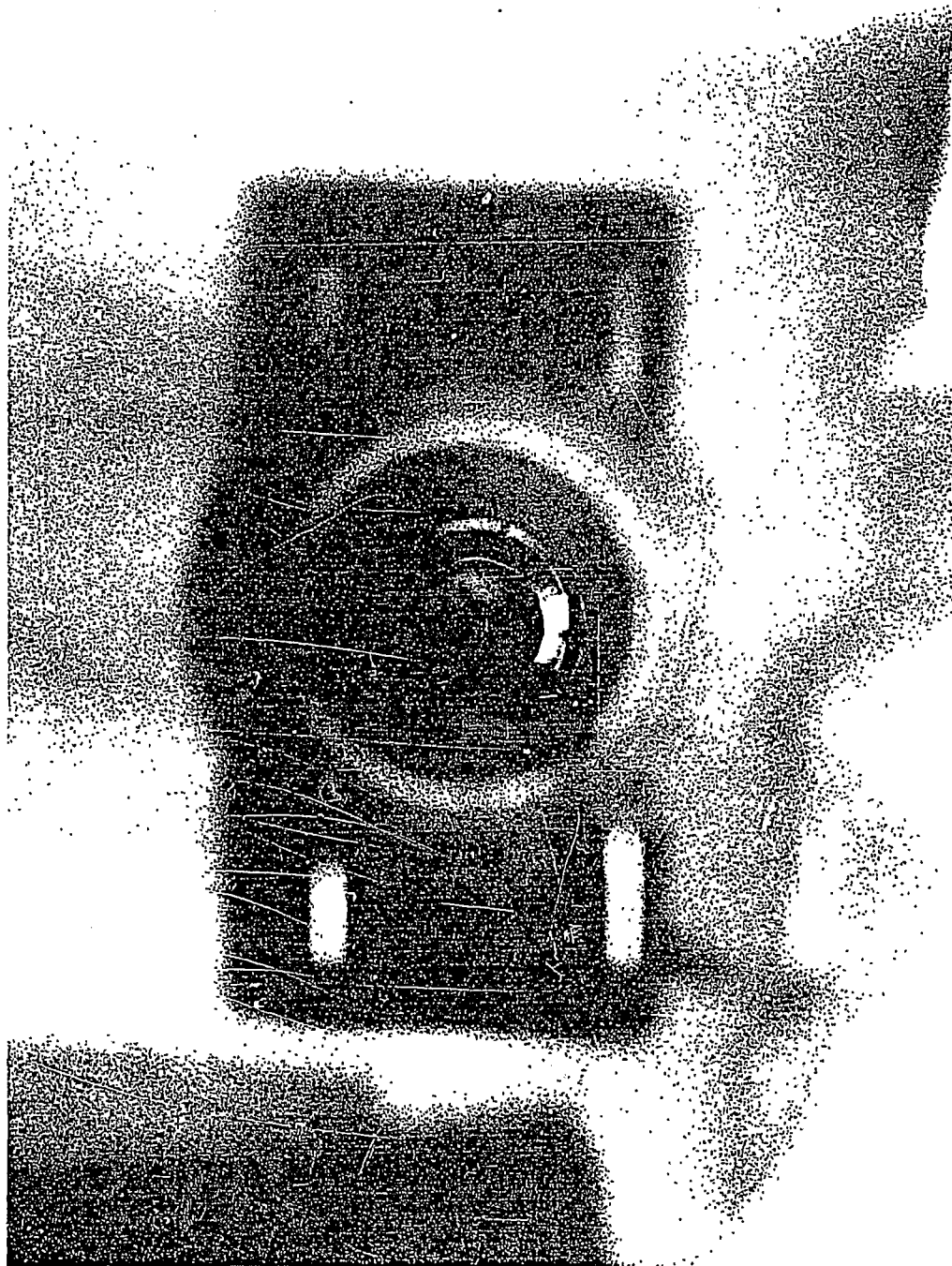


Fig. A.46

XBC 857-5519

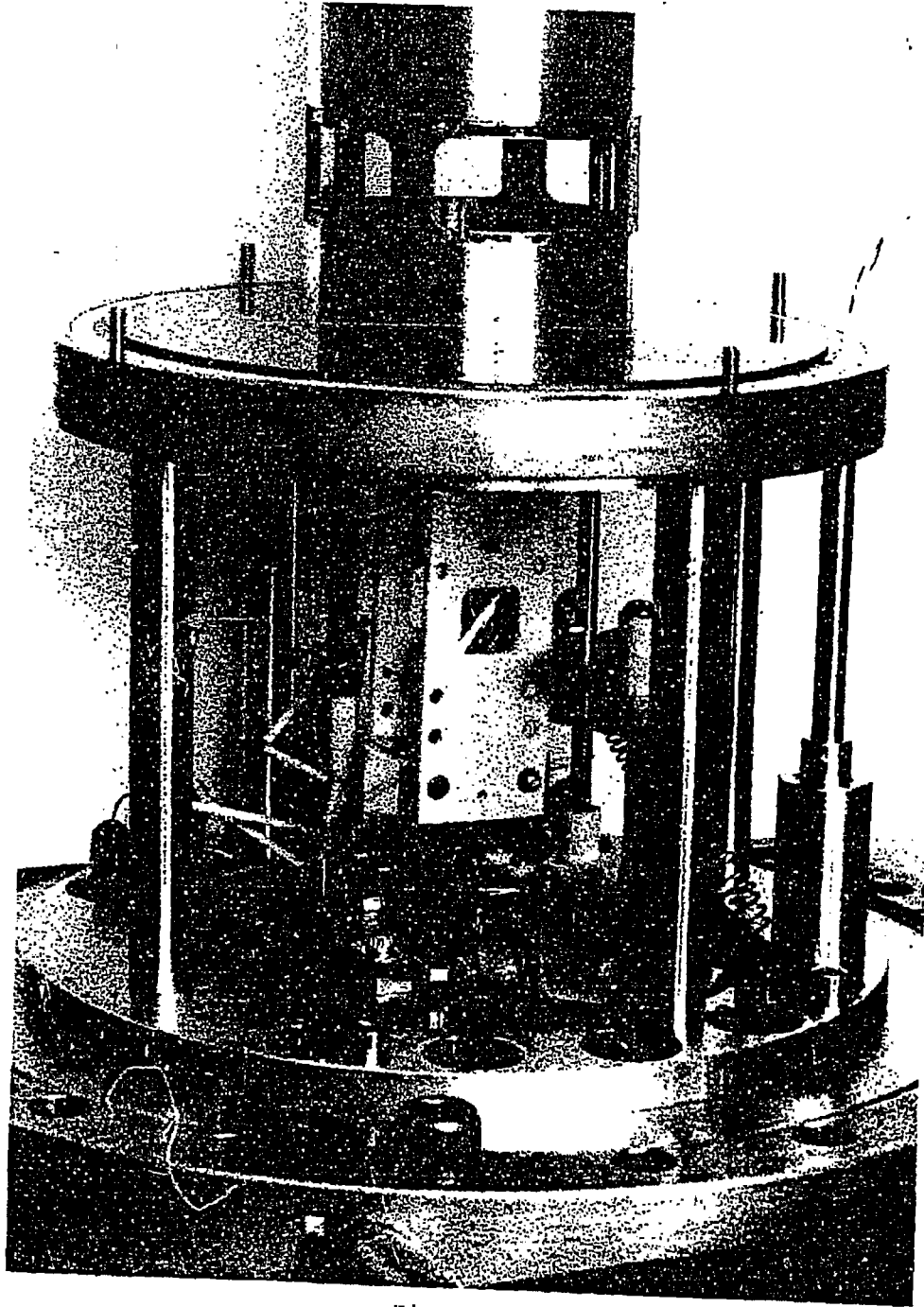


Fig. A.17

XBC 857-5532

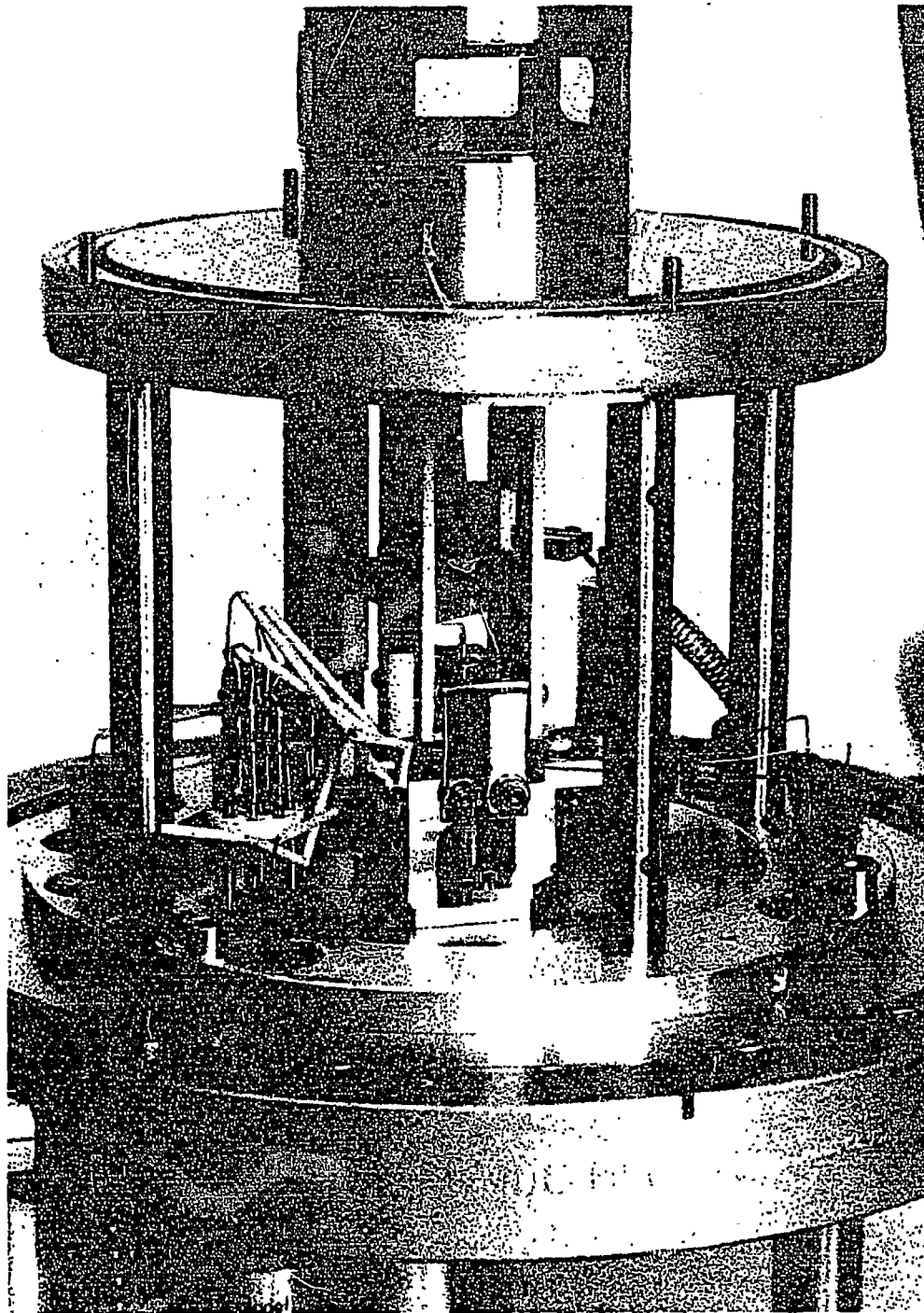


Fig. A.48

XBC 857-5533

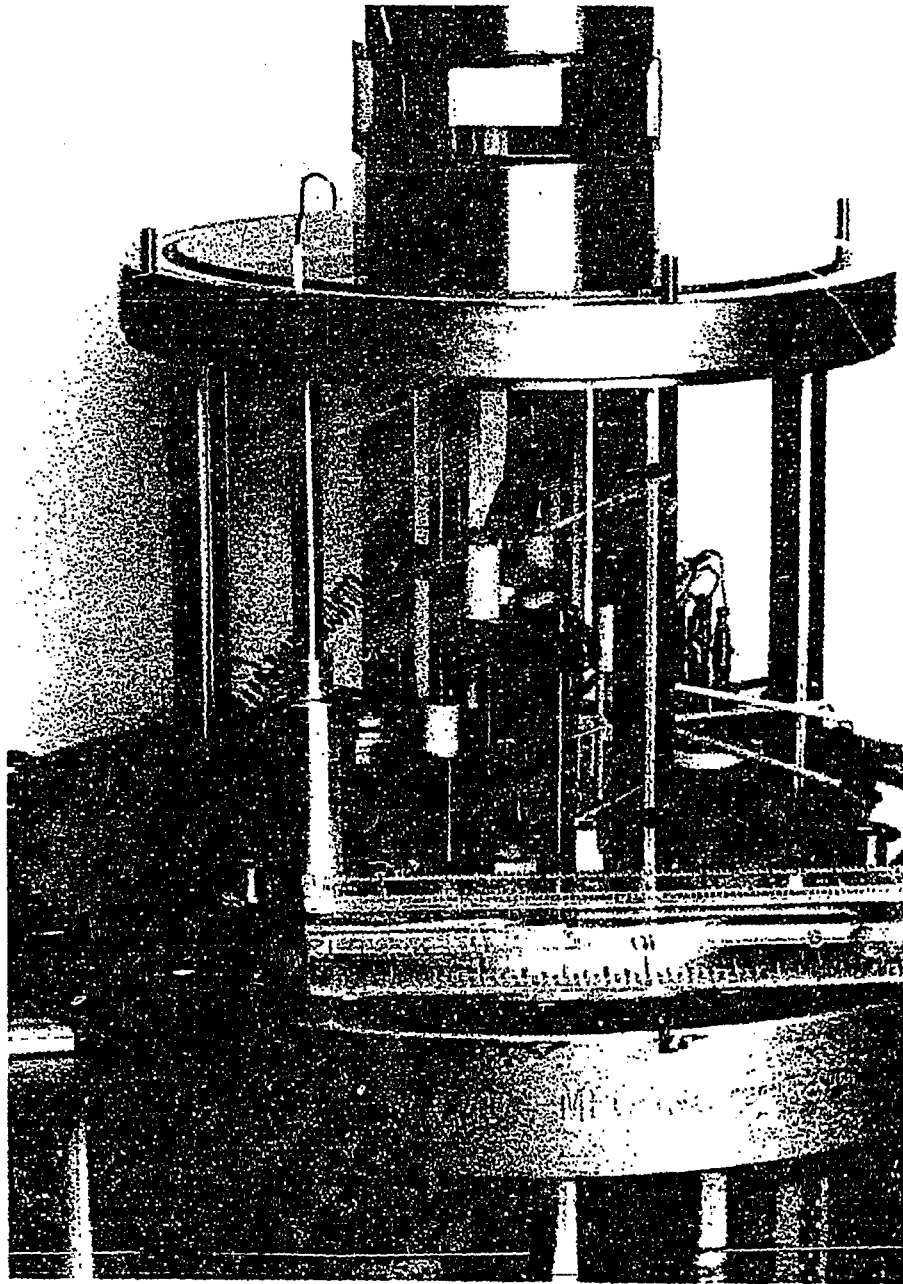


Fig. A.49

XBC 857-5534

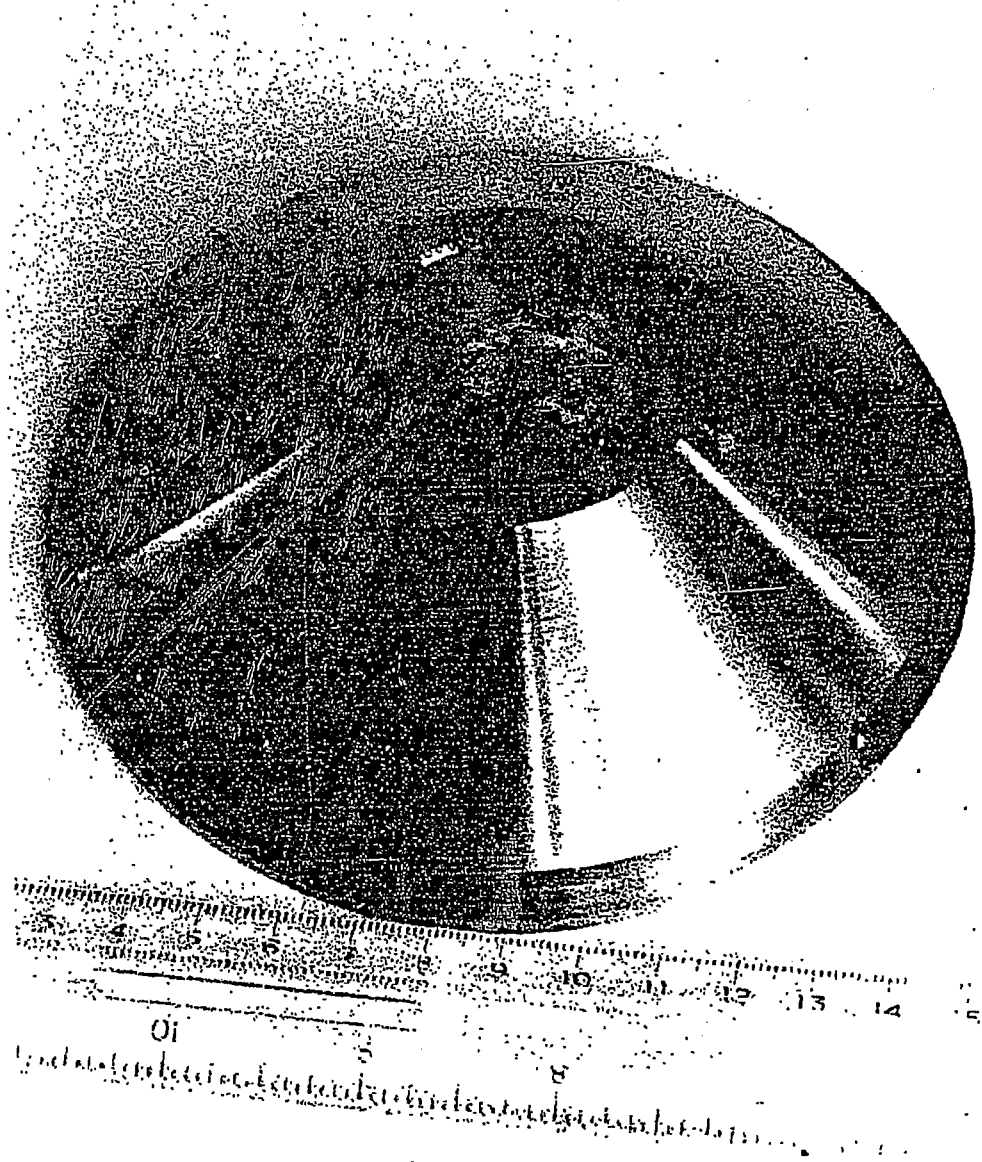


Fig. A.50

XBC 857-5535



Fig. A.51

XBC 857-5537

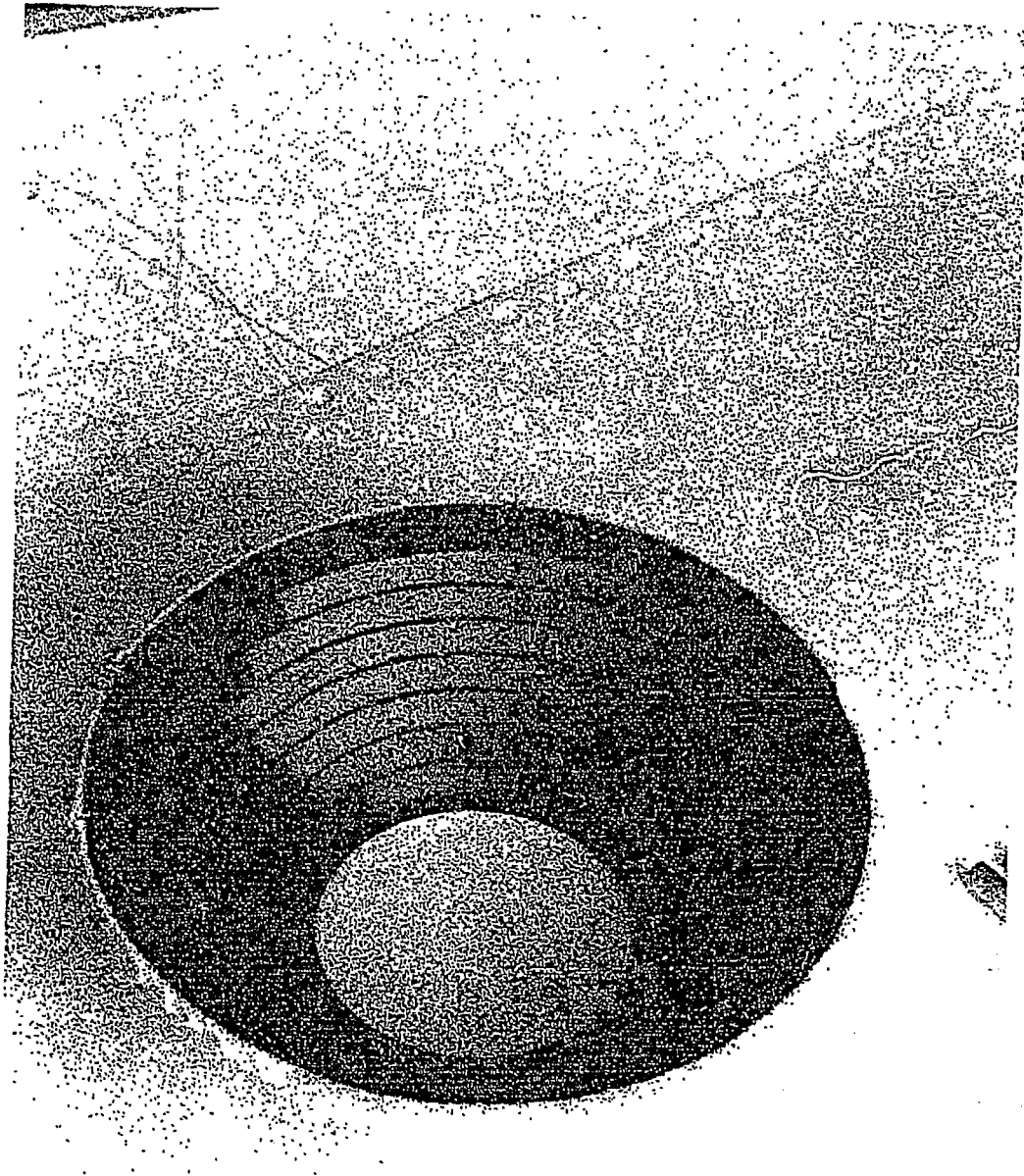


Fig. A.52

XBC 857-5538

This report was done with support from the Department of Energy. Any conclusions or opinions expressed in this report represent solely those of the author(s) and not necessarily those of The Regents of the University of California, the Lawrence Berkeley Laboratory or the Department of Energy.

Reference to a company or product name does not imply approval or recommendation of the product by the University of California or the U.S. Department of Energy to the exclusion of others that may be suitable.

SATISFACTION GUARANTEED

NTIS strives to provide quality products, reliable service, and fast delivery. Please contact us for a replacement within 30 days if the item you receive is defective or if we have made an error in filling your order.

▲ **E-mail: info@ntis.gov**

▲ **Phone: 1-888-584-8332 or (703)605-6050**

Reproduced by NTIS

National Technical Information Service
Springfield, VA 22161

This report was printed specifically for your order from nearly 3 million titles available in our collection.

For economy and efficiency, NTIS does not maintain stock of its vast collection of technical reports. Rather, most documents are custom reproduced for each order. Documents that are not in electronic format are reproduced from master archival copies and are the best possible reproductions available.

Occasionally, older master materials may reproduce portions of documents that are not fully legible. If you have questions concerning this document or any order you have placed with NTIS, please call our Customer Service Department at (703) 605-6050.

About NTIS

NTIS collects scientific, technical, engineering, and related business information – then organizes, maintains, and disseminates that information in a variety of formats – including electronic download, online access, CD-ROM, magnetic tape, diskette, multimedia, microfiche and paper.

The NTIS collection of nearly 3 million titles includes reports describing research conducted or sponsored by federal agencies and their contractors; statistical and business information; U.S. military publications; multimedia training products; computer software and electronic databases developed by federal agencies; and technical reports prepared by research organizations worldwide.

For more information about NTIS, visit our Web site at <http://www.ntis.gov>.

NTIS

**Ensuring Permanent, Easy Access to
U.S. Government Information Assets**



U.S. DEPARTMENT OF COMMERCE
Technology Administration
National Technical Information Service
Springfield, VA 22161 (703) 605-6000
